Single Molecule Probes of Lipid Membrane Structure

By

Philip Wayne Livanec
B.S., Sam Houston State University, 2004

Submitted to the Department of Chemistry and the Faculty of the Graduate School of the University of Kansas in partial fulfillment of the requirements for the degree of Doctor of Philosophy

_____
Robert C. Dunn, Ph.D. (Chairman)

_____
Susan M. Lunte, Ph.D.

_____
Cindy L. Berrie, Ph.D.

_____
Richard S. Givens, Ph.D.

_____
Cory Berkland, Ph.D.

Date Approved: December 9, 2009

The Dissertation Committee for Philip W. Livanec certifies that this is the approved version of the following dissertation:

Single Molecule Probes of Lipid Membrane Structure

_____
Robert C. Dunn, Ph.D. (Chairman)

_____
Susan M. Lunte, Ph.D.

_____
Cindy L. Berrie, Ph.D.

_____
Richard S. Givens, Ph.D.

_____
Cory Berkland, Ph.D.

Date Approved: December 9, 2009

ABSTRACT

Philip W. Livanec, Ph.D.
Department of Chemistry, December 2009
University of Kansas

Biological membranes are highly heterogeneous structures that are thought to use this heterogeneity to organize and modify the function of membrane constituents. Probing membrane organization, structure, and changes therein are crucial for linking structural metrics with function in biological membranes.

Single-molecule fluorescence studies were used to measure membrane structure at the molecular level. Several groups have shown that polarized total internal reflection fluorescence microscopy (PTIRF-M) using p-polarized excitation can reveal single-molecule orientations when spherical aberrations are introduced into the optics train. This approach was used here to measure the orientation of fluorescent lipid analogs doped into Langmuir-Blodgett and bilayer films of DPPC and DPPC/sterol mixed monolayers.

Two commonly used fluorescent lipid analogs, BODIPY-PC and $DiIC_{18}$ which have their fluorophores located in the tailgroup and headgroup, respectively were used and a variety of other probes are currently being studied. It was found that the tilt orientation of BODIPY-PC is very sensitive to the surface pressure at which the DPPC films are transferred onto the substrate. At low surface pressures, the tailgroups are largely lying in the plane of the film and evolve to an orientation normal to the surface as pressure is increased. For $DiIC_{18}$, however, no evolution in orientation with surface

pressure is observed which is consistent with the headgroup located fluorophore being less sensitive to changes in membrane packing.

The monolayer / bilayer "equivalent surface pressure" was also found to be ~23 mN/m by directly comparing the molecular structure in the two films. Using this information, the condensing affect of cholesterol and other biologically relevant sterols on monolayers and bilayers at the equivalent surface pressure was studied. Molecular dynamics simulations were also compared with the experimental results to probe the insertion of BODIPY-PC into membrane lipids.

Dedicated to Maggie, the best wife a man could ever have
and my new son Austin

Acknowledgements

Looking back over the five years that I have been here at the University of Kansas, I realize that one of the most important decisions I made, was the research group I chose to join. Not only was it important for me to pick research that I enjoyed, it was as equally important to pick a research advisor I could get along with. Well, I think I hit the jackpot. Bob Dunn has served as, not only a great advisor and mentor, but also a great friend. He has given me the opportunity to pursue research in a manner that has given me a mixture of guided direction and personal freedom. For this I will be forever grateful. Thank you Bob, for being a great advisor and an even better friend.

The faculty and staff in the KU chemistry office also played an integral part of my education. The people in the front office are the reason that the chemistry department achieves what it does. Without them, life would be much more difficult. Specifically, I would like to thank Sonjia Payne, Jan Akers, Susan Teague, Yvonne Martinez, Teri Herberger, Gary Webber, Carla Ramirez, and Ann Smith. Any time I needed something done, I knew I could go to anyone of them, and they would make it happen. I can only hope that wherever I end up, the people are as dedicated to their jobs as they have been.

I am also grateful for the numerous friends that I have made here at KU. I have worked along side some great people in the lab. When I first got here, Beth Erickson and Olivia Mooren helped with the daunting task of training me. I had many great conversations with these two and miss them a great deal. Also when I joined the group, Nick Dickenson was in the lab. Not only did he help me get through learning what I needed in the lab, but he was one of the best friends a guy could have. We never had a hard time convincing each other that nothing else was going to work that day, and we

should just go shoot some pool instead. Thank you Nick, for being that true friend, and I wish you were still here. I would also like to thank the current members of the Dunn lab, Heath Huckabay and Kevin Armendariz. We have had many useful and not-so-useful conversations in lab that make it fun just being here and I know that they will carry on the Dunn group legacy.

Along the way, I gained several more friends that helped make graduate school a great experience. Specifically I would like to mention, Nick Dickenson, Carl Cooley, Megan Dorris, Matt Culpepper, Megen Culpepper, Tom Linz, Heath Huckabay, Angelica Meyer, Dan Clark, Brandy and Tony Recio. These guys were true friends that I found would do anything for me and my wife and for that I am forever grateful. And also I have to mention my best friends in the world that are back home in Texas, Beau and Jenny Payne. They were always willing to take a weekend trip and meet us half way in Oklahoma, just so we could spend the weekend together and make home not seam so far away.

I would also like to thank my family for the support they have provided me. My parents, Mike and Sandy Livanec have been there for me through every step of the way. From buying me groceries and clothes when money was low, to the emotional support needed to get through this entire process. I have always thought highly of my parents, but going through this stage in my life, and seeing how happy they were for me, made me realize that I am the luckiest son in the world to have parents that care so deeply about me. I would also like to thank my sister, Brandy Price for the support she has given me from the moment I was born. Her and my brother-in-law, Wayne Price, are the best siblings a guy could ask for.

And last, but definitely not least, I would like to thank my wife, Maggie Livanec. She has stood by my side through thick and thin. Even though I drug her over 800 miles away from our family and friends to pursue my dreams and goals, she has always kept a smile on her face in support of me. I could not have ever done any of this without the loving support that she provides. We meet back in high school and I knew from that day, that I was never going to let this one slip away. She is the BEST thing that has ever happened to me, and I wouldn't change a thing. Plus, she has provided me with my greatest accomplishment in my life, my new son, Austin Livanec. I can't wait until he gets older and I get to tell him stories about how he was born a month early and made daddies' life crazy while trying to write a dissertation and take care of a new born baby all at once. He is the most beautiful baby boy, and I love him and his mom more than anything in this world.

Table of Contents

Chapter 7: Conclusions and Future Directions

List of Figures

List of Tables

Chapter 1

The Structure, Function, and Heterogeneity of Biological Membranes

1.1 Introduction

Since the discovery of cells by Robert Hooke and Anton van Leeuwenhoek in the mid 1600's using homemade microscopes, scientists have studied these minute structures that make up the smallest unit of life. Cells are intricate and complex structures that have many different roles in maintaining life. In order for cells to perform their basic functions, their intracellular components need to be kept safe and separate from their extracellular environment. This is one role provided by cell membranes. Cell membranes provide a semi-permeable barrier that allows the movement of substances in and out of the cell.

The cell membrane forms the defining structures of the cell. Biological membranes are made from a highly complex and diverse set of, among other things, phospholipid molecules, proteins, and cholesterol and are only about 30-50 Å in thickness. Through the studies of lipidomics, it now appears that there are thousands of different lipids incorporated into these membranes that total about 5% of a cell's genes.[1] There is great diversity in the number and types of lipids used in the membranes of different cells and even between the organelles within the same cell. It is thought that the cells use this large variety of lipid molecules to fine tune the properties and structures of their membranes. There is a hypothesis that there must be an evolutionary advantage that derives from the complex lipid collection found in membranes, but it remains unclear exactly what this advantage is.

1.2 Composition of Biological Membranes

1.2.1 The Structural Diversity of Lipids

All lipid molecules are amphipathic in nature, with a hydrophobic tail group and a hydrophilic headgroup. They vary, however, in headgroup structure, acyl chain saturation, and tailgroup lengths. Figure 1.1 shows some of the structural diversity found in the lipid headgroup. As Table 1.1 suggests, the structural diversity in membranes is large.[2] This table shows only a few different animal and bacterial membranes and the large diversity that exists within them. The tailgroup can consist of different chain lengths and different degrees of saturation and unsaturation that greatly change their properties. One of the most abundant lipids in eukaryotic cells is dipalmitoylphosphatidylcholine (DPPC) lipid, which has two 16 carbon chains that are saturated (16:0), as shown in Fig. 1.1.

The structures of lipids are extremely important in determining the properties of membranes. As discussed above, by simply changing the head group, the properties can be drastically changed. Most lipids are zwitterionic (without overall charge) but some lipids are charged. Negatively charged lipids make up about 10-20 % of lipids in membranes and are important in many ways.[3] For example, if the outer leaflet of the cell membrane contains the negatively charged lipid phosphatidylserine (PS), macrophages will be able to detect that the cell has undergone apoptosis and will digest the cell. Also, by varying the saturation and length of the lipid acyl chains, properties such as the transition temperature can be altered. This allows membranes to be in a condensed or fluid state at a given temperature. At the chain melting transition, the film is transformed from a highly ordered crystalline solid state to a less ordered liquid state. Changes in lipid

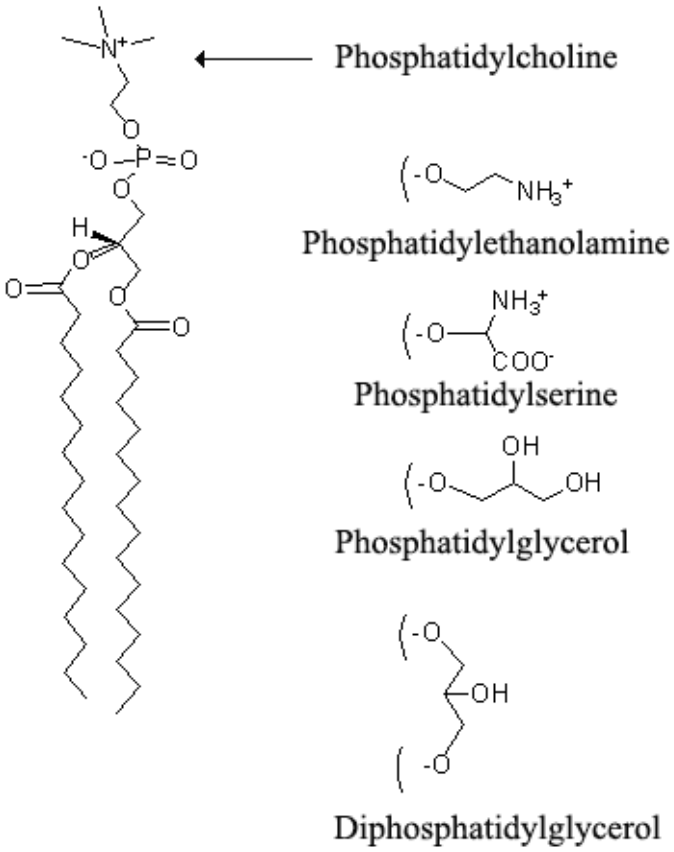

Figure 1.1 The structure of the phospholipid molecule dipalmitoyl-phosphatidylcholine (DPPC) is represented schematically. Head groups for other classes of phospholipids are also shown.

Table 1.1 Lipid composition of some animal cell and bacterial membranes

Membranes	Major Lipids
Myelin (human)	PC 10% PE 20% PS 8.5% SM 8.5% Ganglioside 26% Cholesterol 27%
Disk Membranes (bovine)	PC 41% PE 39% PS 13% Trace of Cholesterol
Erythrocytes (human)	PC 25% PE 22% PS 10% SM 18% Cholesterol 25%
Rectal Gland Plasma Membrane (dogfish)	PC 50.4% PE 35.5% PS 8.4% PI 0.5% SM 5.7% Cholesterol
Cholinergic receptor membranes *(Torpedo marmorata)*	PC 24% PE 23% PS 9.6% Cholesterol 40%
Sarcoplasmic reticulum (rabbit)	PC 66% PE 12.6% PI 8.1% Cholesterol 10%
E. coli (inner membrane)	PE 74% PG 19% CL 3%
Purple membrane *(Halobacterium halobium)*	PG 52% Glycolipids 30% Neutral lipids 6%

Abbreviations used: PC, phosphatidylcholine; PE, phosphatidylethanolamine; PS, phosphatidylserine; SM, sphingomyelin; PI, phosphatidylinositol; PG, phosphatidylgylcerol; CL, cardiolipin. Data from reference [2].

transition temperature, therefore, can lead to domain formation, which will become important as discussed later.

1.2.2 Lipid Structures Formed in Solution

Due to the amphiphilic nature of lipids, when lipids are added into solution, they tend to congregate with one another. This property allows for several different structures to be obtained based on the structure and properties of the lipid molecules. Because water exists in an energetically favored state of maximum entropy, this leads to the segregation of the hydrophobic domains away from the water molecules, causing the hydrophobic portions to congregate with one another. This interaction has been termed the *hydrophobic effect* and leads to acyl chains minimizing their interactions with the bulk aqueous phase. This is the basis for the formation of monolayers, bilayers, and micelles.[4]

Lipid monolayers are formed at the air/water interface based on these amphiphilic properties. The hydrophilic headgroups are in contact with the water subphase and the hydrophobic tailgroups orient into the air above, in order to minimize their interactions with the water molecules. This provides a convenient way to analyze monolayer structures formed at the air/water interface as will be discussed in further detail in Chapter 2.

Vesicles and micelles are formed by these same types of interactions. A vesicle or a micelle will form depending on the overall shape of the lipid molecule. By changing the headgroup or the tailgroup, the excluded volume can be changed, thereby altering the structure that is formed by the congregation of lipid molecules. The three main classes of

lipid shapes are cones, cylinders, and inverted cones as shown schematically in Fig. 1.2. The shape dictates what type of structure is formed by the lipid. In most biological systems, a bilayer is the most prominent lipid structure present. Bilayers are stabilized by orienting their lipid acyl chains towards each other in order to minimize their interactions with water molecules. This drives spontaneous bilayer formation in aqueous solvents. Planar bilayers are formed by cylindrical shaped lipids, as shown in Fig. 1.2, and exist in a tension free state at equilibrium. Bilayers can also be made by sequential dipping of two monolayers which is known as the Langmuir-Blodgett / Langmuir-Schaffer (LB/LS) method, or by using vesicle fusion on a solid support as will be discussed further in Chapter 2.

Vesicles are formed by bilayers with positive curvature. Lipids such as lysophospholipids and detergent molecules have an inverted cone shape in which the headgroup is larger than the tailgroup, thus forming micelles with positive curvature. Several types of vesicles can be made based on the method used.[5] Multilamellar vesicles (MLVs) are formed by a series of concentric shells that contain multiple bilayers and were the first type of vesicles formed. Later, both small and large unilamellar vesicles (SUVs and LUVs) were created that contain a single bilayer, and are most often used to mimic biological vesicles. Lipids molecules with a conical shape such as diacylglycerol, tend to form structures with negative curvature, such as the inverted hexagonal phase of tubes as shown in Fig. 1.2.

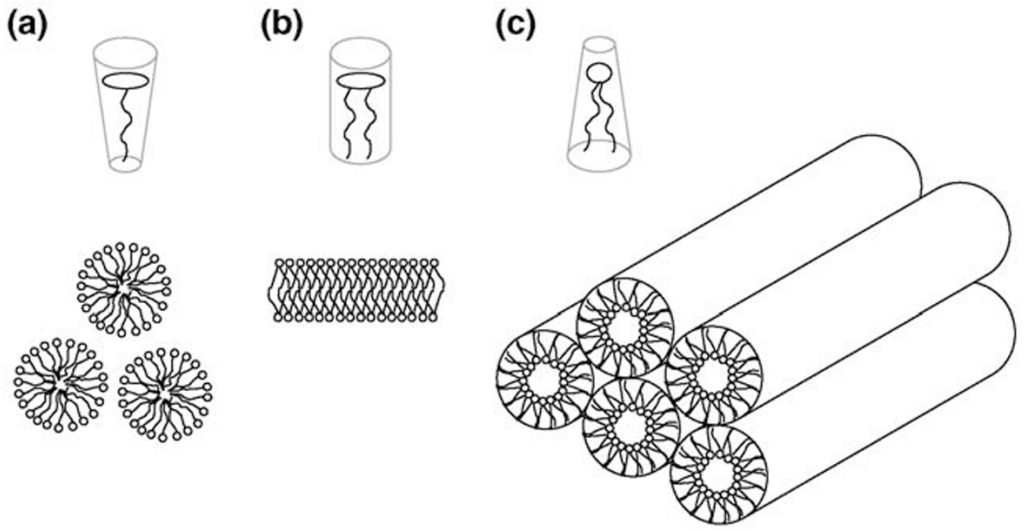

Figure 1.2 Schematic representation of structure formed by different shaped lipid molecules. **(a)** Inverted conical shaped lipid molecules form structures such as micelles, **(b)** cylindrical shaped lipid molecules form flat bilayer structures, and **(c)** conical shaped lipid molecules form inverted hexagonal structures. Figure used with permission from reference.[5]

1.2.3 Various Membrane Structures Found in Biological Systems

Although biological membranes usually exist as bilayers, they can also exist as vesicles and monolayers and each of these structures has a purpose and function. One example of a process in which vesicles are utilized biologically, is in the transport of neurotransmitters such as dopamine. Dopamine is synthesized and packaged into vesicles to be delivered to the synaptic terminal. Once at the synaptic terminal, the vesicles can fuse and burst open, releasing the dopamine. Monolayers are also present in biological systems. Lung surfactant (LS) is a monolayer mixture of lipids and proteins that coat the inner surface of the lungs and help the lungs to compress and expand as will be further discussed in Chapter 2. There is a long standing history in the literature of studying LS monolayers as many pre-mature infants are born every year with respiratory distress syndrome (RDS). RDS is a debilitating disease that can result in labored breathing, reduced oxygen transport, and even death.

1.3 Lipid Rafts

1.3.1 Brief History of Lipid Rafts

Biological membranes were once believed to be a homogenous fluid-like structure with proteins adsorbed or embedded. This idea was termed the fluid mosaic model and was proposed by Singer and Nicolson in 1972 to explain the structural features in biological membranes.[6] Shortly after, experimental results, such as X-ray diffraction studies supported the idea that some molecules do not diffuse freely, but rather congregate, creating lateral heterogeneities in the lipid bilayer. In 1982 Karnovsky and co-workers formalized the concept of lipid rafts by using the dye, 1,6-dipenyl-1,3,5-

hexatriene (DHP), which indicated there were multiple phases present in the membrane,[7] as will be discussed in further detail later.

Numerous other experiments were performed which suggested membranes contain small regions of coexisting lipid phases or microdomains, termed lipid rafts, which segregate or isolate different membrane components. While the functional roles of lipid rafts are not completely understood, experimental evidence shows that they can sequester membrane bound proteins thereby altering their biological activity. The small size and dynamic nature of lipid rafts has made direct physical measurements difficult. These structures, however, have long been studied by a host of techniques including AFM, NSOM, NMR, fluorescence microscopy, electron microscopy, and X-ray diffraction to name just a few.

Lipid rafts are enriched in sphingolipids, cholesterol and certain proteins. There are two main classes of lipid rafts; glycosphingolipid enriched membranes (GEM) and caveolae. GEM enriched rafts are the traditional detergent resistant portions of the membrane and some are thought to be enriched with certain proteins such as Immunoglobulin E (IgE). Caveolae are flask shaped invaginations of the plasma membrane that contain caveolin proteins. It is thought that rafts are responsible for certain cell signaling processes involving, for example, IgE.[8-10]

Historically, lipid rafts were first identified through detergent resistant fractions isolated by Triton X-100. Evidence of lipid rafts included the decreased solubility in Triton X-100 of FcεR (a high affinity IgE receptor) from steady state to the cross-linking state. These results show that specialized membrane domains may be involved in the coupling of receptor aggregation to the activation of signaling events.[9] This was among

the first convincing evidence of lipid rafts involving signaling processes. It was also reported by Brown and Rose that GPI-anchored proteins selectively partitioned into a Triton-insoluble membrane fraction that was enriched with glycosphingolipids and cholesterol.[11] These initial results led to numerous reports of proteins that were selectively found in the detergent-resistant lipid rafts and caveolae.[12-13]

An additional example of protein enrichment in lipid rafts is illustrated by the case of T-cell antigen receptors (TCR). TCRs are molecules found on the surface of T lymphocytes (T-cells) and comprised of αβ-heterodimers. The α and β subunits contain extracellular binding sites for peptides and proteins on the surface of the antigen presenting cells. During the signaling process, peptides and proteins bind to the TCRs and bring two or more receptors together forming small domains for signal transduction.[14-15] The results presented here are examples of only a few processes that are believed to be influenced by lipid rafts.

The complexity of biological membranes has driven the need to find better and more controlled ways to study the structure and function of these systems. According to the Gibbs Phase Rule, the maximum number of phases that can coexist is determined by the equation:

$$P = C - F + 2 \qquad \textbf{(1.1)}$$

Where P is the number of phases present, C is the number of components in the system, and F is the degrees of freedom, i.e., the number of intensive variables that are independent of other intensive variables. For example, in a one component system (C = 1), with two intensive variables (F = 2, temperature and pressure), then the maximum number of coexisting phases is three (P = 3). As shown in Fig. 1.3, a schematic of a

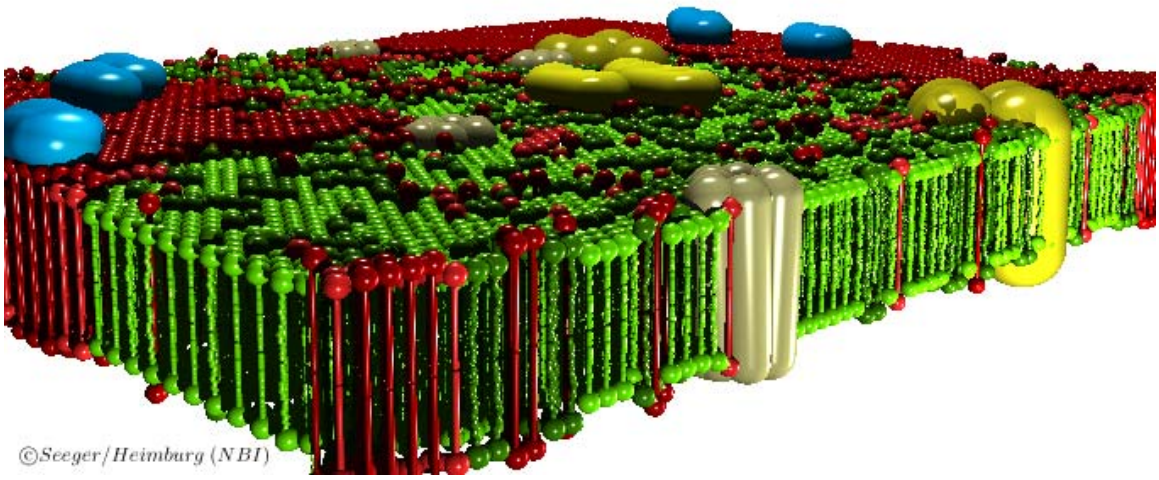

Figure 1.3 A schematic representation illustrating the complex and heterogeneous nature of biological membranes. Figure used with permission from reference [16].

representative biological membrane illustrates the heterogeneity and complexity of the system.[16] There are many different lipids and proteins in natural membranes; therefore the number of possible phases that can coexist becomes extremely high. If we want to understand the role of lipids in domain formation or the effects of additives such as the addition of cholesterol on the lipid structure, we need simpler models for examining these properties. There is a long standing history in the literature of utilizing model membrane systems to better control properties, in order to better understand exactly what is being probed.

1.3.2 Fabrication of Model Membranes

Due to the high complexity and heterogeneous nature of biological membranes, model membranes are often used as a mimic of natural systems. By utilizing model membranes, the complexity associated with biological membranes is reduced and studies can be performed in an environment where membrane constituents and properties can be precisely controlled. By studying these types of systems, we can add to our basic understandings of membrane structure, phase behavior, and mechanisms of protein insertion.

Model membranes can be fabricated by the use of several different techniques. These techniques can create monolayers, bilayers, multilayers, vesicles, and micelles just to name a few. The Langmuir-Blodgett (LB) technique offers a simple way to control several variables of the film, for example, the surface pressure which affects the lipid phase structure. Another benefit that LB deposition offers is that the film can be transferred to a solid substrate for easy analysis. Methods such as vesicle fusion lack the

control over some of these parameters, but are equally as important in the elucidation of membrane structure and function as they offer a much more representative mimic of natural membranes. Both of these methods for fabricating model membranes will be discussed in detail in Chapter 2. These methods have been instrumental in understanding the phase behavior of lipids.

1.3.3 Experimental Studies of Phase Behavior in Biological and Model Membranes

Some of the earliest studies of phase behavior involved freeze fracture sample preparation followed by imaging using scanning electron microscopy (SEM). One study measured the X-ray diffraction patterns of lipid films before and after freeze-fracture in order to study the lateral packing of the acyl chains. It was determined that different phases do exist in model membranes, and that this method could be used to monitor phase domain formation.[17] However, while this technique is useful for analyzing domains in lipid membranes, the sample preparation methods are involved and require vacuum compatible samples for analysis with SEM.

Fluorescence microscopy is a commonly used technique to study domain formation in model membranes. One of the earliest studies, as discussed above, involved using the membrane dye DHP which has been shown to partition equally between the fluid and less fluid regions of the membrane.[7] This dye molecule locates in the hydrophobic acyl chains of the membrane and its fluorescence lifetime decay has been shown to be dependent on the phase of the lipids in which it resides. In homogenous systems the decay rate is exponential while in heterogeneous systems the decay rate is multiexponential. Moreover, the lifetimes are seen to be shorter in fluid phases than in

the more solid-like phases. This early study was among the first to support the idea that lipid rafts could exist.

Later, measurements utilizing fluorescence recovery after photobleaching (FRAP) were performed to study the diffusion rates between raft like domains and the rest of the membrane. This method has been used extensively to probe microdomains in many different model and biological lipid membranes.[18-22] In FRAP, a tightly focused intense beam of light is used to irreversibly photobleach a desired membrane area containing a fluorophore. By monitoring the recovery in fluorescence signal after photobleaching, the rate at which the fluorophore diffuses back into the bleached region is measured. From this, diffusion coefficients of the probe molecules can be quantified. It has been shown that by monitoring the lateral diffusion rates of the probe molecules, multiple diffusion rates are often observed which are attributed to the presence of different lipid domains. For example, Jones et al tracked the diffusion rates of the reporter probe, 5-(N-octadecanoyl)aminofluorescein (ODAF), loaded into various membranes of 5 species of mammalian spermatozoa.[23] By utilizing FRAP measurements, they were able to show that the diffusion rates of the reporter probe differed significantly depending on what region of the spermatozoa was being analyzed. It was concluded that the lipid diffusion in the plasma membrane is highly dependent on the presence of surface domains. This could be due to the heterogeneity, differences in constituents, or the presence of intramembranous barriers that can hinder diffusion between domains. This study stressed the importance of membrane lipids in regulating the migration of sperm surface antigens during developmental stages and further suggests the presence of submicron domains on the surface of living cells.

Studies have also looked at the effects that different environmental conditions, such as the effect of additives, can have on lipid membranes. One recent study investigated the effects of Ganglioside G_{M1} on lipid films of DPPC at the air-water and solid-air interfaces. By utilizing the propensity of a fluorescent lipid analog to partition into the more expanded or fluid regions of the film, they were able to analyze the fluid and condensed regions with increasing concentration of Ganglioside G_{M1}. It was found that with increasing concentrations of Ganglioside G_{M1} (up to 25 mol %), that the mixed monolayers were continually condensed. But with concentrations over 25 mol %, the mixed monolayers became more expanded or fluid-like.[24]

The main limitation to optical techniques is that the spatial resolution is limited to the diffraction limit of light or ~ $\lambda/2$. This has created the need for higher resolution methods such as atomic force microscopy (AFM), which can detect the small height differences between lipid phases. AFM has been widely used to study domains and phases present in model membranes. One early study utilized AFM to analyze the domains present in LB monolayers of DPPC. Wei and group analyzed the liquid-expanded to liquid-condensed (LE / LC) phase transition of DPPC monolayers and they studied the effects of compression rates on domain formation.[25] By utilizing AFM, they were able to see the formation of small domains with chiral structure for the first time.

1.4 Motivation and Overview of this Dissertation

As indicated in the previous sections, many experiments have been done in order to understand the structure and function of biological membranes through the use of model membranes. What was once thought to be a homogenous fluid like structure is

now understood to be much more complex. Through the use of different biological and biophysical techniques, the heterogeneity and complex structure of membranes has been brought to the forefront.

Chapter 2 of this dissertation will discuss the techniques utilized in this dissertation to investigate model membrane structure. Specifically, the fabrication of model membranes, using both the Langmuir-Blodgett deposition technique and the vesicle fusion technique is discussed. These deposition methods offer a reliable and well controlled way to produce supported model membranes used for these studies. The use of confocal microscopy, Atomic Force Microscopy (AFM), and Near Field Scanning Optical Microscopy (NSOM) to probe the structure of model membranes will also be discussed. These complimentary methods are used to study membrane structure from the mesoscale to the micron length scales. Finally, single molecule fluorescence measurements using polarized total internal reflection fluorescence microscopy (PTIRF-M) will be discussed. These measurements enable the characterization of single molecule orientations which, as we shall show, provides a new approach for measuring membrane structure at the molecular level.

The ordering and lateral packing of lipid acyl chains is a very important property of both model and natural membranes. We show in Chapter 3 that by utilizing single molecule orientation measurements, we can analyze the orientation of reporter molecules doped into model membrane films. By using a tailgroup labeled lipid analog as the reporter molecule, the ordering of the lipid acyl chains with increasing surface pressure can be tracked at the single molecule level. Furthermore, we show that the effects of additives such as cholesterol to lipid membranes can be probed using this method.

Monolayers are useful models of membrane behavior due to the ease of control over important properties, but bilayers, provide a better mimic of biological membranes. Bilayers, however, exist in a tension free state at equilibrium so surface pressure is not a well defined parameter. Therefore, establishing corresponding states between monolayers and bilayers is important for comprehensive studies of model membranes. As will be shown in Chapter 4, we are able to extend the linear trend of acyl chain ordering vs. surface pressure in monolayers to bilayers in order to assign a monolayer / bilayer "equivalent surface pressure" which is important for establishing a baseline for future comparisons. In chapter 4, these measurements are extended to probe the effects that sterols have on both monolayers and bilayers at the "equivalent surface pressure" found earlier.

A collaboration was also initiated with Dr. Wonpil Im and Kevin Song at the University of Kansas to use molecular dynamics (MD) simulations to model the effect of the reporter molecule on the membrane and understand its orientation as a function of surface pressure. A comparison between the average tilt angle of the reporter molecule in bilayers and monolayers in the MD simulations was made. This study showed that at higher pressures, comparisons between monolayers and bilayers agreed relatively well. Chapter 5 also compares the MD simulations with the experimental data performed at temperatures above the transition temperature of the lipid, and showed the same trends in ordering of the lipid acyl chains with an increase in surface pressure.

Chapter 6 describes a method to easily nano-pattern large surfaces quickly and efficiently using model lipid membranes as templates of the desired structure. Micro-patterning techniques often require expensive equipment and long periods of time to

pattern surfaces. The method developed here utilizes the LB technique as well as a diblock copolymer deposition technique to create nanometric patterns on flat or curved solid substrates that template the growth of 3-D structures. A host of different patterns can be created on fairly large scales that range from the micron-scale to the nano-scale. By simply fuming the template structure with cyanoacrylate, 3-D structures can be fabricated.

Finally, chapter 7 discusses preliminary studies underway and continuing that are related to the previous chapters. The possible directions and implications of future studies will be outlined and discussed. First, the placement of the fluorophore on the lipid analog will be probed. The depth dependence and sensitivity of reporter molecules can be analyzed based on these measurements. Secondly, the effect of relative humidity of model membranes will be discussed. The goal is to achieve more biological-like samples to examine the orientations of single molecules. Lastly, antibody orientations will be discussed. By utilizing the single molecule method presented in this dissertation, antibody orientations may be able to be directly probed.

1.5 References

1. van Meer, G.; Voelker, D. R.; Feigenson, G. W., Membrane lipids: where they are and how they behave. *Nature Reviews Molecular Cell Biology* **2008,** *9* (2), 112-124.

2. Gennis, R. B., *Biomembranes*. Springer-Verlag: New York, 1989.

3. Dickey, A.; Faller, R., Examining the contributions of lipid shape and headgroup charge on bilayer behavior. *Biophys. J.* **2008,** *95* (6), 2636-2646.

4. Voelker, D. R., Lipid Assembly into Cell Membranes. *New Compr. Biochem.* **1991,** *20*, 489-523.

5. Janmey, P. A.; Kinnunen, P. K. J., Biophysical properties of lipids and dynamic membranes. *Trends Cell Biol* **2006,** *16* (10), 538-546.

6. Singer, S. J.; Nicolson, G. L., Fluid Mosaic Model of Structure of Cell-Membranes. *Science* **1972,** *175* (4023), 720.

7. Karnovsky, M. J.; Kleinfeld, A. M.; Hoover, R. L.; Klausner, R. D., The Concept of Lipid Domains in Membranes. *J. Cell Biol.* **1982,** *94* (1), 1-6.

8. Sheets, E. D.; Holowka, D.; Baird, B., Membrane organization in immunoglobulin E receptor signaling. *Curr. Opin. Chem. Biol.* **1999,** *3* (1), 95-99.

9. Field, K. A.; Holowka, D.; Baird, B., Fc-Epsilon-Ri-Mediated Recruitment of P53/56(Lyn) to Detergent-Resistant Membrane Domains Accompanies Cellular Signaling. *P Natl Acad Sci USA* **1995,** *92* (20), 9201-9205.

10. Baird, B.; Sheets, E. D.; Holowka, D., How does the plasma membrane participate in cellular signaling by receptors for immunoglobulin E? *Biophys. Chem.* **1999,** *82* (2-3), 109-119.

11. Brown, D. A.; Rose, J. K., Sorting of Gpi-Anchored Proteins to Glycolipid-Enriched Membrane Subdomains during Transport to the Apical Cell-Surface. *Cell* **1992,** *68* (3), 533-544.

12. Liu, P. S.; Rudick, M.; Anderson, R. G. W., Multiple functions of caveolin-1. *J. Biol. Chem.* **2002,** *277* (44), 41295-41298.

13. Simons, K.; Toomre, D., Lipid rafts and signal transduction. *Nature Reviews Molecular Cell Biology* **2000,** *1* (1), 31-39.

14. Janes, P. W.; Ley, S. C.; Magee, A. I.; Kabouridis, P. S., The role of lipid rafts in T cell antigen receptor (TCR) signalling. *Semin Immunol* **2000,** *12* (1), 23-34.

15. Langlet, C.; Bernard, A. M.; Drevot, P.; He, H. T., Membrane rafts and signaling by the multichain immune recognition receptors. *Curr Opin Immunol* **2000,** *12* (3), 250-255.

16. Seeger, H.; Heimburg, T., Membrane, B., Ed. University of Copenhagen, 2009.

17. Costello, M. J.; Gulikkrzywicki, T., Correlated X-Ray-Diffraction and Freeze-Fracture Studies on Membrane Model Systems Perturbations Induced by Freeze-Fracture Preparative Procedures. *Biochim. Biophys. Acta* **1976,** *455* (2), 412-432.

18. Axelrod, D.; Koppel, D. E.; Schlessinger, J.; Elson, E.; Webb, W. W., Mobility Measurement by Analysis of Fluorescence Photobleaching Recovery Kinetics. *Biophys. J.* **1976,** *16* (9), 1055-1069.

19. Cezanne, L.; Lopez, A.; Loste, F.; Parnaud, G.; Saurel, O.; Demange, P.; Tocanne, J. F., Organization and dynamics of the proteolipid complexes formed by annexin V and lipids in planar supported lipid bilayers. *Biochemistry* **1999,** *38* (9), 2779-2786.

20. Edidin, M., *Mobility and Proximity in Biological Membranes*. CRC Press, Inc.: 1994; p 339.

21. Lalchev, Z. I.; Mackie, A. R., Molecular lateral diffusion in model membrane systems. *Colloid Surface B* **1999,** *15* (2), 147-160.

22. Salome, L.; Cazeils, J. L.; Lopez, A.; Tocanne, J. F., Characterization of membrane domains by frap experiments at variable observation areas. *Eur Biophys J Biophy* **1998,** *27* (4), 391-402.

23. Wolfe, C. A.; James, P. S.; Mackie, A. R.; Ladha, S.; Jones, R., Regionalized lipid diffusion in the plasma membrane of mammalian spermatozoa. *Biol Reprod* **1998,** *59* (6), 1506-1514.

24. Frey, S. L.; Chi, E. Y.; Arratia, C.; Majewski, J.; Kjaer, K.; Lee, K. Y. C., Condensing and fluidizing effects of ganglioside G(M1) on phospholipid films. *Biophys. J.* **2008,** *94* (8), 3047-3064.

25. Yang, X. M.; Xiao, D.; Xiao, S. J.; Wei, Y., Domain-Structures of Phospholipid Monolayer Langmuir-Blodgett-Films Determined by Atomic-Force Microscopy. *Appl Phys a-Mater* **1994,** *59* (2), 139-143.

Chapter 2

Preparation of and Techniques Used to Image Model Membranes

2.1 Introduction

There are numerous techniques used to study biological and model membranes as briefly mentioned in chapter 1. This chapter will focus on the high resolution techniques employed in this dissertation to study model membranes. First, several methods used to prepare model membranes will be briefly discussed. This is followed by a discussion of fluorescence microscopy and two higher resolution techniques, atomic force microscopy (AFM) and near field scanning optical microscopy (NSOM). While fluorescence microscopy provides a convenient and powerful approach for probing membrane structure with micron spatial resolution, the latter techniques enable measurements with nanometric spatial resolution. Finally, we introduce a new single molecule approach for characterizing membrane structure and dynamics at the molecular level

2.2 Preparation of Model Membranes

2.2.1 Langmuir Blodgett Monolayers

In 1773, Benjamin Franklin dropped a teaspoon on oil on the surface of a pond and noticed that the oil spread for about half an acre. Lord Rayleigh was able to quantify this phenomenon over a century later.[1] By knowing the volume of the oil and the total coverage, he was able to calculate the thickness of the film and show it was a monolayer. Afterward Lord Rayleigh received a letter written from Agnes Pockels who found that these monolayers could be compressed in her kitchen sink using barriers.[2] This set the

stage for the work of Irving Langmuir and Katherine Blodgett. Langmuir created what is now known as the Langmuir trough,[3] and Blodgett discovered that when a solid substrate is inserted into the monolayer created at the air/water interface, that this monolayer could be controllably deposited onto this solid substrate.[4] With the help of Blodgett, in 1932 Langmuir was rewarded with the Nobel Prize for his work. The compression of a monolayer at the air/liquid interface, followed by its transfer onto a substrate is now known as the Langmuir-Blodgett (LB) technique. This technique is widely used to create mimics of biological membranes.

Figure 2.1 shows a typical LB trough used for transferring monolayers onto substrates. Briefly, amphiphilic molecules dissolved in a volatile solvent are deposited onto a water subphase in the LB trough, as shown in Fig. 2.1. Once the solvent evaporates, a movable barrier compresses the amphiphilic molecules trapped at the air-water interface to the desired surface pressure. The surface pressure is monitored with a Wilhelmy plate, which measures the surface or interfacial tension at the air/liquid interface. Once compressed to the desired surface pressure, the monolayer can be transferred to a solid substrate by a mechanical dipping mechanism.

LB films of lipids can be deposited at any point along the pressure-area isotherm. Figure 2.2 shows a typical pressure/area isotherm for the lipid DPPC at room temperature. As the barrier is compressed and the area per lipid is reduced, the lipid monolayer undergoes several phase transitions, which are reflected in the pressure-area isotherm. At low surface pressures, a gas-like state known as the liquid expanded (LE) phase is dominate. As the monolayer is further compressed, there exists a plateau region,

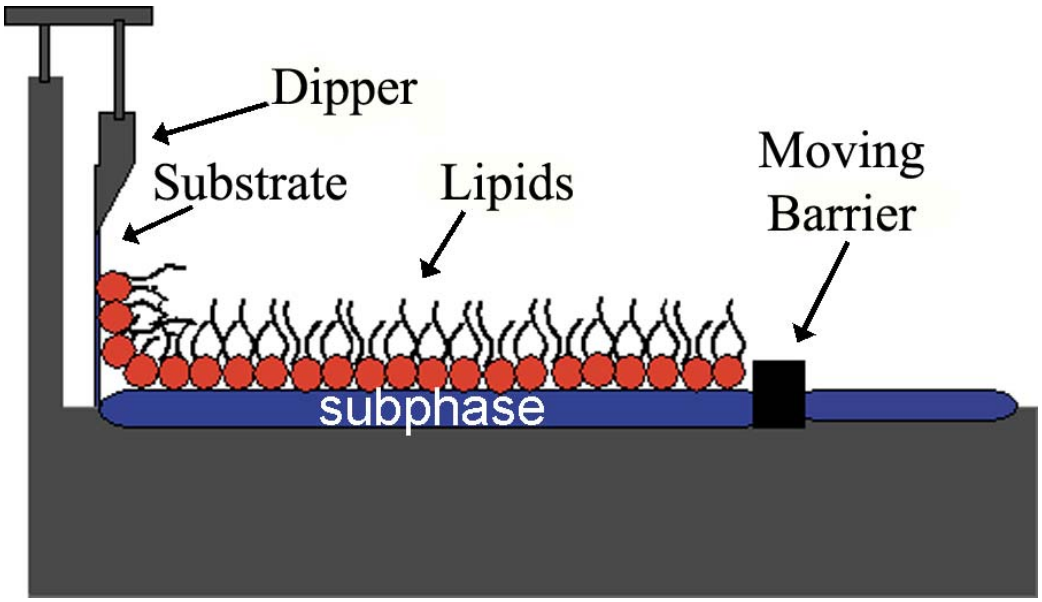

Figure 2.1 Schematic of a Langmuir-Blodgett trough, in which the amphiphilic lipids trapped at the air-water interface are shown. The barrier used to compress the monolayer to a target pressure is shown along with the dipper used to deposit the monolayer onto a solid substrate.

in which the LE/LC (liquid condensed) phases coexist, as shown in the pressure-area isotherm in Fig. 2.2. Upon compression to higher surface pressures, the LC phase is dominant and the lipid molecules are in a tightly ordered state. When the monolayer is compressed to higher pressures above the LC region, the monolayer goes through a solid condensed (SC) phase and eventually collapses into the subphase. Using the LB technique, monolayers are easily created and can be made under highly controlled conditions where membrane constituents, surface pressure, and temperature are easily controlled. However they do not mimic biological membranes as well as bilayers. Bilayers and multilayer films can also be created in which the asymmetry of each leaflet can be controlled.

2.2.2 Vesicle Fusion Technique

Model bilayers made through the vesicle fusion technique also offer a controllable and reproducible way to make lipid films. Vesicle fusion onto solid supports offers many advantages, such as ease of preparation, stability, and they are amendable to a wide variety of surface techniques for their analysis. Two main types of vesicles can be formed for vesicle fusion ranging from tens of nanometers (small unilamellar vesicles or SUVs) to tens of microns (giant lamellar vesicles or GUVs). These vesicles can be free standing in solution, tethered to a substrate, or fused to a substrate to form planar supported bilayers. Numerous studies from protein insertion to domain formation have been performed on these systems. Here we use the vesicle fusion technique to form planar lipid bilayers on a solid supports to study lipid structure in model films at the single molecule level.

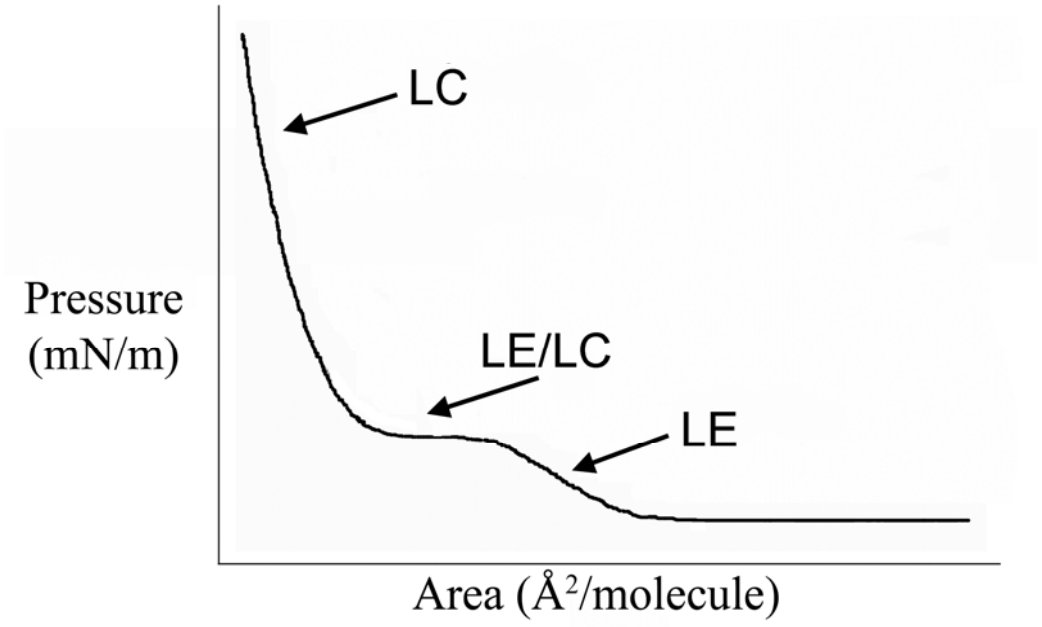

Figure 2.2 Representative pressure-area isotherm for DPPC at room temperature in which the liquid expanded (LE), liquid condensed (LC) and the LE/LC coexistence region are all visible.

Briefly, the lipid is dissolved in a volatile solvent at a desired concentration. The solution is evaporated to dryness using a nitrogen stream, and placed under vacuum to remove any residual solvent. The lipids are then reconstituted in a buffer solution and allowed to hydrate. The suspensions are vortexed and sonicated to clarity to yield small unilamellar vesicles (SUVs). The SUV suspensions are incubated at 60˚C in PDMS wells to form bilayers. Vesicle fusion takes place as illustrated in Fig. 2.3, where vesicles first adsorb to the hydrophilic solid substrate and then accumulate and rupture. Once ruptured, the vesicles coalesce to form a supported bilayer. This is one theory on how vesicle fusion proceeds, however, the molecular level details remain unclear.[5]

Supported lipid bilayers can also be formed using giant unilamellar vesicles (GUVs). Briefly, lipid suspensions are deposited between two indium tin oxide (ITO) coated slides and dried under vacuum. The slides are then rehydrated using water, and sandwiched around a PDMS gasket. The temperature of the slides is controlled using a temperature controlled stage and a function generator applies a 10 Hz, 1V sine wave across the slides to produce GUVs. Reducing the frequency to 1 Hz leads to GUVs detachment and the solution can be used to make supported bilayers as previously discussed.

2.3 Fluorescence Microscopy

Of all the imaging techniques developed to probe biological samples, optical microscopy methods remain the most versatile and popular. The instrumentation is relatively inexpensive, there has been a long historical development in optical contrast agents, and the techniques are compatible with fragile biological tissues under viable

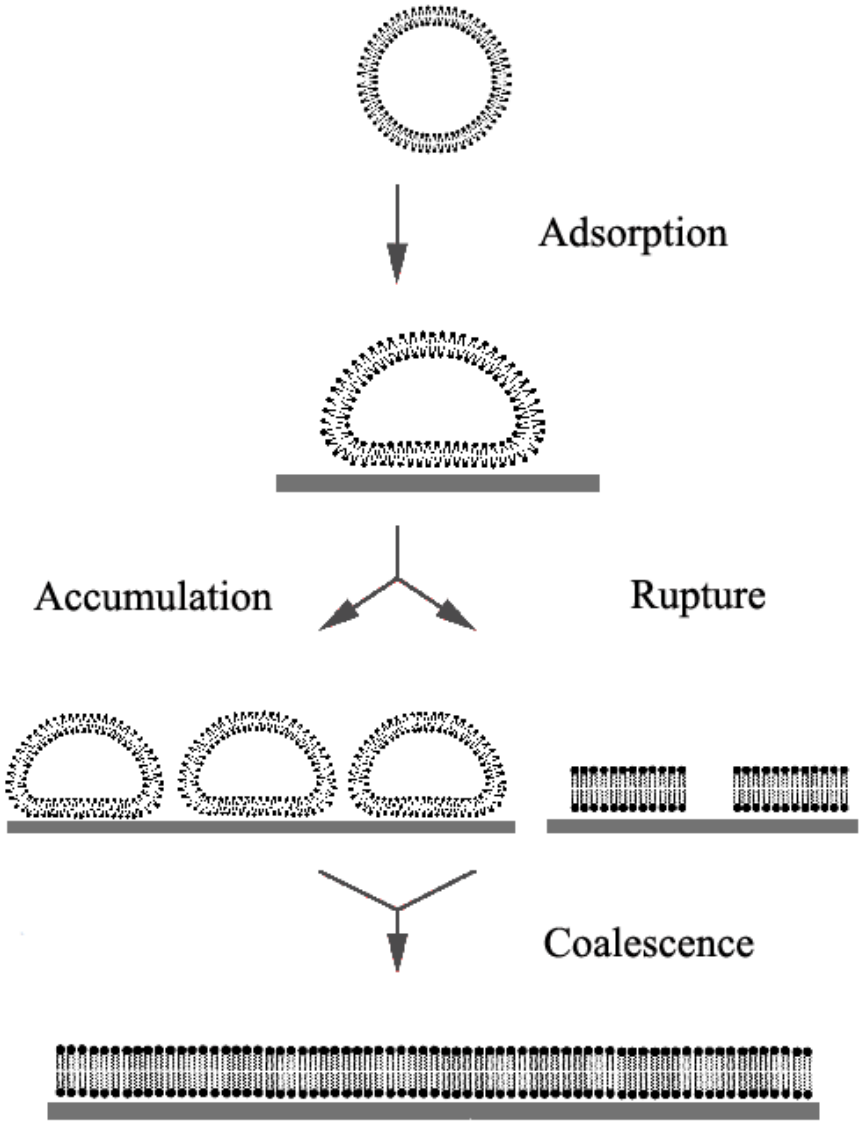

Figure 2.3 A schematic representation of the process of vesicle fusion to form a supported bilayer on a hydrophilic surface. First the vesicles adsorb to the glass, accumulate and rupture, then coalesce into a uniform bilayer.[5]

conditions. Moreover, a vast array of approaches have been developed that take advantage of the unique properties of light to probe various aspects of the samples. In addition to the spectroscopic capabilities available with light microscopy, polarization and time-resolved methods can provide additional information about sample properties. These attributes have made optical microscopy an invaluable tool in the biological sciences.

The propensity of fluorescent lipid analogs to preferentially partition into specific lipid phases makes fluorescence microscopy a convenient technique to analyze phases and domains in model membrane systems. Our lab and others have used confocal microscopy to examine the phase structure present in model membranes. For example, Fig. 2.4 shows a typical 35μm x 35μm confocal fluorescence image of a complete monolayer of DPPC deposited onto mica at 9 mN/m in the LE/LC coexistence region (see Fig. 2.2). While the bright regions denote the less ordered liquid expanded (LE) region in which the dye is incorporated, the semi-circular dark regions are the more ordered liquid condensed (LC) regions that exclude the dye.[6] This provides a convenient way to examine the phase coexistence and domains present in model membranes.

While fluorescence microscopy is a powerful technique to study domains formed in lipid films, one major drawback involves spatial resolution. The resolution of conventional fluorescence microscopy is limited by the diffraction of light, and for coherent radiation can be quantified by equation **(2.1)** as shown later. For high numerical aperture objectives, the resolution is often approximated by ~ λ/2. When working in the visible region of the spectrum, the maximal resolution is ~ 250nm - 300nm. While many model membranes exhibit large domains that are easy to resolve with this method (as

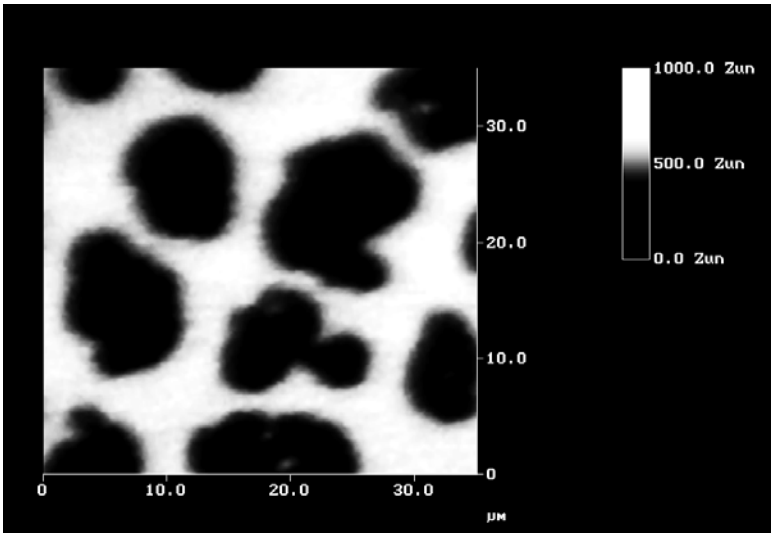

Figure 2.4 A 35µm x 35µm confocal image showing dark and bright domains. The bright regions are the less ordered liquid expanded (LE) regions in which the dye is entropically favored to partition into. The large, semi-circular dark regions are the more ordered liquid condensed (LC) regions in which the dye is excluded.[6]

shown in Fig. 2.4), biologically relevant domains such as lipid rafts are thought to exist on the mesoscale which is beyond the reach of conventional light microscopy. This highlights the need for better resolution which has led to the widespread use of atomic force microscopy to study model membranes.

2.4 Atomic Force Microscopy (AFM) used to Study Model Membranes

Atomic Force microscopy (AFM) is a commonly used surface method that can reveal structural information at the Ångstrom level. In 1986, Gerd Binnig, Calvin Quate, and Christoph Gerber developed the first AFM, which created a new way to measure, manipulate, and image matter on the nanometric scale. This section will focus on a brief overview of AFM and how it can be used to analyze model membranes.

As shown schematically in Fig. 2.5, AFM utilizes a sharp stylus (tip) fabricated at the end of a cantilever to detect small topography features on a sample surface. In contact force AFM, the tip is brought near the surface and repulsive interactions between the tip and the sample cause the deflection of the cantilever. By reflecting a laser off the back of the cantilever onto a quadrant detector, as shown in Fig. 2.5, these small deflections can be detected and used to reveal small topographical changes in the sample surface.

For the tip to track the sample surface, a feedback mechanism needs to be employed. The sample is mounted on a piezoelectric tube that can move the sample in the z-direction to maintain a constant force between the tip and the sample as the tip scans over the surface. This constant force method enables the topography of the sample to be tracked while keeping the tip a constant distance from the sample. The

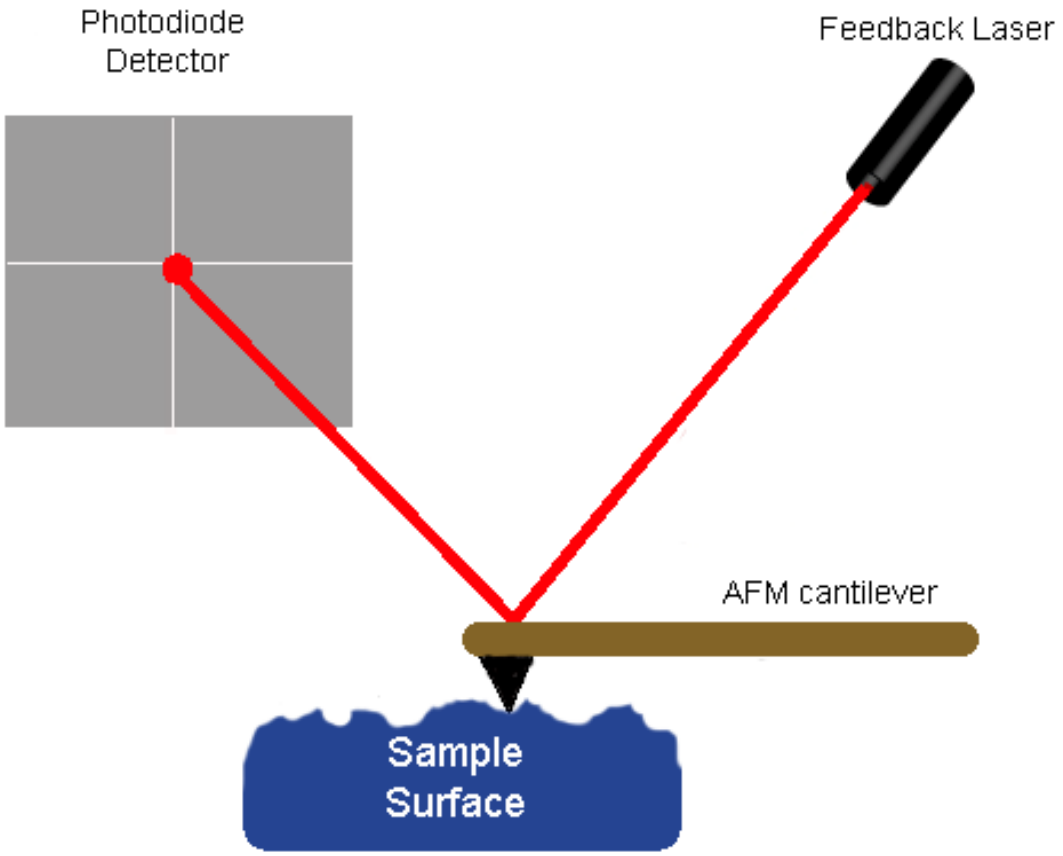

Figure 2.5 Schematic of a typical atomic force microscope. A laser is reflected off the back of the cantilever. In contact mode, as the tip is tracked along the surface, the reflection of the laser spot on a quadrant detector is changed, resulting in a topographical image of the surface.

piezoelectric tube also scans the sample under the tip in the x- and y-directions. Piezoelectric materials, such as many ceramics, expand or contracts proportional to an applied voltage which enables precise control over small distance changes. The piezoelectric tube is fabricated incorporating three different sections responsible for the x, y, and z movements. This forms a scanner that can precisely control the movement of a sample in all three-dimensions with Ångstrom level resolution.

2.4.1 Studies of Model Membranes

Fig. 2.6 shows a representative AFM image of a DPPC monolayer deposited on a mica substrate in the LE/LC coexistence region of the pressure/area isotherm (see Fig. 2.2). The 10μm x 10μm AFM image shows large semi-circular regions of higher topography, which reflect the LC domains present in the film as seen as dark domain in the fluorescence image shown in Fig. 2.4. The LC domains are surrounded by regions of lower topography which reflect the LE phase as was also seen in Fig. 2.4 as bright regions.[6] In the AFM measurements, contrast between the LE and LC regions arises from the small height difference between these two phases which is only ~6-8 Å. Also visible in Fig. 2.6 are small coexisting domains in the LE region.[6] These small domains, not resolved in the fluorescence image (Fig. 2.4), suggest that the LE domains are not homogenous and illustrate the need for high resolution techniques in studying domain formation in model membranes.

While the use of monolayers is valuable in characterizing the structure and function of biological membranes, bilayers often provide a more faithful representation of biological membranes. However, even though the system gets only slightly more

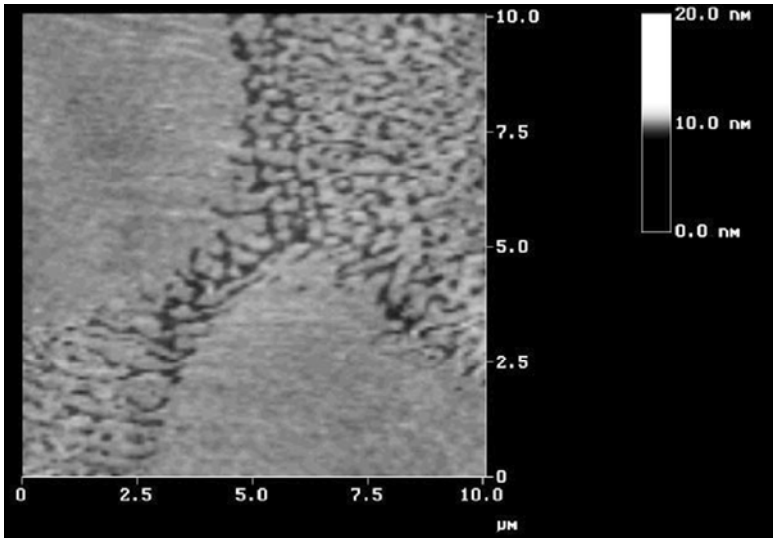

Figure 2.6 A 10µm x 10µm AFM scan of a DPPC monolayer deposited in the LE/LC coexistence region. The small ~6-8 Å height differences can be seen illustrating the two phases present.[6]

complicated in going from monolayers to bilayers, the analysis becomes much more difficult with AFM. For example, Fig. 2.7 shows a 10μm x 10μm AFM image of a DPPC bilayer which was deposited on mica using the LB / LS (Langmuir-Schaffer) technique.[6] Each layer of the bilayer was deposited in the LE/LC phase coexistence region (at 9 mN/m). For monolayers, shown in Fig. 2.6, the small ~ 6 to 8 Å height differences between the two lipid phases enable their characterization with AFM. However, the AFM image of the bilayer shown in Fig. 2.7 reveals three distinct height levels which represent the convolution of height information from each monolayer of the bilayer. The lowest topography regions correspond to LE on LE while the tallest features correspond to LC on LC, with the intermediate height level corresponding to LE on LC or LC on LE. While it is clear that both monolayers of the bilayer have distinct phase partitioning, assigning a particular phase structure within either leaflet is not possible because of the convolution of height information from each side.[6]

The difficulty therefore becomes identification of the phase structure present in each leaflet in the bilayer using AFM. Asymmetry, as discussed previously, is an important property of biological membranes and it is important to be able to probe this property with high spatial resolution. Confocal fluorescence microscopy can delineate the larger domains present when the dye is incorporated into one monolayer of the bilayer, but still lacks the resolution to see the sub-micron domains as detected by AFM. These limitations motivated the development of a method that combines fluorescence and topography information with high spatial resolution. Near field scanning optical microscopy (NSOM), combines sub-diffraction limited optical resolution with high

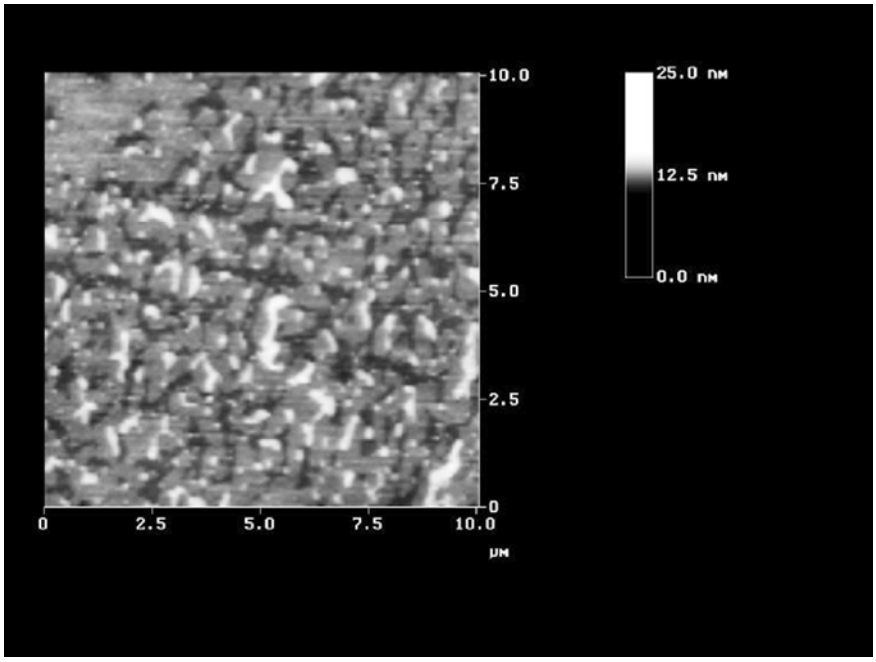

Figure 2.7 A 10μm x 10μm AFM scan of a DPPC bilayer deposited by the LB/LS method in the LE/LC coexistence region.[6]

resolution topographical information needed to differentiate the small domains present, as illustrated below.

2.5 Near Field Scanning Optical Microscopy (NSOM)

Near field scanning optical microscopy (NSOM) was designed to combine the favorable aspects of several different techniques. By utilizing NSOM, we can combine the specificity, high time resolution, and spectral properties of optical microscopy with the high spatial resolution that AFM provides. This section will focus on a brief overview of NSOM and how it can be used to study model membrane systems, with an emphasis on research performed in our group.

When a lens is used to focus light, spatial resolution is limited by the diffraction of light from the aperture. Light passing through this circular lens interferes around the focal point and thus generates a diffraction pattern. This forms a well known Airy disk pattern that was described in the early 1870's by Ernst Abbe. He defined the size of the Airy disk pattern as the distance from the highest intensity point within the center of the disk to the first node of the pattern that was created. The size of the central spot of the Airy disk pattern is defined as:

$$\textbf{spot size} = 0.61\,\lambda_{vac} / n \sin\theta \qquad (2.1)$$

where, λ_{vac} = the vacuum wavelength, n = refractive index of the medium, and θ = the half angle through which the light is focused by the objective. The **n sinθ** term in equation **(2.1)** determines the spot size and is known as the numerical aperture (NA) of

the objective. In order to resolve two features, the features must be separated by a distance greater than or equal to that given in equation **(2.1)**. This is referred to as the Rayleigh criterion and is the generally accepted criterion for the minimum resolvable detail. This diffraction limit dictates the maximum resolution possible in conventional microscopy and is often approximated by ~ λ/2. When working in the visible region of the spectrum, therefore, spatial resolution is limited to several hundred nanometers, or ~ 250 – 300 nm.

Due to these limitations, in 1928, E.H. Synge proposed the idea of using a small aperture to image a surface with sub-wavelength resolution.[7] His original idea was based on illuminating the backside of a thin opaque metal film containing a small pinhole as shown in Fig. 2.8. The aperture, which is smaller than the wavelength of light, is placed within one wavelength of the sample such that light exiting the aperture interacts with the sample before diffracting out. This results in wavelength independent spatial resolution on the order of the size of the aperture.

Although conceptually straightforward, it was not until 1972 that Ash and Nichols implemented Synge's idea using microwave radiation with a wavelength of 3 centimeters.[8] This long wavelength simplified aperture fabrication and placement and they were able to demonstrate resolution of ~ λ/60. Not until about 12 years later did Pohl *et. al.* publish a paper that used a submicron, metal coated optical aperture to make similar high resolution measurements using visible light.[9] A feedback mechanism was implemented to maintain a constant probe distance of a few nanometers of the sample surface. They were able to obtain sub-diffraction limited resolution using a visible wavelength of 488nm.

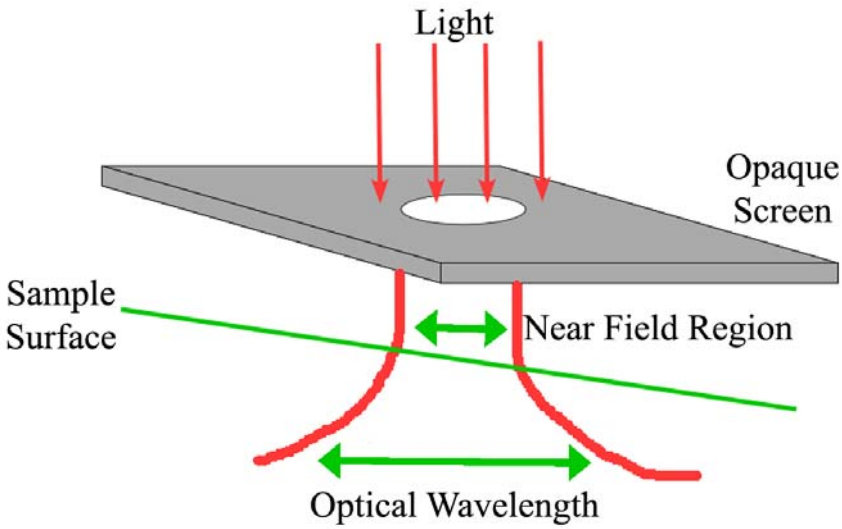

Figure 2.8 Schematic representation of E.H. Synge's original experiment. Light is passed through a sub-wavelength diameter aperture (~100nm) of an opaque screen producing a near field region and held in close proximity to the sample surface.[7]

.

This has lead to the development of NSOM which combines the favorable attributes inherent to optical microscopy with the high spatial resolution of the other techniques. There are several ways that NSOM can be implemented, but for the purpose of this dissertation we will restrict our discussion to fluorescence measurements using aperture NSOM. In aperture NSOM, light is delivered to the nanometer dimension using specially fabricated tapered single-mode optical fibers coated with a reflective coating around the tapered region. Figure 2.9a and 2.9b shows magnified views of a typical NSOM probe. In the electron microscopy image shown in Fig. 2.9a, the aperture at the distal end can be seen along with the metal coating around the sides of the taper that is used to confine the light. Light emerging from the end of the NSOM probe can be seen in the magnified optical image shown in Fig. 2.9b.[10] The aperture size and transmission characteristics are strongly tied to the exact geometry of the NSOM probe, but typically probe apertures have sub-100 nm diameters and can deliver hundreds of nanowatts of light.

To achieve high spatial resolution, the NSOM probe must be positioned and held within nanometers of the sample surface as the probe is scanned across the surface. Numerous feedback systems have been introduced to achieve this, with most based on force interactions between the probe and the surface. The schematic shown in Fig. 2.9 (bottom panel), for example, outlines one approach implementing feedback based on shear-force. Because of this force feedback, a topography image of the surface is also generated along with the NSOM fluorescence information, which can be particularly informative for biological applications.

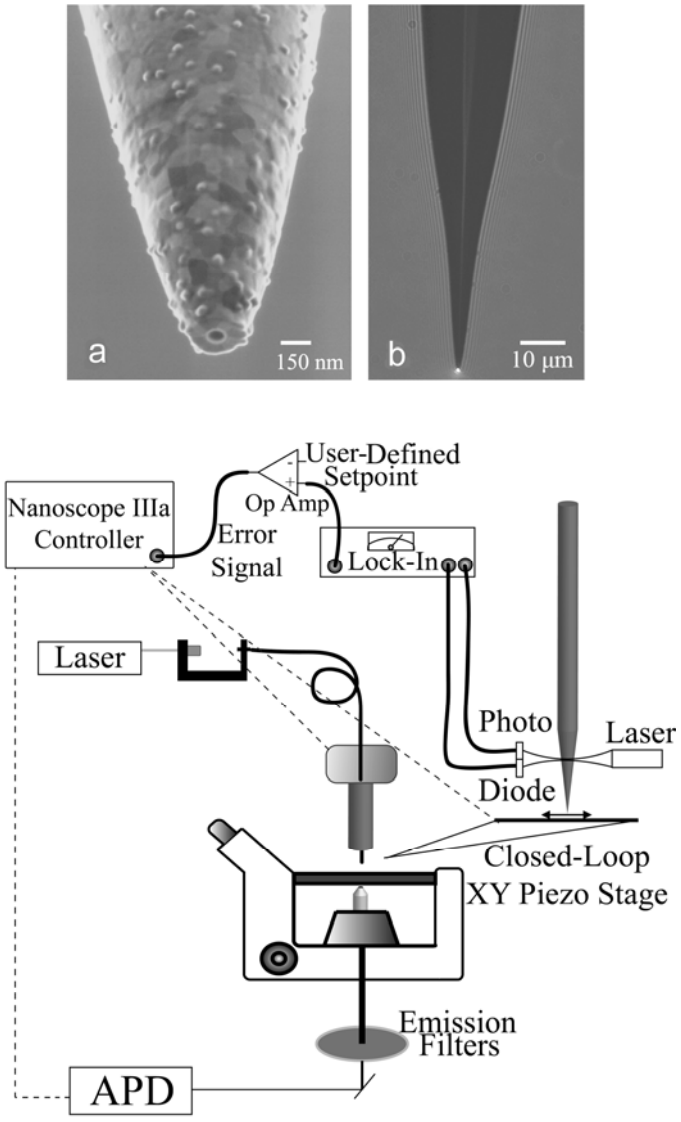

Figure 2.9 **(a)** An SEM image of an aluminum coated NSOM probe with the aperture clearly visible. **(b)** A magnified view of a typical aluminum coated NSOM probe with a well-defined spot of light emerging from the aperture at the end. A schematic of a typical NSOM microscope is shown at bottom. Laser light is directed into an optical fiber, the end of which is fashioned into a NSOM tip as shown above **(a and b)**. The sample is scanned below the NSOM tip and fluorescence is collected from below with a high numerical aperture objective. The fluorescence is filtered and detected with an avalanche photodiode detector (APD). To maintain the tip-sample gap, a shear-force feedback mechanism is implemented. In the shear-force feedback method, the NSOM probe is dithered laterally with respect to the sample surface and the amplitude of the motion is detected by shining a laser across the tip and onto a split photodiode. The dither amplitude is detected by a lock-in amplifier, the output of which creates an error signal that is used to maintain a constant gap between the tip and sample.[10]

The high-resolution optical and topography information available from NSOM measurements has proven particularly useful in probing the microscopic structure of membranes.[11-17] For example, the addition of fluorescent lipid markers to model membranes can reveal information about the phase partitioning of the lipids which can be compared to the simultaneously collected NSOM topography.[18-19] Much of this work has been motivated by the implication of small lipid domains, such as the lipid rafts discussed in chapter 1, in a number of functional pathways. Because of their small size, however, most evidence for lipid rafts remains indirect and it was hoped that the high-resolution afforded by NSOM could directly probe these elusive structures.

2.5.1 Monolayer Systems

NSOM measurements on LB monolayers have been used to probe the phase partitioning in lipid films,[16, 18-19] measure models of lipid rafts,[11-13, 17, 20] understand the distribution of membrane proteins,[21-23] and map the physical characteristics of model lung surfactants.[24] Initial NSOM studies compared high-resolution fluorescence images with the simultaneously collected topographical information to understand the phase partitioning in lipid monolayers.[6] For example, Figs. 2.10a and 2.10b show 15 μm x 15 μm NSOM fluorescence and topography images, respectively, of a LB monolayer of DPPC transferred onto cleaved mica in the phase coexistence region (~9 mN/m) of the pressure-area isotherm (as shown in Fig. 2.2 above). At this surface pressure, less ordered LE phase coexists with the more ordered LC lipid phase as discussed before. In these studies, ~0.25 mol% of the fluorescent lipid analog, 1,1'-dioctadecyl-3,3,3',3'-tetramethylindocarbocyanine perchlorate ($DiIC_{18}$), was doped into the monolayer, which

gives rise to the contrast seen in the NSOM fluorescence image. As mentioned before, this fluorescent lipid analog preferentially partitions into the LE phase and is excluded from the LC regions, thus allowing each phase to be quantified from images such as that shown in Fig. 2.2.

The LE and LC domains are also distinguishable in the NSOM topography image shown in Fig. 2.10b through the small ~ 6 to 8 Å height differences between the two phases. A direct correlation is observed between bright domains in Fig. 2.10a with regions of lower topography in Fig. 2.10b, confirming that these areas represent regions of LE phase lipid.[6] These measurements help illustrate the utility of NSOM in measuring both fluorescence and topography simultaneously and how the high-resolution can detect small domains such as that expected for lipid rafts.

The effects of proteins or peptides added to model lipid monolayers have also been studied with NSOM. Often these studies rely on the high-resolution fluorescence capabilities of NSOM to reveal structures previously unseen in far-field measurements. However, the unique collection of a simultaneous force mapping of the surface topography can be particularly informative, especially when complementing the fluorescence information. For example, both NSOM fluorescence and topography measurements were recently used to probe the mechanism of monolayer collapse in models of the lung surfactant (LS) [24].

2.5.2 Bilayer Systems

In moving from model monolayers to bilayers, the level of complexity vastly increases and the development of new high-resolution methods becomes especially

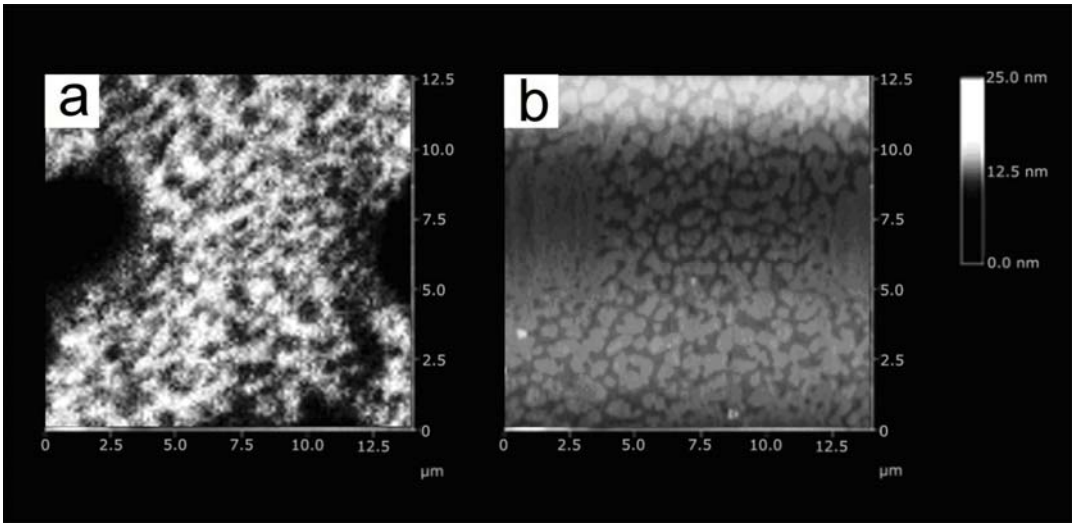

Figure 2.10 A 15µm x 15µm high resolution NSOM scan of a DPPC monolayer deposited at 9 mN/m onto freshly cleaved mica. **(a)** Fluorescence image showing sub-diffraction limited domains. The bright domains show the LE phases where the dye partitions and the dark domains show the LC phase where the dye is excluded. **(b)** NSOM topography image collected simultaneously with the fluorescence image shown in **(a)**. The same LE/LC coexistence regions are found as with AFM, but now a pixel-by-pixel mapping of the fluorescence and topography can be compared.[6]

important. The asymmetry that biological membranes are known to contain across their bilayer membranes has been studied by many different techniques. Loss of this asymmetry can be a sign that the cell is undergoing apoptosis and is therefore an important indicator. However, the thickness of the bilayer, typically ~50Å, makes studying these systems difficult. As shown with AFM before (Fig. 2.7), bilayer systems can be problematic because of the convolution of height information from domains present in each leaflet. Figures 2.11a and 2.11b displays NSOM topography and fluorescence images, respectively, of a DPPC bilayer similar to that shown in Fig. 2.7 above.[6] As in the AFM measurement, the NSOM topography image in Fig. 2.11a measures the convolution of height information from both sides of the bilayer making specific domain assignments complicated. However, by selectively adding a fluorescent lipid analog to one leaflet of the bilayer, the NSOM fluorescence image shown in Fig. 2.11b is able to selectively map the submicron phase partitioning present in this leaflet. These capabilities suggest that NSOM will be an asset in characterizing the structural characteristics of model lipid bilayers and become a useful tool in determining submicron heterogeneities in biological membranes.

Recent progress using aperture NSOM to probe model and biological systems has expanded our understanding of nanometric structures previously hidden from traditional far-field techniques. The examples discussed here help to highlight the utility of collecting both high-resolution fluorescence and topography information with NSOM. The continued evolution in probe design, feedback, and contrast mechanisms, however, is necessary to expand the biological applications of NSOM and reduce some of the barriers that currently limit its use.

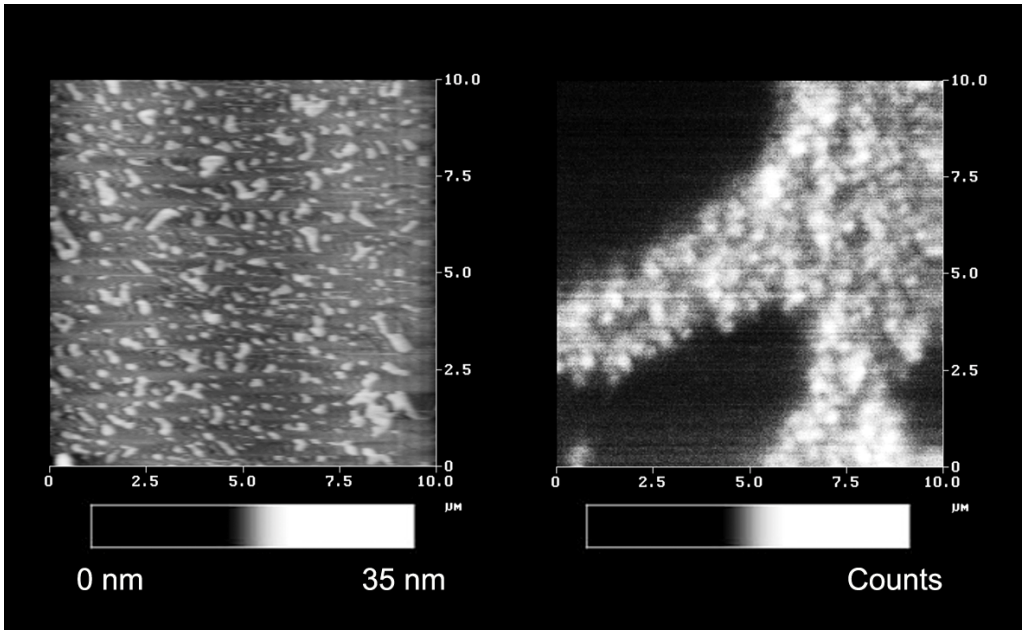

Figure 2.11 A 10μm x 10μm NSOM image of a DPPC bilayer fabricated by the LB/LS method. Three distinct height levels are observed which are due to overlapping LE and LC regions from the two leaflets. NSOM **(Left)** topography and **(Right)** fluorescence images of a DPPC bilayer similar to that shown in Fig. 2.XXX(AFM above). The NSOM fluorescence image shown at **(Right)** reveals the phase structure present in one leaflet of the bilayer.[6]

The examples of fluorescence microscopy, AFM, and NSOM discussed thus far in this chapter illustrate how these methods can be used to probe structural information in model membranes. Fluorescence microscopy, with the addition of a membrane dye, can detect large domains present in model membranes. AFM can further resolve submicron sized domains present that were not previously seen in the fluorescence measurements. NSOM simultaneously collects both the high resolution topography information and fluorescence measurements with high spatial resolution. But even with NSOM, we are limited to about 50 nm resolution. In order to extract more information about the heterogeneity of membrane structures, we want to explore down to the molecular level. By utilizing single molecule measurements as described below, we can achieve structural information at the molecular level.

2.6 Single Molecule Orientations

Single molecule studies in the gas phase at ultralow temperatures have been around for decades, but it wasn't until 1989 that W.E. Moerner and Lothar Kador were able to study single molecules in the condensed phase.[25] With the advent of very sensitive commercial optical detectors, it is now a relatively simple task to image the fluorescence from single molecules. This section will briefly discuss single molecule techniques with an emphasis on defocused imaging to obtain single molecule orientations in model membranes. This technique will be used to obtain information about the structure of model membranes at the molecular level.

Single molecule experiments concentrate on investigating the properties of individual molecules in their environment and distinguishing these properties from the

bulk average. A variety of experiments can be done to study the property, structure, and position of these single molecules. More recently, single molecule fluorescence has been used for analysis of biological samples. Proteins such as myosin/actin enzymes found in muscle tissues have been a widely studied system. In a recent study, Cappello et al tagged individual myosin V motors with quantum dots and introduced them into the cytoplasm of living HeLa cells and recorded their motion at the single molecule level. Myosin V is an actin-associated protein that is involved with transport inside the cell. This motor uses ATP to produce energy that is then used to carry cargo through the cytoplasm. They found discrepancies between the in vitro and in vivo studies performed. In vitro studies have previously shown a mean velocity of 200-450 nm/s while the in vivo studies suggest they move much faster in organelles at a rate of 1 μm/s or faster.[26] It was not until the advent of single molecule studies that the true consecutive step motion of these molecules was realized.

The ability to study the properties of each single molecule and to investigate structural heterogeneity is the true strengths of this method. When the bulk or ensemble average is analyzed, the true heterogeneity of the system is often missed. It is for this reason that we chose to study single molecule orientations in model membranes for this dissertation. By studying membrane properties at the single molecule level, the structural heterogeneity present can be entirely quantified. A representative single molecule fluorescence image is shown in Fig. 2.12 in which ~ 10^{-8} mol % of a membrane dye was added into a monolayer of DPPC. With a high signal-to-noise ratio, the fluorescence from each individual fluorophore molecule doped into the membrane can be seen in the image.

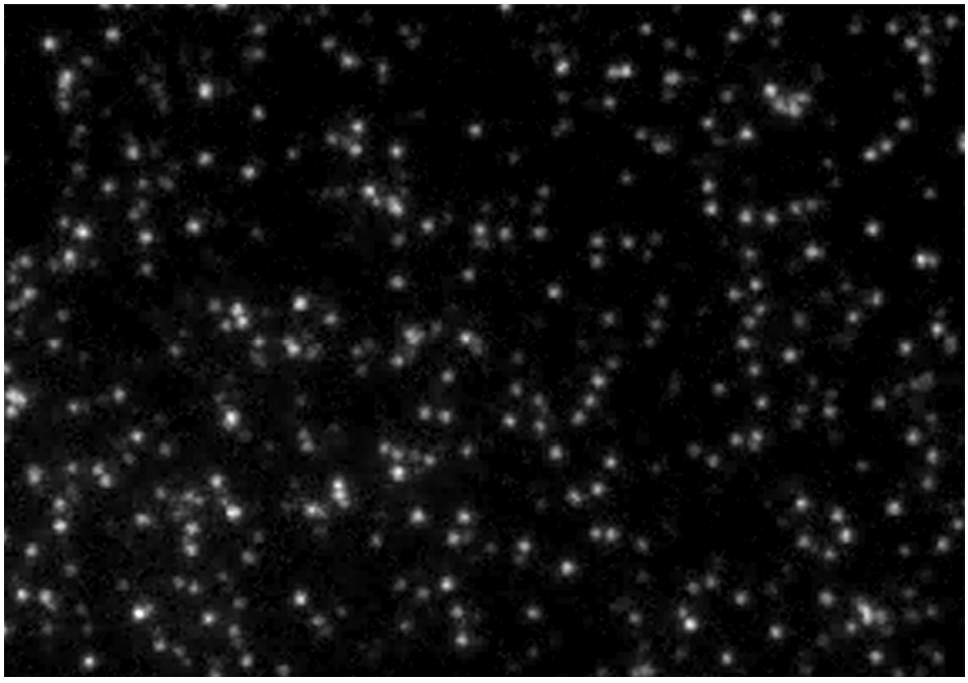

Figure 2.12 A representative in focus single molecule fluorescence image is shown illustrating the fluorescence from each individual molecule with a high signal-to-noise ratio.

Several groups have previously shown that by using polarized total internal reflection fluorescence microscopy (PTIRF-M), single molecule orientations can be measured.[27-31] To understand how this technique works, let's first consider how single fluorophores emit light. Fluorophores emit light in a sine-squared spatial pattern relative to the transition dipole orientation. When a molecule is brought close to an interface with differing refractive index, the emission pattern is distorted.[32] As shown in Fig. 2.13, molecules oriented with their transition dipoles aligned parallel to the membrane plane couple fluorescence predominately along the optical axis. Molecules with their transition dipoles oriented perpendicular to the membrane plane couple fluorescence through the interface at high angles, as shown in Fig. 2.13.

In order to excite randomly oriented fluorophores, we employ polarized total internal reflection fluorescence microscopy (PTIRF-M). The probe molecules are excited by a laser excitation source that is undergoing total internal reflection (TIR) at the glass / air interface. This creates a non-propagating, exponentially decaying, evanescent field into the sample surface, as shown schematically in Fig. 2.14.[32] TIR is achieved by increasing the angle at which the incident ray is brought to the interface of two materials with differing refractive indexes. When the incident beam is brought to the interface from a higher refractive index medium to a lower refractive index medium, the light is refracted away from the normal and totally internally reflected at the critical angle as defined by Snell's law, or $\theta_{crit} = \arcsin(n2/n1)$, where $n1>n2$. This creates evanescent field polarizations in the x, y, and z directions depending on the polarization of the incident beam. P-polarization "cart-wheels" through the sample and allows for interactions with molecules that are oriented in all directions in the film, as shown by the

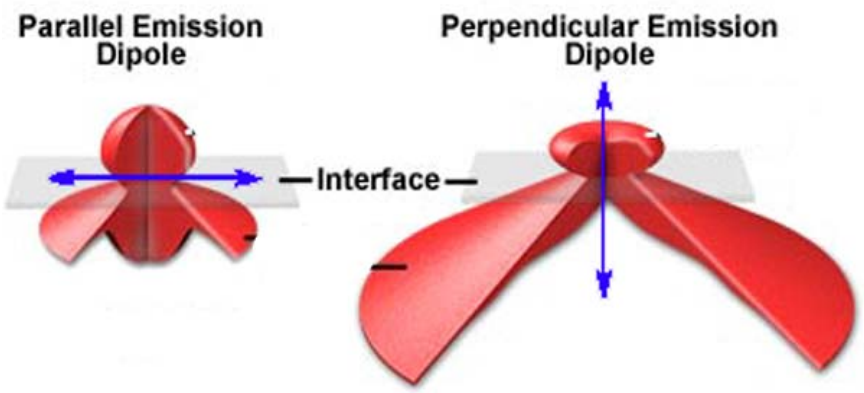

Figure 2.13 Schematic representation of two transition dipole orientations. With the parallel emission dipole as shown on the **left**, most of the fluorescence is reflected straight back into the interface or directly back into the objective. With the perpendicular emission dipole as shown on the **right**, most of the fluorescence is collected at high angles.[32]

red wave in Fig. 2.14, and s-polarized light is in the plane of the glass slide as shown by the blue wave in Fig. 2.14.

The fluorescence from single molecules can then be collected back through the high NA objective in epi-fluorescence geometry. Dichroic and emission filters are used to filter any stray excitation light. In order to probe the distorted emission patterns from single reporter molecules, spherical aberrations were induced. By defocusing the optics by ~500nm, spherical aberrations are created in the optical train, in which the light collected at high angles is out of focus with the light collected directly into the objective. The resulting image contains emission patterns representative of the transition dipole orientation of the single molecules. Fig. 2.15 shows a representative defocused single molecule fluorescence image in which a small amount of a dye (~ 10^{-8} mol %) was doped into the lipid monolayer. Each individual emission pattern collected contains angle dependent information.

Emission patterns of each single reporter molecule can be analyzed and the mathematical representation of these patterns mapped using a MatLab code created by Dr. Jörg Enderlein. The convention shown in Fig. 2.16 will be used where Φ is the polar angle, or tilt away from the membrane normal and θ is the azimuthal angle.

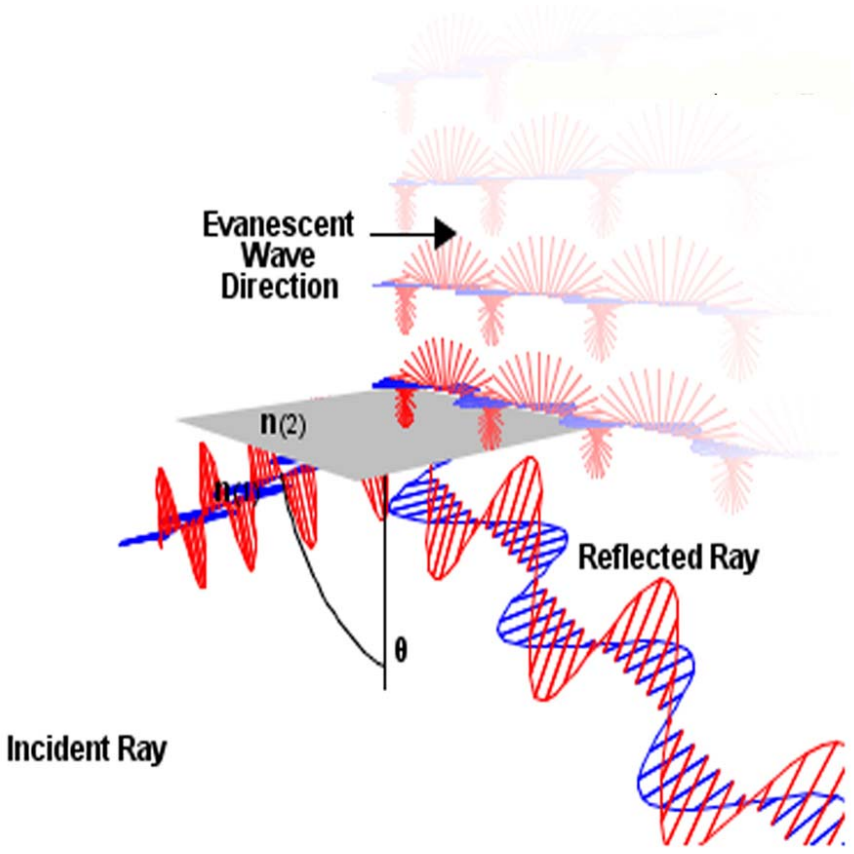

Figure 2.14 Schematic representation of polarized total internal reflection (PTIR). As an incident ray is brought to the interface of two refractive indexes (n1 > n2) the light is refracted away from the normal. At the critical angle, as defined by Snell's law ($\theta_{crit} = \sin^{-1}$ (n2/n1)), the light is totally internally reflected and a non-propagating, exponentially decaying evanescent field is created. P-polarization is represented by the red waves that "cart-wheel" through the sample and s-polarization is represented by the blue wave that "snakes" through the interface. By selecting for p-polarized light, molecules oriented in all directions can be excited.[32]

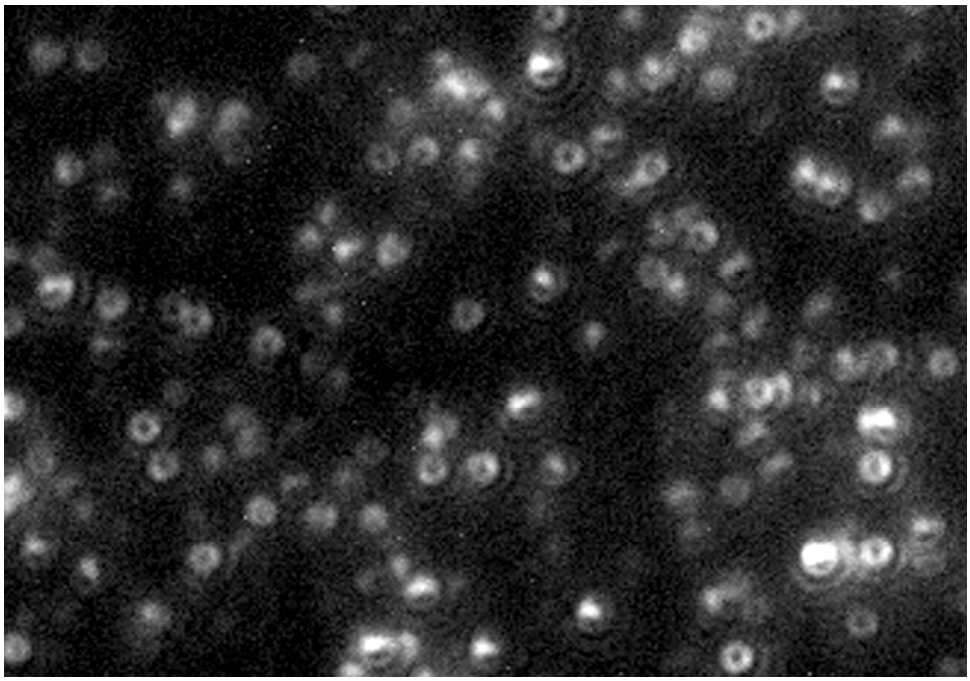

Figure 2.15 By utilizing PTIRF-M, and defocusing ~ 500nm, this representative out of focus single molecule fluorescence image can be obtained. This image contains orientation specific information about each individual probe molecule in the film.

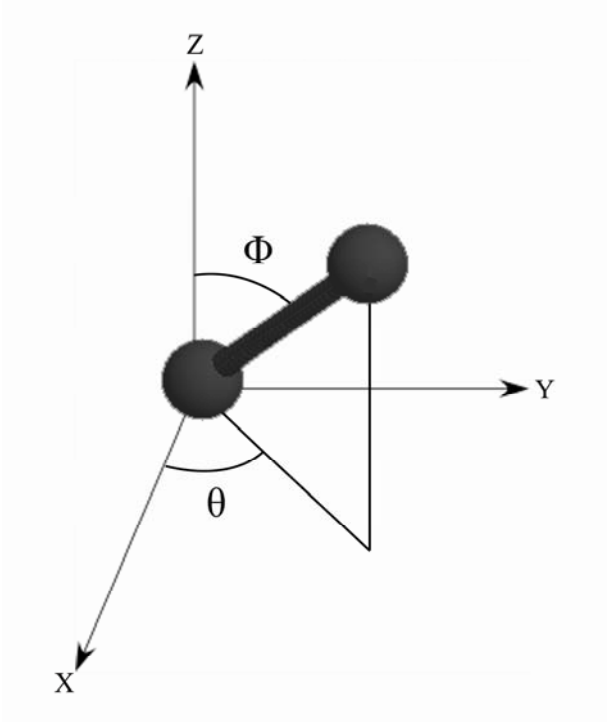

Figure 2.16 Schematic of an emission dipole oriented in space showing the convention used here for the polar (Φ) and azimuthal (θ) angles.

Most of the emitted fluorescence is collected back into the glass at orientation specific angles by using TIRF-M as the imaging technique.[33] As discussed before and shown in the top panel of Fig. 17, molecules oriented perpendicular to the membrane (0˚ from the membrane normal) produce patterns that look like "donuts", or symmetric fluorescent rings, and molecules that are oriented parallel to the membrane (90˚ from the membrane normal) produce "wing-like" features, as shown in the bottom panel of Fig. 2.17. The observed shapes collected are due to the orientation specific coupling of fluorescence into the glass slide. Very small amounts (~ 10^{-8} mol%) of the reporter molecule is required for single molecule imaging and therefore should have extremely low perturbation effects on the membrane. Other scanning techniques such as AFM and NSOM lack the temporal resolution of this technique. Therefore, this method can be used as a complimentary technique to analyze the structure of model membranes.

Using this technique, we may probe single molecule orientations in model membranes. Fig. 2.18 shows a schematic representation of how each reporter molecule is oriented in a monolayer of DPPC (shown in left panel) using modeled bar-bell type molecules (shown in right panel). Both the polar and azimuthal angles can be assigned, but for the purposes of this dissertation, only the polar angles will be assigned, as the distribution of azimuthal angles are isotropic.

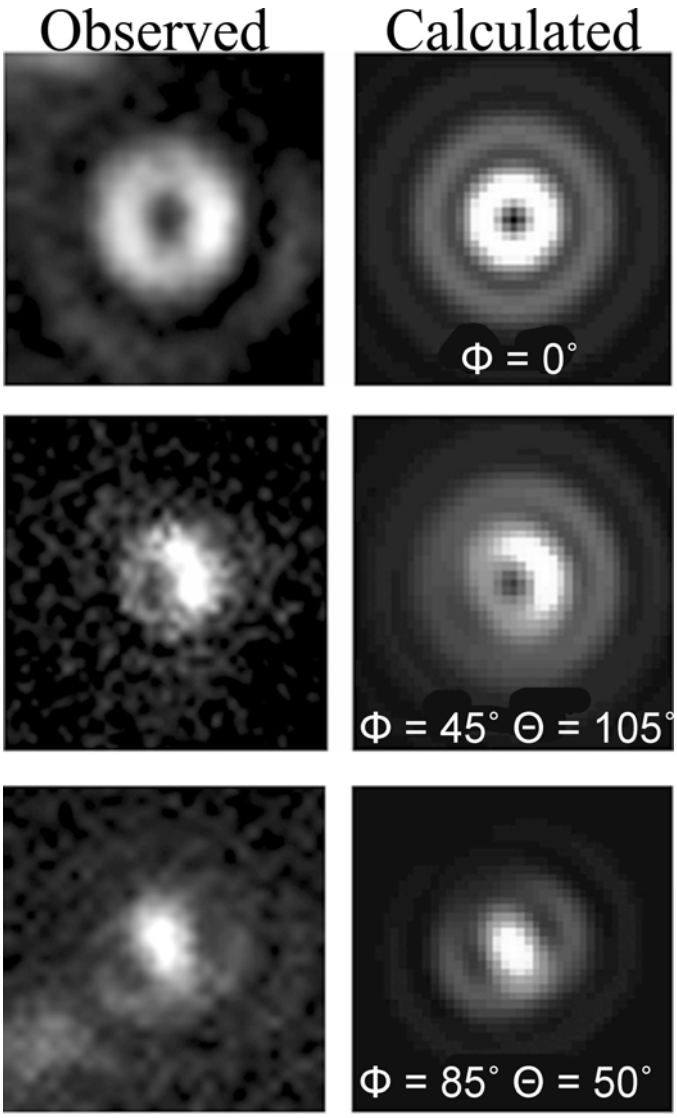

Figure 2.17 Three representative orientations obtained are shown. The observed single molecule orientation images are shown at **left**, while the calculated images are shown at **right**. The **top** image is representative of a transition dipole oriented ~ parallel to the membrane normal, the **middle** image is representative of a transition dipole oriented at a ~ 45˚ tilt from the membrane normal, and the **bottom** image is representative of a transition dipole oriented ~ perpendicular to the membrane normal.

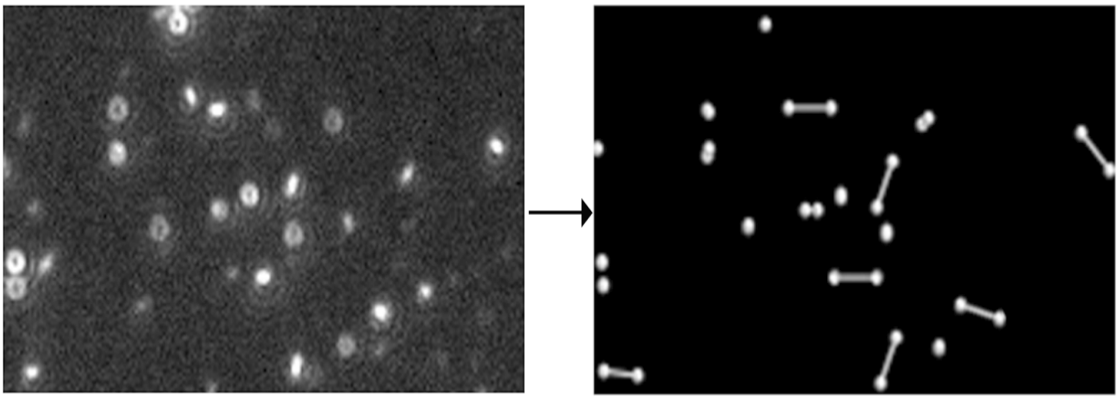

Figure 2.18 Each single molecule emission pattern (shown at **left**) can be schematically represented and modeled to represent its 3-D orientation (shown on **right**).

2.7 Conclusion

The combination of the high resolution techniques described above offers a particularly informative view of membranes. Model membranes can be fabricated in a controllable fashion and used as biological mimics to study their structure and function. Fluorescence microscopy is commonly used to study domains formation in model membranes, due to the propensity of fluorescent lipid analogs to partition into one phase. While this technique is useful in studying the microscopic domains present, the nanoscopic domains present has created the need for higher resolution techniques. AFM is a high resolution technique that can be used to study structural features of model membranes. This technique has Ängstrom level resolution, but lacks the specificity of optical microscopy. To combine the optical benefits of fluorescence microscopy, and the nanometric topographical resolution of AFM, NSOM is used. NSOM can obtain simultaneous topographical and fluorescence information with high spatial resolution. However, as stated before, even with NSOM, we are limited to ~ 50nm at best.

In order to study the structure and function of model membranes and to probe the structural heterogeneity, we use a single molecule technique that allows for large, simultaneous areas of individual molecules to be collected and analyzed. The majority of this dissertation will discuss single molecule orientations in model membranes. The following chapter will show that these measurements can be made in a predictable and accurate fashion by studying how the molecular order is affected by an increase in surface pressure. We will also discuss the comparisons between monolayer and bilayer systems using single molecule orientation measurements and also study the effects of sterols on model membranes.

2.8 References

1. Rayleigh, F. R. S., *Proc. R. Soc.* **1890,** *47*, 364.

2. Pockels, A., On the dispersion of pure and mixed liquids on water. *Phys Z* **1916,** *17*, 142-145.

3. Langmuir, I., The constitution and fundamental properties of solids and liquids. II. Liquids. *J. Am. Chem. Soc.* **1917,** *39*, 1848-1906.

4. Blodgett, K. B., Films built by depositing successive monomolecular layers on a solid surface. *J. Am. Chem. Soc.* **1935,** *57* (1), 1007-1022.

5. Reviakine, I.; Brisson, A., Formation of supported phospholipid bilayers from unilamellar vesicles investigated by atomic force microscopy. *Langmuir* **2000,** *16* (4), 1806-1815.

6. Hollars, C. W.; Dunn, R. C., Submicron structure in L-alpha-dipalmitoylphosphatidylcholine monolayers and bilayers probed with confocal, atomic force, and near-field microscopy. *Biophys. J.* **1998,** *75* (1), 342-353.

7. Synge, E. H., A suggested method for extending microscopic resolution into the ultra-microscopic region. *Philosophical Magazine* **1928,** *6* (35), 356-362.

8. Ash, E. A.; Nicholls, G., Super-Resolution Aperture Scanning Microscope. *Nature* **1972,** *237* (5357), 510.

9. Pohl, D. W.; Denk, W.; Lanz, M., *Appl. Phys. Lett.* **1984,** *44*, 651-653.

10. Dickenson, N. E.; Armendariz, K. P.; Huckabay, H. A.; Livanec, P. W.; Dunn, R. C., Near-field scanning optical microscopy: a tool for nanometric exploration of biological membranes *Anal Bioanal Chem* **2009,** *In press*.

11. Burgos, P., Yuan, C., Viriot, M., Johnston, L. J., Two-Color Near-Field Fluorescence Microscopy Studies of Microdomains ("Rafts") in Model Membranes. *Langmuir* **2003,** *19* (19), 8002-8009.

12. Coban, O., Popov, J., Burger, M., Vobornik, D., Johnston, L. J., Transition from Nanodomains to Microdomains Induced by Exposure of Lipid Monolayers to Air. *Biophys. J.* **2007,** *92* (8), 2842-2853.

13. Coban, O., Burger, M., Laliberte, M., Ianoul, A., Johnston, L.J., Ganglioside Partitioning and Aggregation in Phase-Separated Monolayers Characterized by Bodipy GM1 Monomer/Dimer Emission. *Langmuir* **2007,** *23* (12), 6704-6711.

14. Hollars, C., Dunn RC, Submicron Structure in L-α-Dipalmitoylphosphatidylcholine Monolayers and Bilayers Probed with Confocal, Atomic Force, and Near-Field Microscopy. *Biophys. J.* **1998,** *75*, 342-353.

15. Ianoul, A., Strekal, N., Maskevich, S., Imaging Nanometer Scale Optical Heterogeneities in Phospholipid Monolayers Deposited on Metal Island Films. *Journal of Nanoscience and Nanotechnology* **2006,** *6*, 61-65.

16. Johnston, L. J.; Abulrob, A.; Lu, Z. F.; Pulla, D.; Stanimirovic, D., Near field microscopy studies of epidermal growth factor receptor partitioning between lipid rafts and caveolae. *Biophys. J.* **2007**, 548a-549a.

17. Tokumasu, F.; Hwang, J.; Dvorak, J. A., Heterogeneous Molecular Distribution in Supported Multicomponent Lipid Bilayers. *Langmuir* **2004,** *20* (3), 614-618.

18. Ianoul, A.; Burgos, P.; Lu, Z.; Taylor, R. S.; Johnston, L. J., Phase Separation in Supported Phospholipid Bilayers Visualized by Near-Field Scanning Optical Microscopy in Aqueous Solution. *Langmuir* **2003,** *19* (22), 9246-9254.

19. Yuan, C., Johnston, L. J., Phase evolution in cholesterol/DPPC monolayers: atomic force microscopy and near field scanning optical microscopy studies. *Journal of Microscopy* **2002,** *205* (2), 136-146.

20. Yatsui, T.; Kourogi, M.; Ohtsu, M., Increasing throughput of a near-field optical fiber probe over 1000 times by the use of a triple-tapered structure. *Appl. Phys. Lett.* **1998,** *73* (15), 2090-2092.

21. Kramer A, W. A., Sieber M, Galla HJ, Amrein M, Guckenberger R, Distribution of the Surfactant-Associated Protein C within a Lung Surfactant Model Film Investigated by Near-Field Optical Microscopy. *Biophys. J.* **2000,** *78* (1), 458-465.

22. Murray, J., Louis Cuccia, L., Ianoul, A., Cheetham, J.J., Johnston, L.J., Imaging the Selective Binding of Synapsin to Anionic Membrane Domains. *ChemBioChem* **2004,** *5*, 1489-1494.

23. Trudel, E., Gallant, J., Mons, S., Mioskowski, C., Lebeau, L., Jeuris, K., Foubert, P., De Schryver, F., Salesse, C., Design of Functionalized Lipids and Evidence for Their Binding to Photosystem II Core Complex by Oxygen Evolution Measurements, Atomic Force Microscopy, and Scanning Near Field Optical Microscopy. *Biophys. J.* **2001,** *81*, 563-571.

24. Sibug-Aga, R., Dunn, R.C., High-resolution Studies of Lung Surfactant Collapse. *Photochem. Photobiol.* **2004,** *80* (3), 471-476.

25. Moerner, W. E.; Kador, L., Optical-Detection and Spectroscopy of Single Molecules in a Solid. *Phys. Rev. Lett.* **1989,** *62* (21), 2535-2538.

26. Pierobon, P.; Achouri, S.; Courty, S.; Dunn, A. R.; Spudich, J. A.; Dahan, M.; Cappello, G., Velocity, Processivity, and Individual Steps of Single Myosin V Molecules in Live Cells. *Biophys. J.* **2009,** *96* (10), 4268-4275.

27. Bartko, A. P.; Dickson, R. M., Imaging three-dimensional single molecule orientations. *J. Phys. Chem. B* **1999,** *103* (51), 11237-11241.

28. Bartko, A. P.; Dickson, R. M., Three-dimensional orientations of polymer-bound single molecules. *J. Phys. Chem. B* **1999,** *103* (16), 3053-3056.

29. Forkey, J. N.; Quinlan, M. E.; Goldman, Y. E., Measurement of single macromolecule orientation by total internal reflection fluorescence polarization microscopy. *Biophys. J.* **2005,** *89* (2), 1261-1271.

30. Patra, D.; Gregor, I.; Enderlein, J., Image analysis of defocused single-molecule images for three-dimensional molecule orientation studies. *J. Phys. Chem. A* **2004,** *108* (33), 6836-6841.

31. Toprak, E.; Enderlein, J.; Syed, S.; McKinney, S. A.; Petschek, R. G.; Ha, T.; Goldman, Y. E.; Selvin, P. R., Defocused orientation and position imaging (DOPI) of myosin V. *Proc. Natl. Acad. Sci.* **2006,** *103* (17), 6495-6499.

32. http://www.olympusmicro.com/.

33. Dickson, R. M.; Norris, D. J.; Moerner, W. E., Simultaneous imaging of individual molecules aligned both parallel and perpendicular to the optic axis. *Phys. Rev. Lett.* **1998,** *81* (24), 5322-5325.

Chapter 3

Single-Molecule Probes of Lipid Membrane Structure

3.1 Introduction

Because of the importance that membranes play in biological function, a host of techniques have been applied to probe the microscopic structure in both natural and model membranes. Fluorescence microscopy and atomic force microscopy (AFM) have proven especially useful for understanding the phase partitioning in model membranes.[1-6] These methods are particularly useful for reasons discussed in Chapters 1 and 2.

Bulk lipid order and orientational information has been obtained by methods such as quasielastic neutron scattering (QENS),[7] NMR relaxation studies,[8-11] small angle x-ray diffraction,[12] and wide angle x-ray scattering.[13] Structural information has also be obtained from optical techniques such as infrared (IR) spectroscopy,[14-16] polarized total internal reflection fluorescence (PTIRF) microscopy,[17-18] variable acquisition angle polarized TIRF (VAATIRF),[19] and polarized epifluorescence (PEF).[18-19] These techniques, however, often average over large populations of molecules and therefore provide an ensemble view of membrane organization and lack information at the single-molecule structural level.

The recent advances in single molecule fluorescence detection provide new opportunities for probing membrane structure at the molecular level. Single molecule fluorescence detection is now well established using both near-field and far-field approaches.[20-25] Moreover, these measurements have been extended to probe the three-dimensional orientation of fluorescent molecules doped into samples. For example,

several groups have shown that polarized total internal reflection fluorescence microscopy (PTIRF-M) measurements with p-polarized excitation can probe single molecule orientation in a sample.[17, 26-33] As shown in Chapter 2, the orientation of single molecules can be mapped by analyzing their emission patterns created when brought near an interface, such as a glass substrate.

Briefly, by defocusing the optics, distinct emission patterns are observed in the single molecule fluorescence image which reflects the orientation of the molecule in the sample. As has been shown, these emission patterns can be modeled to extract the orientation of the emission dipole moment for each molecule. Here we show that this provides a powerful new approach for probing membrane structure.

Langmuir-Blodgett monolayers of dipalmitoylphosphatidylcholine (DPPC) and arachidic acid (AA) are doped with small amounts of commonly used fluorescent lipid analogs. Taken with slightly defocused PTIRF-M, single-molecule fluorescence images reveal changes in the single-molecule orientation as the surface pressure of the monolayer is changed. The reorientations of the reporter dye reflect the evolution in order within the film as the surface pressure is increased and demonstrates that this technique can be used to probe membrane structure at the molecular level. Having shown that single molecule emission patterns can track membrane order, similar measurements are made on DPPC monolayers incorporating cholesterol. The addition of cholesterol is known to lead to dramatic ordering in membranes[34-36] which is reflected in the single molecule emission patterns. These measurements yield both the orientation and location of the dye molecules in the film which should be particularly informative in cellular applications. Moreover, unlike ensemble averaging techniques, the entire orientation distribution is

measured in single-molecule measurements which should be very useful for heterogeneous membrane systems. Finally, because only trace quantities of the reporter dye are incorporated into the membranes, this approach is less perturbative than conventional fluorescence approaches.

3.2 Experimental and Methods

3.2.1 Langmuir-Blodgett (LB) Monolayers

1,2-dipalmitoyl-*sn*-glycero-3-phosphocholine (DPPC) (Avanti Polar Lipids, Alabaster, AL), arachidic acid, and cholesterol (Sigma Aldrich, St Louis, MO) were obtained at >99% purity and used without further purification. The fluorescent lipid analogs 2-(5-butyl-4,4-difluoro-4-bora-3a,4a-diaza-*s*-indacene-3-nonanoyl)-1-hexadecanoyl-*sn*-glycero-3-phosphocholine (β-C_4-BODIPY 500/510 C_9 HPC) (BODIPY-PC) (Invitrogen Corporation, Carlsbad, CA, B3794) and 1,1'-dioctadecyl-3,3,3',3'-tetramethylindocarbocyanine perchlorate ($DiIC_{18}$) (Invitrogen Corporation, Carlsbad, CA, D-282) were doped into lipid films at a concentration of approximately $1x10^{-8}$ mol%.

DPPC and arachidic acid were dissolved in chloroform (1mg/ml), doped with an appropriate reporter dye, and dispersed on a subphase of ultra-pure water (18 MΩ) in a Langmuir-Blodgett trough (Type 611, Nima Technology, Coventry, England). Once dispersed on the subphase, the chloroform was allowed to evaporate for 15 minutes. DPPC monolayers were compressed at a speed of 100 cm^2/min to approximately 42 mN/m and then expanded at a speed of 80 cm^2/min. The compression cycles were repeated twice to anneal the monolayer and it was then compressed to the target pressure

and held there for approximately 15-20 minutes. The film was then transferred in a heads-down geometry onto a Piranha cleaned glass substrate at a dipping speed of 25 mm/min. For DPPC films containing cholesterol, the appropriate amount of cholesterol (from a 1mg/ml in chloroform stock solution) was added to the DPPC solution to make the appropriate concentration in mol%.

For arachidic acid films, glass slides were first treated in a 3% octatriethoxysilane (OTS) / toluene (v/v) solution for 6 hours and rinsed with water (18 M Ω) to produce a hydrophobic surface. The first monolayer of pure AA was transferred onto the OTS treated substrate with tailgroups down. A second layer of AA doped with ~10^{-8} mol% $DiIC_{18}$ was then deposited on top to produce a Y-type film. All films were prepared at a temperature of ~21˚C.

3.2.2 Imaging Technique

The films were imaged using a total internal reflection fluorescence microscope (TIRF-M) (Olympus IX71, Center Valley, PA) equipped with a 100x objective (1.45 NA achromat). The 514 nm line from an argon ion laser (Coherent Innova 70 Spectrum, Santa Clara, CA) was directed through half-wave and quarter-wave plates (Newport, Irvine, CA) to generate p-polarized excitation. Excitation was directed through the objective, and fluorescence was collected in an epifluorescence geometry with the optics defocused ~500 nm. The fluorescence was filtered with a combination of a dichroic mirror and long pass filters (Chroma, Rockingham, VT) and imaged onto a CCD camera (Cascade 650, Roper Scientific, Tucson, AR). Image collection was controlled with

Slidebook software (Version 4.2, Intelligent Imaging Innovations, Denver, CO) and analyzed using MatLab software (Natick, MA).

3.3 Results and Discussion

3.3.1 Single Molecule Orientations – Tracking Acyl Chain Order in Membranes

To explore the structural information available from single molecule orientation measurements, PTIRF-M studies on the fluorescent lipid analogs BODIPY-PC and $DiIC_{18}$ doped into Langmuir-Blodgett (LB) films were studied over a range of surface pressures. For these studies, lipid monolayers were formed from DPPC, arachidic acid (AA), and DPPC/cholesterol mixed monolayers. Figure 3.1 shows the structures of DPPC, AA, cholesterol, and the two fluorescent lipid analogs that were doped into the films. The two fluorescent lipid analogs shown in Fig. 3.1 were chosen for the placement of the fluorophore. For DPPC monolayers transferred onto glass with headgroups down, the BODIPY-PC probe with the fluorophore in the tailgroup is expected to be more sensitive to changes in membrane packing while the $DiIC_{18}$, with the fluorophore in the headgroup, should be less sensitive and will act as a control in these studies. Each of these fluorophores has an emission dipole aligned along the long axis of the chromophore as shown schematically in Fig. 3.1. For the BODIPY chromophore, anisotropy measurements suggest there is an angle of $\sim 13^{o}$ between the absorption and emission dipoles.[37] Previous studies have shown the propensity of fluorescent lipid analogs to partition into the more expanded phase in these films

Figure 3.2 shows a pressure-area isotherm for DPPC with arrows denoting the surface pressures at which monolayers were transferred onto a glass substrate. The

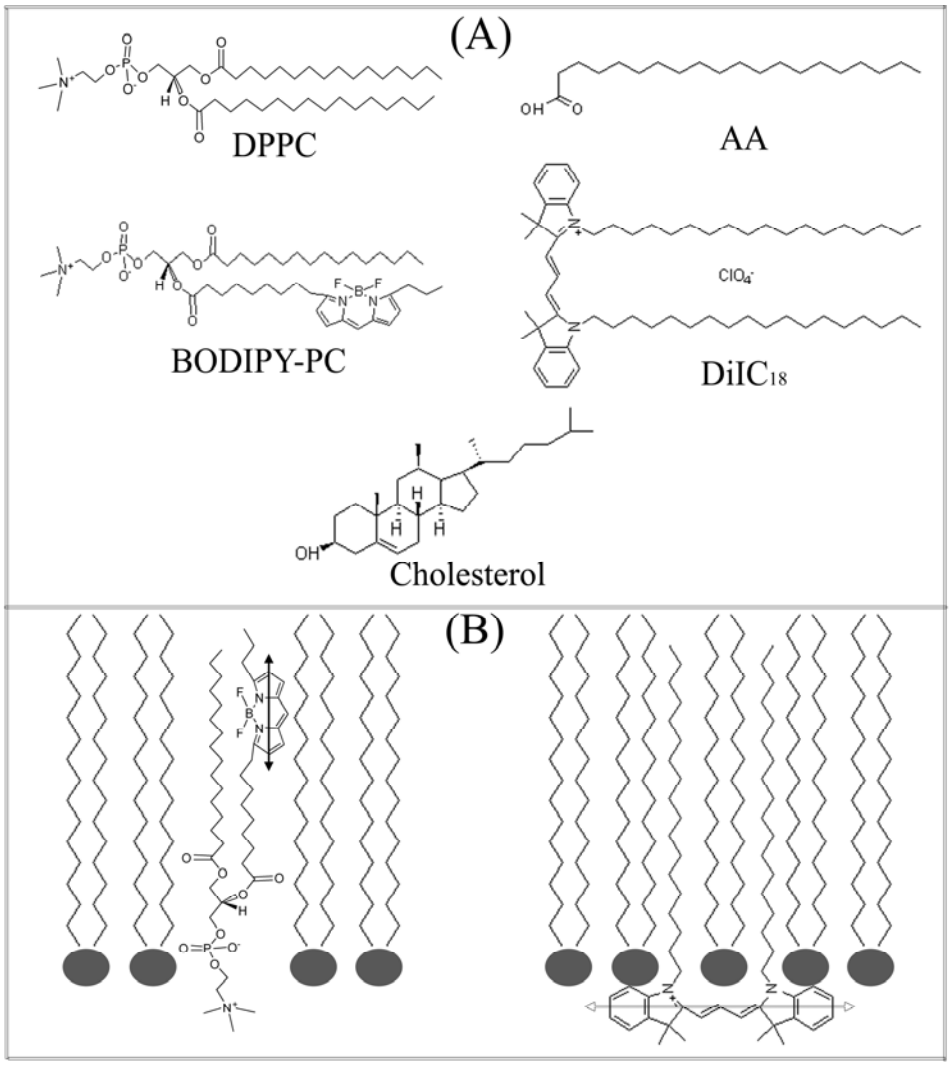

Figure 3.1 **(A)** Structures of the lipids, cholesterol, and fluorescent lipid analogs used in film formation are shown. **(B)** A schematic of how BODIPY-PC and $DiIC_{18}$ insert into the monolayer is also shown.

pressure-area isotherm for DPPC shows the phase coexistence plateau region where liquid expanded (LE) and liquid condensed (LC) phases coexist. Also shown in Fig. 3.2 are AFM images (as described in Chapter 2) of the DPPC monolayers transferred at pressures of 25 mN/m and 40 mN/m. Height differences indicative of coexisting phases remain visible in the AFM image of the film transferred at 25 mN/m, where a single phase is expected for an ideal single component film. The departure from ideal behavior is common and arises from small amounts of impurities.[38] At 40 mN/m, the AFM image reveals a nearly homogeneous film with only small, < 15 nm width, structures remaining.

As an example of how out-of-focus PTIRF-M measurements can probe lipid membrane organization, Fig. 3.3 shows a typical single molecule fluorescence image taken of a DPPC monolayer doped with ~10^{-8} mol% of the reporter molecule BOPIPY-PC. This monolayer was transferred onto a glass substrate at a surface pressure of 25 mN/m. Each bright spot in the image reflects the emission from a single BODIPY-PC molecule in the monolayer. With the optics defocused ~500 nm, the single molecule fluorescence shows distinct shapes that reflect the orientation of the BODIPY-PC fluorophores in the monolayer. As shown previously by others, donut-like shapes in the fluorescence image reflect emission dipoles oriented normal to the substrate.[26-33] At this defocus length, these features become asymmetric as the dipole orients away from the normal and appear as elliptical bright spots surrounded by wings when the emission dipole lies in the plane of the membrane. As seen in Fig. 3.3, a range of single molecule emission patterns are observed that qualitatively reflect the order present in the lipid membrane at this surface pressure.

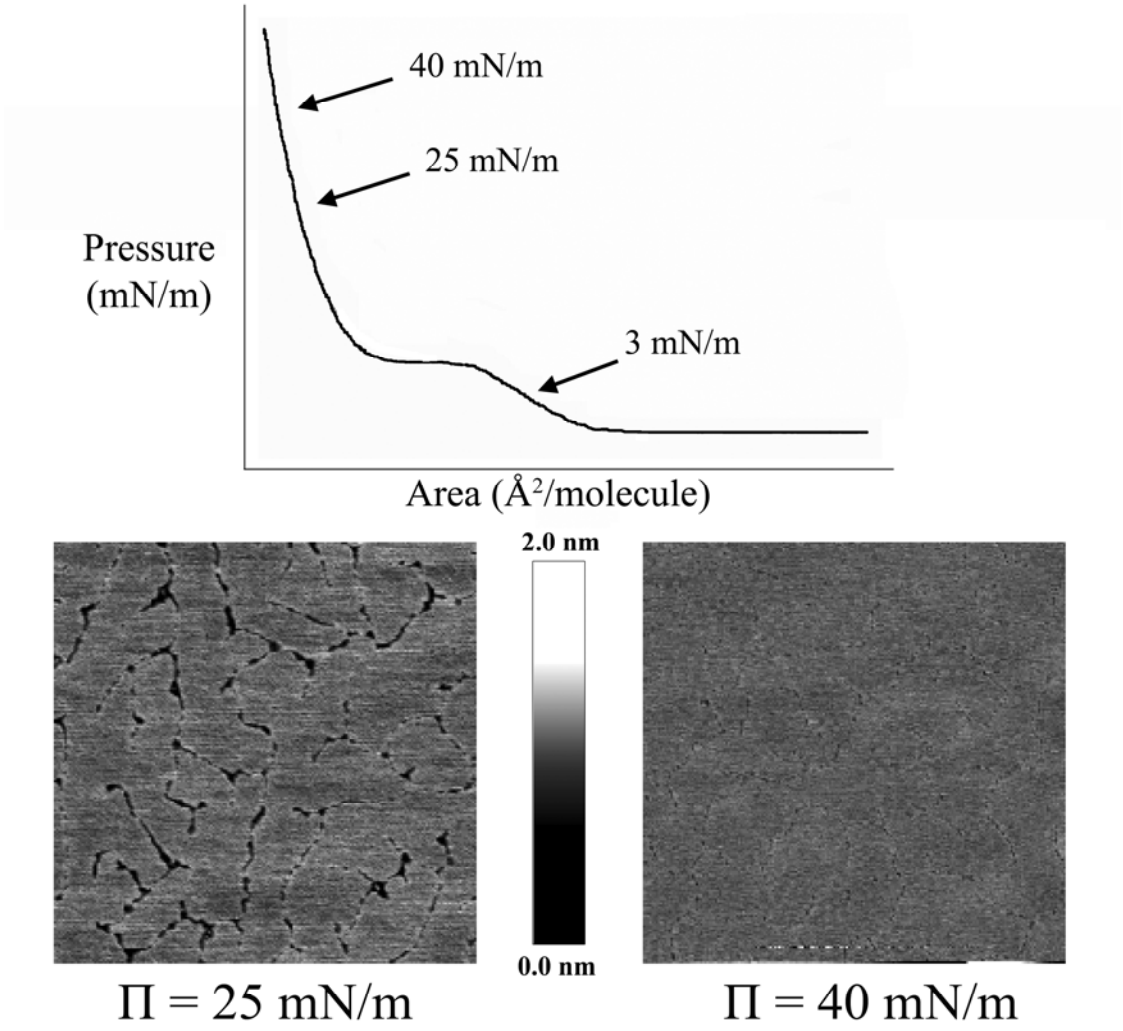

Figure 3.2 Pressure-area isotherm for DPPC with arrows denoting pressures used to transfer monolayers onto the glass substrate. Below are AFM images of typical films transferred at the higher pressures.

Representative single molecule emission patterns, extracted from the full image, are also shown in Fig. 3.3. The top single molecule emission feature shows the donut-like shape indicative of molecules oriented normal to the surface. The middle image shows an asymmetric emission suggesting a molecule tilted away from the normal while the bottom image reveals the emission pattern measured for molecules lying in the plane of the film. As shown previously,[26-33] the degraded imaging system that leads to the emission shapes can be modeled to extract the emission dipole orientation. For LB films this is simplified because the thinness of the film leads to all dye molecules being located at the same *z* position.

Figure 3.3 shows modeled emission patterns for the three extracted single molecule features, along with the angles used in the modeling. As shown in Fig. 2.16, we use the convention that ϕ represents the polar angle and θ denotes the azimuthal angle. Figure 3.3 also shows a schematic representation of the emission dipole orientation for each extracted emission pattern.

To explore the use of single molecule emission measurements to reveal membrane structure, DPPC monolayers were doped with ~10^{-8} mol% BODIPY-PC and transferred onto substrates at surface pressures of π = 3 mN/m, 25 mN/m, and 40 mN/m. Figure 3.4 shows representative emission images taken on monolayers transferred at these pressures. Qualitatively, comparison of the emission images shows an evolution in the emission patterns as the surface pressure increases and the films become more ordered. At low surface pressure (3 mN/m) where there is maximal orientational freedom around the probe molecule, the single molecule emission patterns consist primarily of patterns associated with emission dipoles lying in the plane of the film. Relatively few

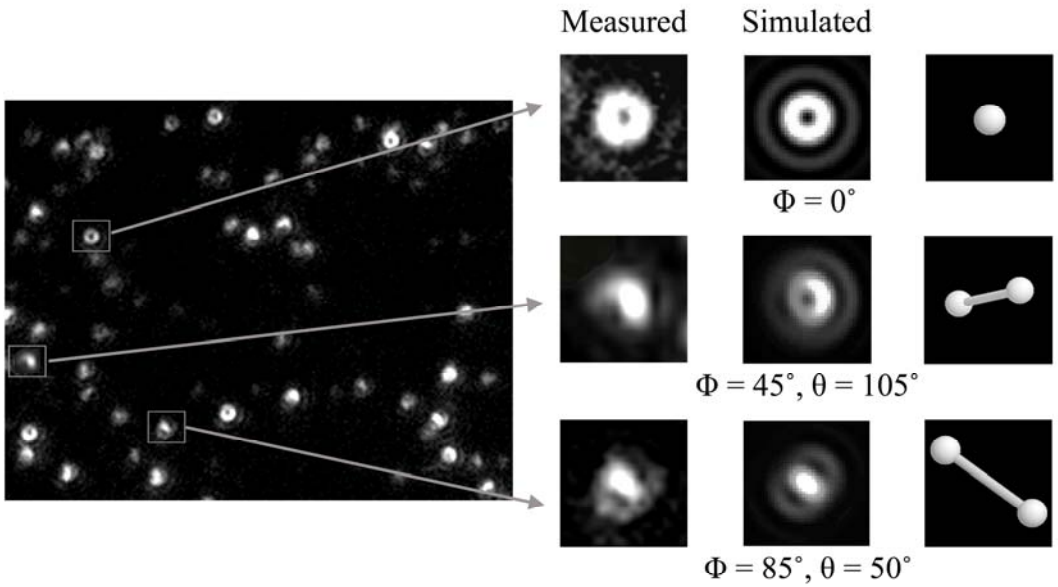

Figure 3.3 Typical single-molecule fluorescence image of a DPPC monolayer doped with BODIPY-PC. This monolayer was transferred onto a glass substrate at a surface pressure of 25 mN/m. Representative single-molecule emission patterns have been extracted to illustrate the range of patterns observed. Modeling of the emission patterns leads to the orientation of the emission dipole.

donut-like single molecule emission patterns are observed at this pressure where the average area per molecule is approximately 75 - 80 $Å^2$/molecule.

As shown in Fig. 3.4, as the surface pressure of the film is raised, an increase in the appearance of donut-like emission patterns is observed. For example, the emission image shown in Fig. 3.4 for the DPPC monolayer transferred at 40 mN/m shows single molecule patterns that are dominated by donut-like features. These features arise from emission dipoles oriented normal to the membrane plane and are consistent with the tailgroups of the fluorescent probe positioned vertically in the monolayer. At this surface pressure, the area per molecule of DPPC is ~40 $Å^2$/molecule which is approximately half that for monolayers transferred at 3 mN/m, where few donut-like features are observed.

Using the same procedure outlined in Fig. 3.3, the three-dimensional orientation of each emission feature in the images can be extracted. These orientations are mapped schematically below each of the measured emission images shown in Fig. 3.4. A clear trend towards vertically oriented emission dipoles is seen as the surface pressure of the film increases. A more quantitative view is found in population histograms of the polar angle (ϕ) extracted from the modeled emission patterns. For each pressure studied, at least three different films where analyzed at various locations to create the histograms shown in Fig. 3.4. In all, at least 700 individual molecules where analyzed at each surface pressure with the exact number for each histogram shown in Fig. 3.4. At a surface pressure of 3 mN/m, this measure of the tilt from the membrane normal shows that most of dye probes have their emission dipoles lying in the plane of the film with an average tilt angle of 67.4° ± 5°. As the pressure is increased to 25 mN/m, a bimodal histogram is found with roughly ~ 39% of the molecules oriented in the plane ($\geq 81^o$) and

~ 42% orientated normal to the plane (≤ 10^{o}), with the remaining 19% approximately evenly spread through the remaining orientations.

The AFM measurements in Fig. 3.2 show that expanded phases in the DPPC monolayer persist even at 25 mN/m. The bimodal distribution of BODIPY-PC orientations, seen in Fig. 3.4, reflects dye molecules located in the differing phases. Emission dipoles oriented normal to the surface arise mainly from dye molecules in condensed regions of the film while those located parallel to the film plane reflect expanded regions. Even though the AFM measurements show a nearly 95% to 5% condensed to expanded phase distribution in the films by area, the dye orientations in the histogram are almost evenly divided between upright and parallel due to the selective partitioning of BODIPY-PC into the expanded phase. If the bimodal distribution is combined, the average tilt angle at 25 mN/m is 48.7˚ ± 5˚.

At a surface pressure of 40 mN/m, the increased packing in the film produces a histogram with the majority of probes oriented normal to the film. At this elevated surface pressure, ~68% are oriented normal to the surface and only ~ 12% lie in the plane of the film producing an overall average tilt angle of 22.4˚ ± 5˚. These results show a clear trend towards vertically oriented tailgroups as the surface pressure increases.

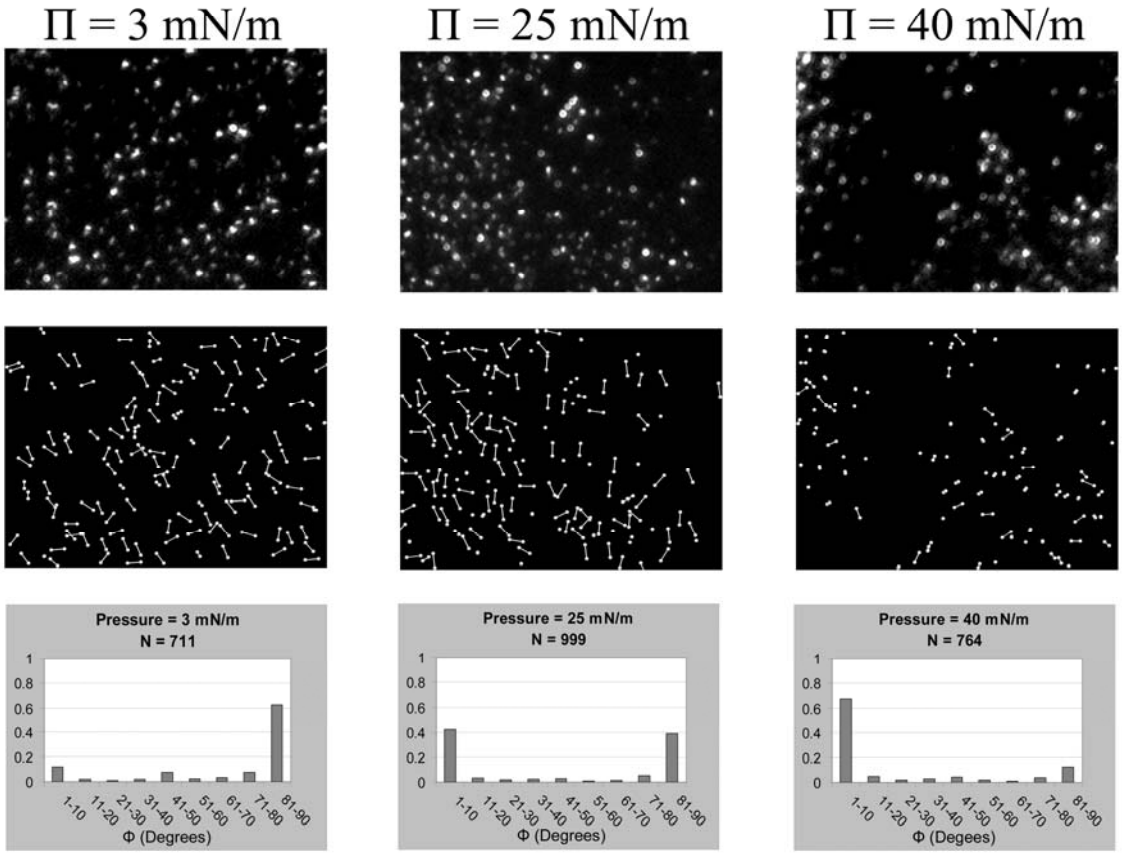

Figure 3.4 Single-molecule fluorescence images of DPPC monolayers doped with BODIPY-PC and transferred at the surface pressures shown at the top. As the pressure increases, more donut-like features are observed reflecting the increased packing and order in the monolayers. The orientation for each molecule is shown schematically in the middle row of images with the polar angle (Φ) population histograms plotted below.

3.3.2 Control Studies Using a Headgroup Labeled Probe

Measurements similar to those shown in Fig. 3.4 were conducted on DPPC monolayers incorporating the fluorescent lipid analog $DiIC_{18}$. As shown in Fig. 3.1, this probe has the fluorophore located in the headgroup with the transition dipole aligned along the long axis of the conjugated ring system. This positions it along the plane of the membrane when incorporated into a lipid monolayer as shown schematically in Fig. 3.1. With the fluorophore located in the headgroup, $DiIC_{18}$ should be much less sensitive to membrane packing in LB monolayers transferred in headgroup down geometry. These studies, therefore, act as a control to confirm that membrane packing is the predominant metric leading to changes in the observed emission patterns.

Figure 3.5 shows representative single molecule emission images of ~10^{-8} mol% $DiIC_{18}$ incorporated into DPPC monolayers transferred at surface pressures of 3 mN/m, 25 mN/m, and 40 mN/m. As before, Fig. 3.5 also shows schematic representations of the extracted emission dipole orientations and population tilt histograms for each surface pressure studied. As before, at each pressure several areas were imaged from at least three different films to construct the histograms. In contrast to the studies carried out with BODIPY-PC, the tilt histograms measured for $DiIC_{18}$ are not sensitive to the surface pressure or packing of the DPPC monolayer. The histograms reveal that most of the probes are oriented with their emission dipoles lying in or near the plane of the film. At a surface pressure of 3 mN/m, for example, approximately 88% of the dye molecules are oriented in the plane of the film ($\geq 81^{o}$). As surface pressure is increased to 25 mN/m and 40 mN/m, approximately 96% and 94% are oriented in the plane of the films, respectively. From the population histograms, average tilt angles of 80.7˚ ± 5˚, 83.5˚ ±

5˚, and 81.9˚ ± 5˚ are calculated for surface pressures of 3 mN/m, 25 mN/m, and 40 mN/m, respectively, showing no appreciable changes in tilt angle with surface pressure. Since these films are deposited with the headgroups on the glass substrate and $DiIC_{18}$ has its emission dipole in the headgroup aligned along the plane of the film, the insensitivity to membrane packing is expected. The BODIPY-PC, on the other hand, with the emission coming from the tailgroup region is much more sensitive to membrane packing as shown in Fig. 3.4.

3.3.3 Comparison of Single Molecule Measurements to Previous Bulk Studies

Other groups have used polarized fluorescence techniques to measure the ensemble orientation of fluorescent probes doped into thin films. In particular, several studies have reported on the orientation of $DiIC_{18}$ doped into thin films of arachidic acid. In one study, LB films consisting of three layers of pure cadmium arachidate followed by

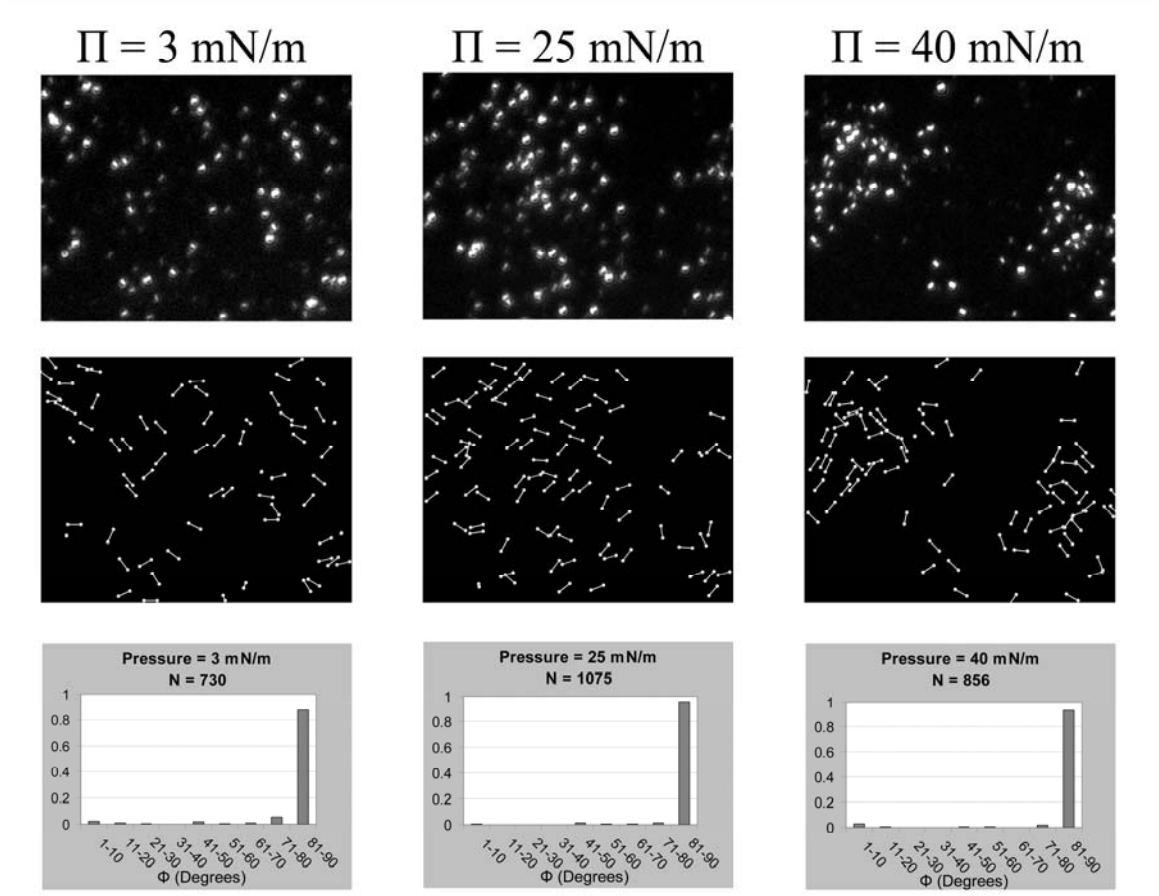

Figure 3.5 Single-molecule fluorescent images of DPPC monolayers doped with $DiIC_{18}$ and transferred at the surface pressures shown at the top. As in Figure 3.4, the top shows representative single-molecule fluorescence images, the middle displays schematic representation of the emission dipole orientations, and polar angle (Φ) population histograms are shown below. With the fluorophore aligned along the long axis of the headgroup in $DiIC_{18}$ and by insertion into the headgroup region of the monolayer, this probe is less sensitive than BODIPY-PC at sensing changes in membrane packing.

two layers of arachidic acid doped with $DiIC_{18}$. These measurements found a mean tilt angle of 75˚ ± 4.1˚ away from the membrane normal.[39] A similar tilt angle of 77˚ ± 5˚ was measured using polarized epifluorescence and polarized total internal reflectance fluorescence measurements.[18] This study measured the $DiIC_{18}$ tilt angle in LB films consisting of a doped bilayer of arachidic acid deposited on top of a pure bilayer of cadmium arachidate.

Figure 3.6 shows the results from single molecule measurements on $DiIC_{18}$ doped into an arachidic acid film. For these measurements, a pure arachidic acid monolayer was transferred in a tailgroup down geometry onto an OTS treated glass substrate. A second monolayer doped with ~10^{-8} mol% $DiIC_{18}$ was then transferred onto the first. Both layers of the film were transferred at a surface pressure of 35 mN/m to match that used in previous studies. The results shown in Fig. 3.6 reveal that most of the $DiIC_{18}$ molecules are oriented with their emission dipoles lying in or near the plane of the film. Averaging all the orientations results in an average orientation of 71^{o} ± 5˚ of the dye molecules, which is close to that measured in the previous studies on similar films. This suggests the single molecule measurements agree well with other bulk averaging techniques.

3.3.4 Condensation Effect of Cholesterol on Model Membranes

Having shown that single molecule orientation measurements can probe membrane structure, the influence of cholesterol on monolayers of DPPC was investigated. Cholesterol is ubiquitous in biological membranes and influences a vast number of biological functions.[35-36, 40-43] Cholesterol inserts into membranes with its

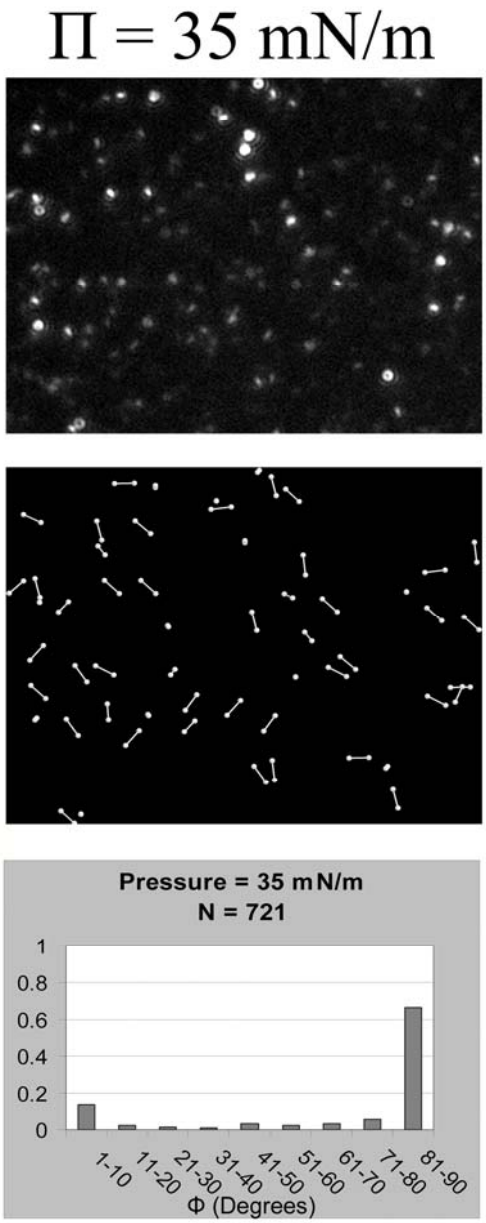

Figure 3.6. From these measurements, the average tilt angle (Φ) calculated from the histogram is approximately 71 ± 5°. This is in good agreement with bulk measurements in similar systems.

rigid four-ring structure aligned along the tailgroups of the lipids in the bilayer and its single hydroxyl group oriented towards the headgroups. The incorporation of cholesterol leads to dramatic changes in the biophysical properties of membranes which has been the subject of many excellent reviews.[35-36, 41-42]

In general, the incorporation of cholesterol leads to ordering in lipid membranes.[36] Cholesterol increases the average motional order of the hydrocarbon chains in lipid bilayers, thus leading to a decreased average area per lipid and a new physical state known as the liquid-ordered (l_o) state.[35-36, 40-42] For phospholipids with chain lengths up to approximately 16 carbon atoms, this cholesterol induced ordering leads to an overall increase in membrane thickness and decrease in membrane permeability.

Figure 3.7 shows single molecule emission measurements of DPPC monolayers doped with increasing amounts of cholesterol at a surface pressure of 25 mN/m. As shown previously in Fig. 3.4, pure monolayers of DPPC doped with BODIPY-PC exhibit a predominantly bimodal distribution of dye molecule orientations at this surface pressure. This is shown in the top image of Fig. 3.7with 0 mol% added cholesterol. With no added cholesterol to the DPPC monolayer, approximately 42% of the dye molecules are oriented normal to the surface ($\leq 10^o$). As seen in Fig. 3.7, the addition of small amounts of cholesterol into the DPPC monolayer leads to a dramatic shift in the single molecule orientations. With the addition of just 5 mol% cholesterol, the population histogram shows that ~ 59% of the dye molecules orient normal to the surface. This increases to ~ 65% at 10 mol% and finally ~ 70% at 33 mol%. These measurements agree with previous studies illustrating the ordering effect that cholesterol has on lipid

membranes and illustrates the utility of single molecule measurements in more complicated and hence biologically relevant membrane models.

The results presented here suggest that single molecule emission patterns can be used to reveal structural changes in membranes. This technique compliments other approaches for studying membrane structure and provides several advantages. There is minimal perturbation to the membrane from the fluorescent lipid probe because of the small amount of probe needed. Typical fluorescence studies of membranes use dyes doped at concentrations ranging from ~0.25 to ~2 mol%. While this is typically considered non-perturbative and does not affect the monolayer transition pressures, miscibility studies on mixed membranes have found an effect from the added fluorescent lipid analogs at concentrations as low as 0.05 mol%.[44] To avoid crowding in the single molecule emission images, dye concentrations of approximately 10^{-8} mol% where utilized here which are several orders of magnitude lower than that in typical studies.

Probing membrane order at the single molecule level also has the advantage that the entire distribution of orientations is measured. Even simple membranes can be highly heterogeneous and this heterogeneity can be lost in bulk measures of average properties. For example, the results shown in Fig. 3.4 for DPPC monolayers transferred at 25 mN/m reveal a bimodal tilt distribution. This would be lost in average measures of tilt and reflects the structure remaining in this monolayer even at pressures where single phase behavior is expected for an ideal single component film. Moreover, because this is a microscopy technique, both dye orientation and location are measured which may prove especially informative in natural biological membranes where correlations may provide new insights.

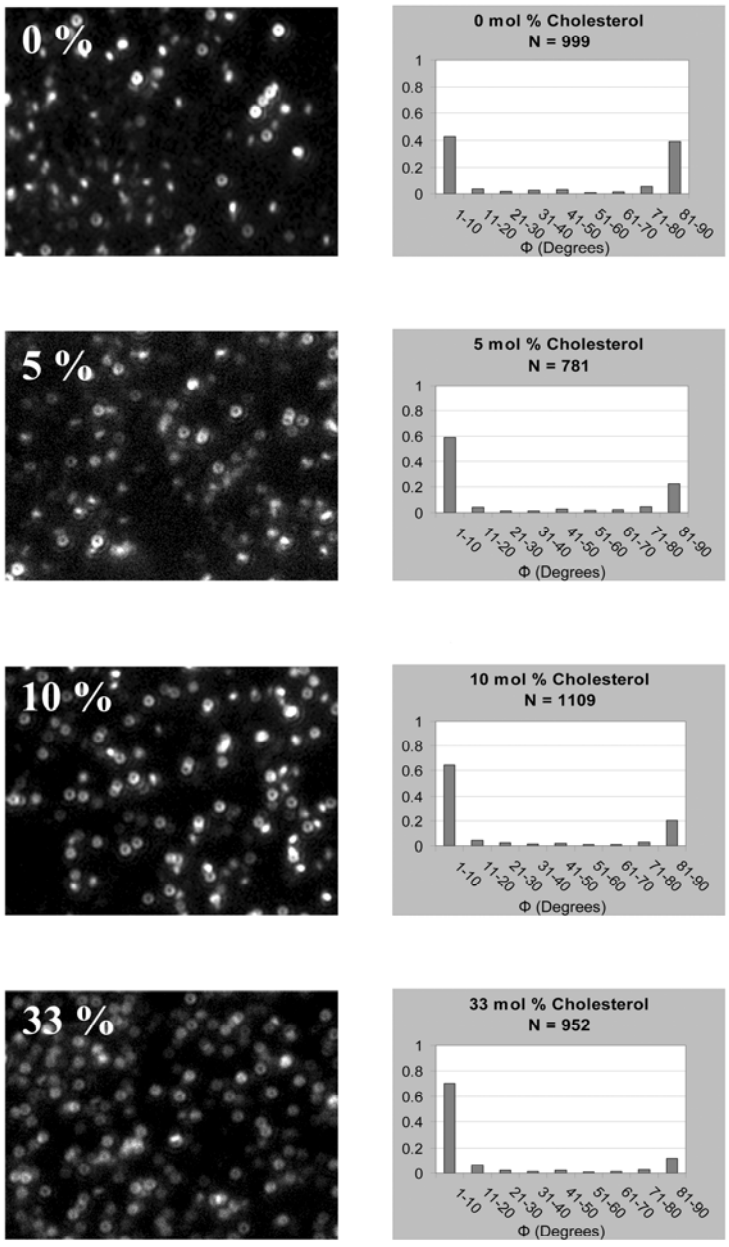

Figure 3.7 Single-molecule emission images and tilt histograms from measurements on DPPC monolayers as a function of mol% cholesterol. All monolayers were doped with ~10^{-8} mol % of the reporter dye BODIPY-PC and transferred at the same surface pressure of 25 mN/m. As the percentage of cholesterol is increased, the films become more ordered as seen in the increased observation of donut-like single-molecule emission patterns in the images. Analysis of the images reflects this ordering as an increase in the number of dye molecules with emission dipoles oriented normal to the film (tilt angle ≤10°).

3.4 Conclusions

Molecular orientations measured at the single molecule level are used here to probe the microscopic order in model membranes. Using TIRF-M with p-polarized excitation, the single molecule emission from the fluorescent lipid analogs BODIPY-PC and $DiIC_{18}$ doped into LB films of DPPC and AA are measured. As shown by others, defocusing of the optics leads to distinct emission patterns in the single molecule images which reflect the orientation of the dye.[26-33] DPPC monolayers doped with ~10^{-8} mol% BODIPY-PC were deposited at a range of surface pressures and changes in the single molecule orientations tracked the increasing order in the monolayer. At low surface pressures, the emission dipole in the tailgroup of the BODIPY-PC was mostly lying in the plane of the film which evolved to a more upright orientation at high surface pressures where the area per molecule is reduced and the order of the monolayer increased. Similar experiments using $DiIC_{18}$ found no significant changes in emission dipole orientation with surface pressure, as expected since its fluorophore is located in the headgroup. Measurements of $DiIC_{18}$ in films multilayer of AA transferred at 35 mN/m found an average tilt away from normal of $71^{o} \pm 5^{\circ}$, which compares favorably with previous bulk measurements.[18, 39] Incorporation of cholesterol into monolayers of DPPC is shown to increase the number of BODIPY-PC dye molecules oriented normal to the membrane, consistent with the known propensity of cholesterol to condense membrane structure. These results show that orientational measurements taken at the single molecule level provide a useful approach for probing membrane structure.

3.5 References

1. Burns, A. R., Domain structure in model membrane bilayers investigated by simultaneous atomic force microscopy and fluorescence imaging. *Langmuir* **2003,** *19* (20), 8358-8363.

2. Burns, A. R.; Frankel, D. J.; Buranda, T., Local mobility in lipid domains of supported bilayers characterized by atomic force microscopy and fluorescence correlation spectroscopy. *Biophys. J.* **2005,** *89* (2), 1081-1093.

3. Ekelund, K.; Sparr, E.; Engblom, J.; Wennerstrom, H.; Engstrom, S., An AFM study of lipid monolayers. 1. Pressure-induced phase behavior of single and mixed fatty acids. *Langmuir* **1999,** *15* (20), 6946-6949.

4. Shaw, J. E.; Epand, R. F.; Epand, R. M.; Li, Z. G.; Bittman, R.; Yip, C. M., Correlated fluorescence-atomic force microscopy of membrane domains: Structure of fluorescence probes determines lipid localization. *Biophys. J.* **2006,** *90* (6), 2170-2178.

5. Sparr, E.; Ekelund, K.; Engblom, J.; Engstrom, S.; Wennerstrom, H., An AFM study of lipid monolayers. 2. Effect of cholesterol on fatty acids. *Langmuir* **1999,** *15* (20), 6950-6955.

6. Yang, X. M.; Xiao, D.; Lu, Z. H.; Wei, Y., Structural Investigation of Langmuir-Blodgett Monolayers of L-Alpha-Dipalmitoylphosphatidylcholine by Atomic-Force Microscopy. *Appl. Surf. Sci.* **1995,** *90* (2), 175-183.

7. Gliss, C.; Randel, O.; Casalta, H.; Sackmann, E.; Zorn, R.; Bayerl, T., Anisotropic motion of cholesterol in oriented DPPC bilayers studied by quasielastic neutron scattering: The liquid-ordered phase. *Biophys. J.* **1999,** *77* (1), 331-340.

8. Guo, W.; Hamilton, J. A., A Multinuclear Solid-State Nmr-Study of Phospholipid-Cholesterol Interactions - Dipalmitoylphosphatidylcholine-Cholesterol Binary-System. *Biochemistry* **1995,** *34* (43), 14174-14184.

9. Scheidt, H. A.; Huster, D.; Gawrisch, K., Diffusion of cholesterol and its precursors in lipid membranes studied by H-1 pulsed field gradient magic angle spinning NMR. *Biophys. J.* **2005,** *89* (4), 2504-2512.

10. Vermeer, L. S.; de Groot, B. L.; Reat, V.; Milon, A.; Czaplicki, J., Acyl chain order parameter profiles in phospholipid bilayers: computation from molecular dynamics simulations and comparison with H-2 NMR experiments. *Eur. Biophys. J. Biophy.* **2007,** *36* (8), 919-931.

11. Vist, M. R.; Davis, J. H., Phase-Equilibria of Cholesterol Dipalmitoylphosphatidylcholine Mixtures - H-2 Nuclear Magnetic-Resonance and Differential Scanning Calorimetry. *Biochemistry* **1990,** *29* (2), 451-464.

12. Fujimori, A.; Araki, T.; Nakahara, H.; Ito, E.; Hara, M.; Ishii, H.; Ouchi, Y.; Seki, K., In-plane X-ray diffraction and polarized NEXAFS spectroscopic studies on the organized molecular films of fluorinated amphiphiles with vinyl esters and their comb-polymers. *Chem. Phys. Lett.* **2001,** *349* (1-2), 6-12.

13. Mills, T. T.; Toombes, G. E. S.; Tristram-Nagle, S.; Smilgies, D. M.; Feigenson, G. W.; Nagle, J. F., Order parameters and areas in fluid-phase oriented lipid membranes using wide angle x-ray scattering. *Biophys. J.* **2008,** *95* (2), 669-681.

14. Kim, Y. H.; Tero, R.; Takizawa, M.; Urisu, T., Characterization of dipalmitoylphosphatidylcholine/cholesterol Langmuir-Blodgett monolayers investigated by atomic force microscopy and Fourier transform infrared spectroscopy. *Japanese Journal of Applied Physics Part 1-Regular Papers Short Notes & Review Papers* **2004,** *43* (6B), 3860-3864.

15. Koppaka, V.; Axelsen, P. H., Evanescent electric field amplitudes in thin lipid films for internal reflection infrared spectroscopy. *Langmuir* **2001,** *17* (20), 6309-6316.

16. Mendelsohn, R.; Davies, M. A., Cd2 Rocking Modes as Quantitative Fourier-Transform Infrared Spectroscopic Probes of Conformational Disorder in Phospholipid-Bilayers. *ACS Symp. Ser.* **1991,** *447*, 24-43.

17. Forkey, J. N.; Quinlan, M. E.; Goldman, Y. E., Measurement of single macromolecule orientation by total internal reflection fluorescence polarization microscopy. *Biophys. J.* **2005,** *89* (2), 1261-1271.

18. Tronin, A.; Xu, T.; Blasie, J. K., In situ determination of orientational distributions in Langmuir monolayers by total internal reflection fluorescence. *Langmuir* **2005,** *21* (17), 7760-7767.

19. Tronin, A.; Blasie, J. K., Variable acquistion angle total internal reflection Fluorescence: A new technique for orientation distribution studies of ultrathin films. *Langmuir* **2001,** *17* (12), 3696-3703.

20. Dunn, R. C., Near-field scanning optical microscopy. *Chem. Rev.* **1999,** *99* (10), 2891.

21. Hollars, C. W.; Dunn, R. C., Submicron fluorescence, topology, and compliance measurements of phase-separated lipid monolayers using tapping-mode near-field scanning optical microscopy. *J. Phys. Chem. B* **1997,** *101* (33), 6313-6317.

22. Hollars, C. W.; Dunn, R. C., Probing single molecule orientations in model lipid membranes with near-field scanning optical microscopy. *J. Chem. Phys.* **2000,** *112* (18), 7822-7830.

23. Johnston, L. J., Nanoscale imaging of domains in supported lipid membranes. *Langmuir* **2007,** *23* (11), 5886-5895.

24. Shiku, H.; Dunn, R. C., Near-field scanning optical microscopy studies of L-alpha-dipalmitoylphosphatidylcholine monolayers at the air-liquid interface. *Journal of Microscopy-Oxford* **1999,** *194*, 461-466.

25. Vickery, S. A.; Hollars, C. W.; Dunn, R. C., Single molecule orientation measurements in Langmuir-Blodgett monolayers of DPPC. *Biophys. J.* **2002,** *82* (1), 46a-46a.

26. Bartko, A. P.; Dickson, R. M., Imaging three-dimensional single molecule orientations. *J. Phys. Chem. B* **1999,** *103* (51), 11237-11241.

27. Bartko, A. P.; Dickson, R. M., Three-dimensional orientations of polymer-bound single molecules. *J. Phys. Chem. B* **1999,** *103* (16), 3053-3056.

28. Bohmer, M.; Enderlein, J., Orientation imaging of single molecules by wide-field epifluorescence microscopy. *J Opt Soc Am B* **2003,** *20* (3), 554-559.

29. Patra, D.; Gregor, I.; Enderlein, J., Image analysis of defocused single-molecule images for three-dimensional molecule orientation studies. *J. Phys. Chem. A* **2004,** *108* (33), 6836-6841.

30. Reifenberger, J. G.; Toprak, E.; Safer, D.; Syed, S.; Enderlein, J.; Sweeney, H. L.; Selvin, P. R., Simultaneous defocused orientation imaging and position imaging of myosin VI. *Biophys. J.* **2007**, 526a-526a.

31. Toprak, E.; Enderlein, J.; Mckinney, S. A.; Syed, S.; Petschek, R. G.; Ha, T.; Goldman, Y. E.; Selvin, P. R., Simultaneous position and orientation analysis using focused and defocused image analysis: Application to quantum dots and myosin V. *Biophys. J.* **2005,** *88* (1), 664a-664a.

32. Toprak, E.; Enderlein, J.; Syed, S.; McKinney, S. A.; Petschek, R. G.; Ha, T.; Goldman, Y. E.; Selvin, P. R., Defocused orientation and position imaging (DOPI) of myosin V. *Proc. Natl. Acad. Sci.* **2006,** *103* (17), 6495-6499.

33. Uji-i, H.; Deres, A.; Muls, B.; Melnikov, S.; Enderlein, J.; Hofkens, J., Defocused Imaging in Wide-field Fluorescence Microscopy. In *Fluorescence of Supermolecules, Polymers, and Nanosystems*, Springer: New York, 2008; p Chapter 4.

34. Ege, C.; Ratajczak, M. K.; Majewski, J.; Kjaer, K.; Lee, K. Y. C., Evidence for lipid/cholesterol ordering in model lipid membranes. *Biophys. J.* **2006,** *91* (1), L1-L3.

35. Silvius, J. R., Fluorescence energy transfer reveals microdomain formation at physiological temperatures in lipid mixtures modeling the outer leaflet of the plasma membrane. *Biophys. J.* **2003,** *85* (2), 1034-1045.

36. Yeagle, P. L., The Roles of Cholesterol in the Biology of Cells. In *The Structure of Biological Membranes*, 2nd ed.; CRC Press LLC: 2005.

37. Karolin, J.; Johansson, L. B. A.; Strandberg, L.; Ny, T., Fluorescence and Absorption Spectroscopic Properties of Dipyrrometheneboron Difluoride (Bodipy) Derivatives in Liquids, Lipid-Membranes, and Proteins. *J. Am. Chem. Soc.* **1994,** *116* (17), 7801-7806.

38. Stottrup, B. L.; Keller, S. L., Phase behavior of lipid monolayers containing DPPC and cholesterol analogs. *Biophys. J.* **2006,** *90* (9), 3176-3183.

39. Edmiston, P. L.; Lee, J. E.; Wood, L. L.; Saavedra, S. S., Dipole orientation distributions in Langmuir-Blodgett films by planar waveguide linear dichroism and fluorescence anisotropy. *J. Phys. Chem.* **1996,** *100* (2), 775-784.

40. McMullen, T. P. W.; Lewis, R. N. A. H.; McElhaney, R. N., Cholesterol-phospholipid interactions, the liquid-ordered phase and lipid rafts in model and biological membranes. *Curr. Opin. Colloid Interface Sci.* **2004,** *8* (6), 459-468.

41. Mouritsen, O. G.; Zuckermann, M. J., What's so special about cholesterol? *Lipids* **2004,** *39* (11), 1101-1113.

42. Ohvo-Rekila, H.; Ramstedt, B.; Leppimaki, P.; Slotte, J. P., Cholesterol interactions with phospholipids in membranes. *Prog. Lipid Res.* **2002,** *41* (1), 66-97.

43. Simons, K.; Vaz, W. L. C., Model systems, lipid rafts, and cell membranes. *Annu. Rev. Biophys. Biomol. Struct.* **2004,** *33*, 269-295.

44. Veatch, S. L.; Leung, S. S. W.; Hancock, R. E. W.; Thewalt, J. L., Fluorescent probes alter miscibility phase boundaries in ternary vesicles. *J. Phys. Chem. B* **2007,** *111* (3), 502-504.

Chapter 4

Exploring the Effects of Sterols in Model Lipid Membranes using Single-Molecule Orientations

4.1 Introduction

As discussed in the previous chapters, the complexity of biological membranes often makes direct studies of membrane properties difficult in intact tissues. The number and distribution of membrane components is highly variable and not easily controlled, complicating both the experimental approaches and interpretation of the resulting data. These difficulties have led to the long historical development of model membrane systems, using both lipid monolayers and bilayers. These simplified models provide more control over parameters such as membrane composition, but questions remain regarding their utility in understanding the vastly more complex natural biomembranes. Regardless, it is clear that these model systems have been invaluable for understanding, for instance, the phase behavior of lipid films and the physical effects of membrane additives such as cholesterol.

Bilayers formed from vesicle fusion onto substrates provide a conceptually appealing mimic of biomembranes while monolayers fabricated using the Langmuir-Blodgett (LB) technique offer the advantage that the surface pressure can be precisely controlled. As discussed in Chapter 2, in the LB technique, the propensity of lipids to spread at the air-water interface is countered by an external mechanical pressure provided by a moving barrier. This enables the precise measurement and control over film lateral surface pressure (Π) which is the first derivative of free energy with respect to surface area. These measurements, therefore, provide a direct link between surface pressure and

film thermodynamics which can be studied over a wide range of pressures, temperatures and film compositions.

For model bilayers, surface pressure is not well defined at equilibrium, since the films exist in a tension free state. For bilayers it is the lateral compressibility that is the useful parameter when discussing such properties as protein insertion or conformational changes. In monolayers, lateral compressibility can be directly measured from the slope of the pressure-area isotherm. This illustrates the utility of comparative studies done with both monolayers and bilayers. While monolayers often provide a more direct measure of quantities such as surface pressure and compressibility, bilayers provide a more faithful representation of biological membranes. This necessitates a need for measureable parameters which establish corresponding states between monolayers and bilayers.

While surface pressure in monolayers is a thermodynamically precise quantity, for bilayers a more relaxed quantity, termed the equivalent surface pressure, is often discussed. The equivalent surface pressure is the collective interactions that balance the cohesive bilayer pressure that arises from the hydrophobic interactions between the lipid acyl chains and water.[1] Quantifying an equivalent surface pressure in bilayers is obviously important for studies comparing properties of monolayers and bilayers and for establishing conditions under which monolayers can be used as bilayer mimics.

While direct measures of surface pressure in bilayers is not possible, the monolayer-bilayer equivalence pressure can be estimated through indirect studies comparing membrane properties. For example, the partitioning of dibucaine, a local anesthetic, in monolayers of 1-palmitoyl-2-oleoyl phosphatidylcholine (POPC) at a surface pressure of 30.7-32.5 mN/m closely matched that in bilayers, suggesting similar

surface pressures.[2] A similar study found that the partitioning of myristic acid into phosphatidylcholine bilayers closely matched that of monolayers compressed to a surface pressure of 35 mN/m.[3] Finally, the partitioning of the small 22 residue peptide, phosphotransferase glucitol permease, into POPC vesicles was found to be similar to POPC monolayers compressed to a surface pressure of 32 mN/m.[4] Assuming that the insertion of species is similar in monolayers and bilayers, these partitioning studies suggest that bilayers have an equivalent surface pressure of ~30-35 mN/m.

Equilibrium spreading experiments have also been used to estimate the bilayer equivalence pressure. Vesicles in a subphase are allowed to form bilayers across an opening separating two solutions and form a monolayer at the air/subphase interface. When these films reach equilibrium, measurement of the surface pressure at the air/subphase interface yields insight into the equivalent surface pressure of the suspended bilayer. Using vesicles from the *Torpedo* electroplax, an equivalence bilayer pressure was estimated to be ~34 mN/m using this technique.[5]

In chapter 3, we used out-of-focus single-molecule fluorescence measurements to quantify the orientation of single dye molecules doped into lipid monolayers of DPPC.[6] Several groups have previously shown that polarized total internal reflection fluorescence microscopy (PTIRF-M) can be used to quantify the three-dimensional orientation of dye molecules in samples when spherical aberrations are introduced into the optics train through defocusing.[7-11] Using this approach, we showed that the orientation of fluorescent lipid analogs doped into LB monolayers of DPPC could be used to track membrane order. In this chapter we extend those measurements to fully explore the single-molecule orientation of BODIPY-PC doped in DPPC monolayers as a function of

surface pressure. Results from these measurements are used to find the equivalent surface pressure in DPPC bilayers formed through vesicle fusion onto a substrate. Single-molecule orientation measurements suggest that supported DPPC bilayers formed from both giant unilamellar vesicles (GUVs) and small unilamellar vesicles (SUVs) exhibit equivalent surface pressures of ~23 mN/m. This value is somewhat smaller than the currently accepted value of ~30 to 35 mN/m.[1-5, 12-13]

Having established a corresponding surface pressure between monolayers and bilayers of DPPC, single-molecule orientation measurements are used to compare the effects of biologically relevant sterols added to the lipid films. Cholesterol is an essential component of biological membranes that contributes up to 40-50 mol % of the plasma membrane in eukaryotic cells and leads to a well known condensing effect when added to membranes containing saturated lipids such as DPPC.[14-15] In general, this condensation of the lipids leads to an increase in lateral packing and ordering of the hydrocarbon chains, a reduction in the area per molecule, decreased membrane permeability, and an increase in membrane mechanical strength.[14-18]

Ergosterol is a plant sterol similar in structure to cholesterol which differs by an extra double bond in the acyl chain. The effects of ergosterol on membrane properties is less clear with some studies suggesting it has a greater condensing effect than cholesterol while others suggest the opposite.[19-21] Finally lanosterol, a biological precursor to cholesterol, is known to induce little condensing effects when added to model membranes.[19-21] These sterols therefore demonstrate a range of effects on membrane properties that are explored at the single-molecule level using defocused PTIRF-M measurements.

4.2 Experimental and Methods

4.2.1 Langmuir-Blodgett (LB) Monolayers

1,2-dipalmitoyl-*sn*-glycero-3-phosphocholine (DPPC) (Avanti Polar Lipids, Alabaster, AL), cholesterol (>99%), ergosterol (≥98), and lanosterol (≥97%) (Sigma Aldrich, St Louis, MO) were obtained and used without further purification. The fluorescent lipid analog 2-(5-butyl-4,4-difluoro-4-bora-3a,4a-diaza-*s*-indacene-3-nonanoyl)-1-hexadecanoyl-*sn*-glycero-3-phosphocholine (β-C_4-BODIPY 500/510 C_9 HPC) (BODIPY-PC) (Invitrogen Corporation, Carlsbad, CA, B3794) was doped into lipid films at a concentration of ~10^{-8} mol %.

For the preparation of monolayers, DPPC was dissolved in chloroform (1mg/ml stock solutions) and the appropriate amount of sterol was added. The solutions were doped with ~10^{-8} mol % BODIPY-PC reporter dye, and dispersed onto a subphase of ultra-pure water (18 MΩ) in a Langmuir-Blodgett trough (Type 611, Nima Technology, Coventry, England). Once dispersed on the subphase, the chloroform was allowed to evaporate for 15 minutes. DPPC monolayers were compressed at a speed of 100 cm^2/min to approximately 45 mN/m and then expanded at a speed of 80 cm^2/min. The compression cycles were repeated twice to anneal the monolayer. The monolayer film was then compressed to the target pressure, held for approximately 15-20 minutes, and then transferred in a heads down geometry onto a Piranha cleaned glass substrate at a dipping speed of 25 mm/min. All monolayers were prepared at a temperature of ~21^oC.

4.2.2 Bilayer Technique – Vesicle Fusion

For the preparation of supported DPPC bilayers, the appropriate mol% of each sterol was added into a 5mg/mL chloroform solution of DPPC. After doping each solution with ~10^{-8} mol % BODIPY-PC reporter dye, 380 μL of DPPC / sterol solution was added to a separate vial, evaporated to dryness with nitrogen, and placed under vacuum for ~1hr to remove residual solvent. The DPPC/sterol films were reconstituted in a buffer solution containing 20mM HEPES, 100mM NaCl, and 0.02 wt % NaN_3 adjusted to neutral pH. The vials were capped and incubated at ~60^{o} C for 1hr to hydrate the phospholipids. The suspensions were vortexed and sonicated to clarity to yield small unilamellar vesicles (SUVs). The SUV suspensions were incubated in PDMS wells on Piranha cleaned glass for 30min at 60^{o}C. The wells were thoroughly washed with nanopure water to remove unruptured vesicles, and the excess water was removed immediately before imaging.

Supported lipid bilayers were also formed using giant unilamellar vesicles (GUVs) prepared by electroformation. Briefly, 50μL of a 5mg/mL chloroform solution of DPPC/sterol with ~10^{-8} mol% BODIPY-PC reporter dye was deposited on two ITO microscope slides coated with the indium tin oxide (ITO). The solution was dried onto the slides under vacuum for ~1hr. The coated sides were rehydrated with ~1mL of ultra pure water (18 MΩ) and sandwiched together with a 1.5 mm thick PDMS gasket. The slide assembly was placed on a temperature-controlled stage set to 50°C and the lipids were allowed to hydrate for ~20 minutes. Following hydration, a function generator was used to apply a 10 Hz, 1 V sine wave across the ITO coated slides for ~3hr to produce

giant unilamellar vesicles. The GUVs were separated from the surface by reducing the frequency to 1Hz for ~30min and the suspension isolated.

4.2.3 Imaging Technique

All films were imaged using a total internal reflection fluorescence microscope (TIRF-M) (Olympus IX71, Center Valley, PA) equipped with a 100x objective (1.45 NA achromat). The 514 nm line from an argon ion laser (Coherent Innova 70 Spectrum, Santa Clara, CA) was directed through half-wave and quarter-wave plates (Newport, Irvine, CA) to generate p-polarized excitation. Excitation was directed through the objective and fluorescence collected in an epifluorescence geometry with the optics defocused ~500 nm. The fluorescence was filtered with a combination of a dichroic mirror and long pass filters (Chroma, Rockingham, VT) and imaged onto a CCD camera (Cascade 650, Roper Scientific, Tucson, AR). Image collection was controlled with Slidebook software (Version 4.2, Intelligent Imaging Innovations, Denver, CO) and analyzed using MatLab software (Natick, MA).

4.3 Results and Discussion

4.3.1 Single Molecule Orientations Studied at a Range of Surface Pressures

Previously we have shown that single-molecule fluorescence measurements using PTIRF-M can reveal insight into membrane structure at the molecular level.[6] Here we expand those initial studies to characterize the equivalent surface pressure in bilayers and compare both monolayers and bilayers doped with the biologically important sterols cholesterol, ergosterol, and lanosterol. Figure 4.1 shows the structures of DPPC and the

sterols studied along with the fluorescent lipid analogue, BODIPY-PC that was doped into the membranes to act as the reporter probe. Other studies have shown that unique single-molecule emission patterns are observed in slightly defocused PTIRF-M images, which reflect the orientation of the dye in the sample.[7-11, 22] Analysis of the emission patterns, therefore, enables the three-dimensional orientation of each dye molecule doped into the lipid film to be characterized. BODIPY-PC was chosen as the fluorescent reporter dye due to its placement of the fluorophore in the tailgroup, which has been shown to be sensitive to membrane order.[6] The absorption and emission dipoles of BODIPY-PC lie along the long axis of the chromophore with ~13˚ between the two.[23]

Figure 4.2 shows representative single-molecule emission images of ~10^{-8} mol% BODIPY-PC doped into DPPC monolayers, which were transferred onto glass substrates at surface pressures of 3 mN/m, 25mN/m, and 40 mN/m using the Langmuir-Blodgett (LB) technique. A shown in Chapter 3, as the surface pressure of the LB monolayers is increased, an evolution towards donut-shaped emission features is observed which arise from emission dipoles oriented normal to the membrane plane. As shown by others, these emission patterns can be modeled to quantitatively extract the three-dimensional orientation of the emission dipoles in the sample.[7-11] Using this approach, each emission feature is analyzed to extract the tilt angle (Φ) away from the membrane normal. Figure 4.2 shows representative tilt angle histograms for monolayers prepared at five different surface pressures along with the number of molecules analyzed at each pressure.

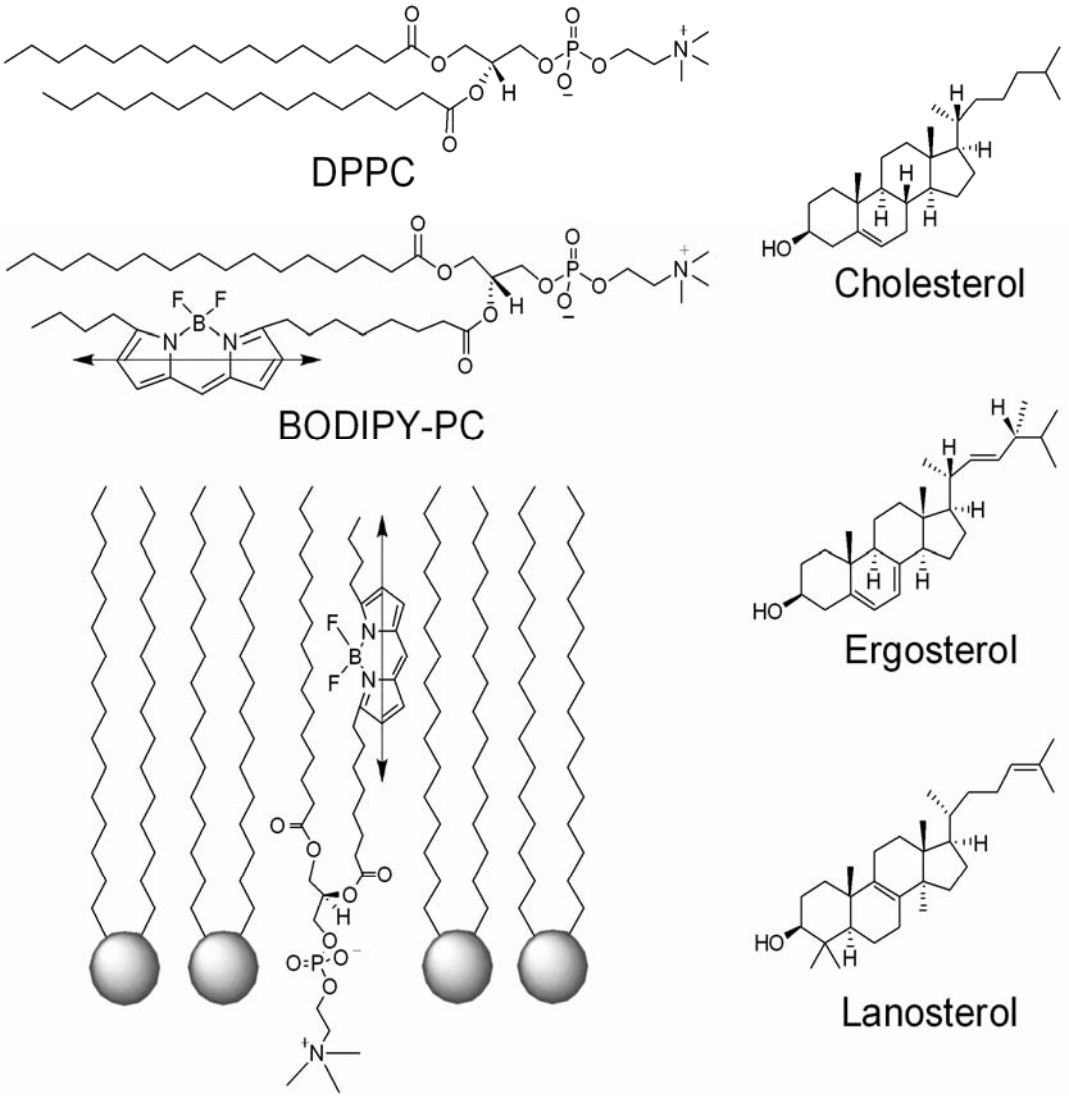

Figure 4.1. Structures of DPPC and the sterols studied in both monolayers and bilayers. Also shown is the structure of the fluorescent lipid analog BODIPY-PC which is used to quantify changes in the surrounding membrane film. BODIPY-PC has its fluorophore located in the tailgroup region so that its emission dipole (arrow) orientation is sensitive to changes in acyl chain orientation.

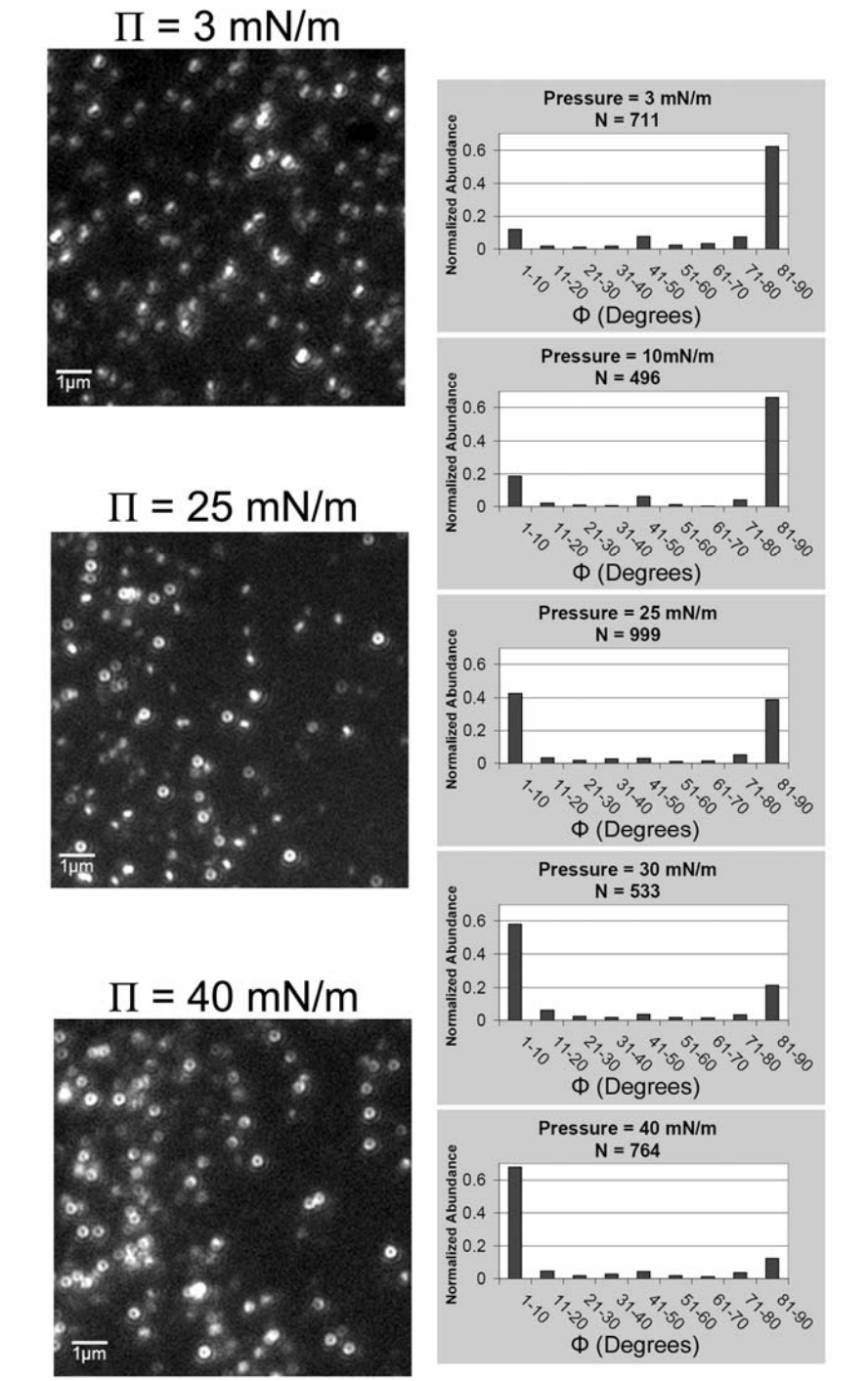

Figure 4.2. Representative single-molecule fluorescence images of DPPC monolayers doped with ~10^{-8} mol% BODIPY-PC, transferred onto glass substrates at the surface pressures (Π) indicated. As the surface pressure is increased, a rise in the number of donut-shaped single-molecule emission patterns is observed. These patterns arise from probes oriented with their emission dipole normal to the film surface and their increase reflects the increased order of the acyl chains at high surface pressures. Single-molecule tilt angle (Φ) histograms for all surface pressures studied are also shown.

At a surface pressure of 3 mN/m, the single-molecule tilt histogram reveals most of the dye probes are oriented in the plane of the film (≥81˚), reflecting the disorder in the DPPC monolayer at low surface pressures. This is seen in the corresponding emission image which contains mostly single-molecule features consisting of bright spots surrounded by wings that are characteristic of molecules oriented with large tilt angles. The tilt angle histogram, therefore, reveals a large population of emission dipoles oriented in the plane of the film with a smaller population spread through the remaining angles. The average tilt angle calculated from the histogram is 67.4 ± 5˚ (N = 711) at a surface pressure of 3 mN/m.

At the other surface pressure extreme, the single-molecule emission image for DPPC transferred at 40 mN/m reveals a large population of donut-like features reflecting emission dipoles that are oriented normal to the membrane surface. The corresponding tilt angle histogram shown in Fig. 4.2 reveals that most of the dye population have tilt angles ≤10˚ at this elevated surface pressure. This reflects the increased membrane order in the lipid monolayer at 40 mN/m, which reduces the average tilt angle to 22.4 ± 5˚ (N = 764).

At intermediate surface pressures, Fig. 4.2 reveals bimodal tilt distributions with the majority of molecules adopting orientations either normal or parallel to the membrane plane, with fewer adopting intermediate tilts. The bimodal distribution in tilt angles reflects BODIPY-PC partitioning into the lipid phases in the DPPC monolayer. At intermediate surface pressures, DPPC monolayers partition into domains of less ordered liquid-expanded (LE) phase and more ordered liquid-condensed (LC) phase leading to the observed bimodal tilt distribution.

As shown in Fig. 4.2 there is a steady rise in the population of molecules oriented normal to the DPPC monolayer as the surface pressure of the film is increased. A plot of the population of molecules oriented normal to the surface ($\Phi \leq 10^{\circ}$) as a function of surface pressure is shown in Fig. 4.3. DPPC monolayers were transferred onto glass substrates at eight different surface pressures between 3 mN/m and 45 mN/m with the results plotted in Fig. 4.3. The linear dependence with surface pressure provides a convenient marker of membrane order and a useful calibration for characterizing the surface pressure in bilayers.

4.3.2 Tracking Single Molecule Orientations in Supported Lipid Bilayers

Figure 4.4 (top panel) shows a defocused single-molecule PTIRF-M fluorescence image of a supported DPPC bilayer doped with ~10^{-8} mol% BODIPY-PC. Analysis of the single-molecule emission patterns leads to the emission dipole orientations shown in the middle panel. Analysis of 743 individual molecules from several bilayers results in the tilt angle histogram shown in the bottom panel of Fig. 4.4. As observed with DPPC monolayers formed with the LB technique, there is a bimodal distribution in the tilt angle histogram of the BODIPY-PC doped into the DPPC bilayers. From the histogram, the average tilt angle for the BODIPY-PC dye doped into DPPC bilayers is measured to be $45.2^{\circ} \pm 5^{\circ}$.

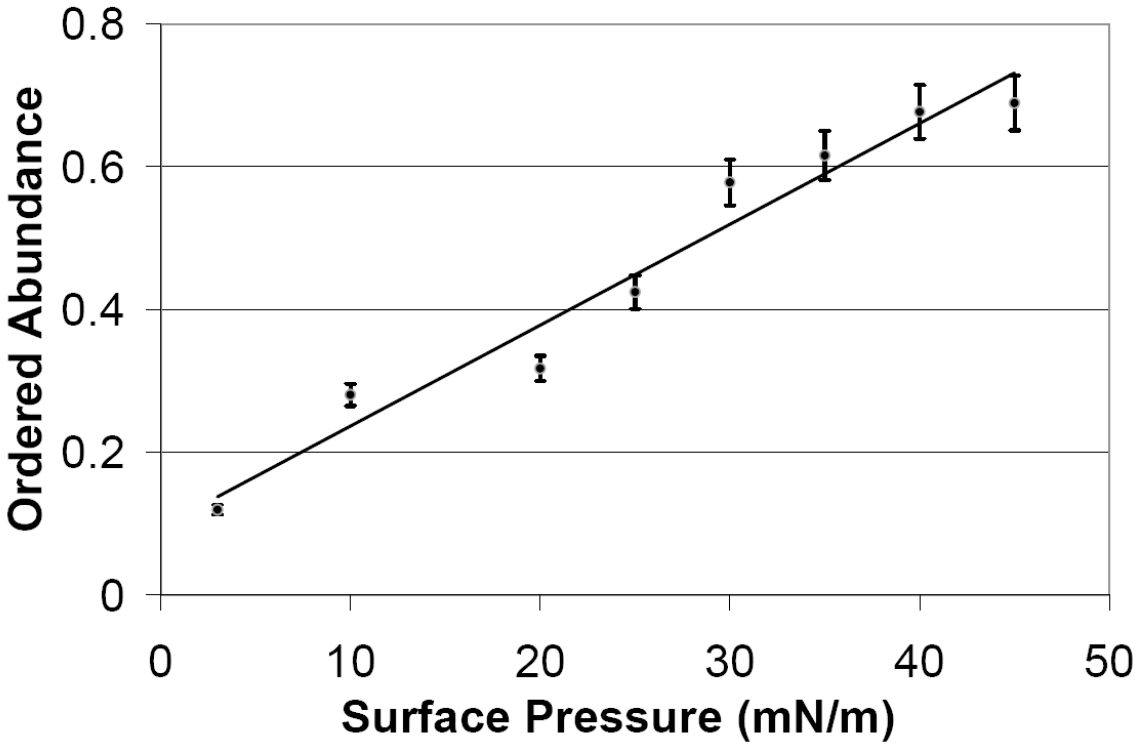

Figure 4.3. The percentage of BODIPY-PC probes oriented normal ($\Phi \leq 10^{o}$) to the membrane plane in DPPC monolayers as a function of surface pressure. A linear dependence ($R^2 = 0.96$) is observed which is used to quantify the equivalent surface pressure of bilayers (Figure 4.4). Also plotted above is the percentage area of LC regions in the DPPC monolayers as a function of surface pressure.

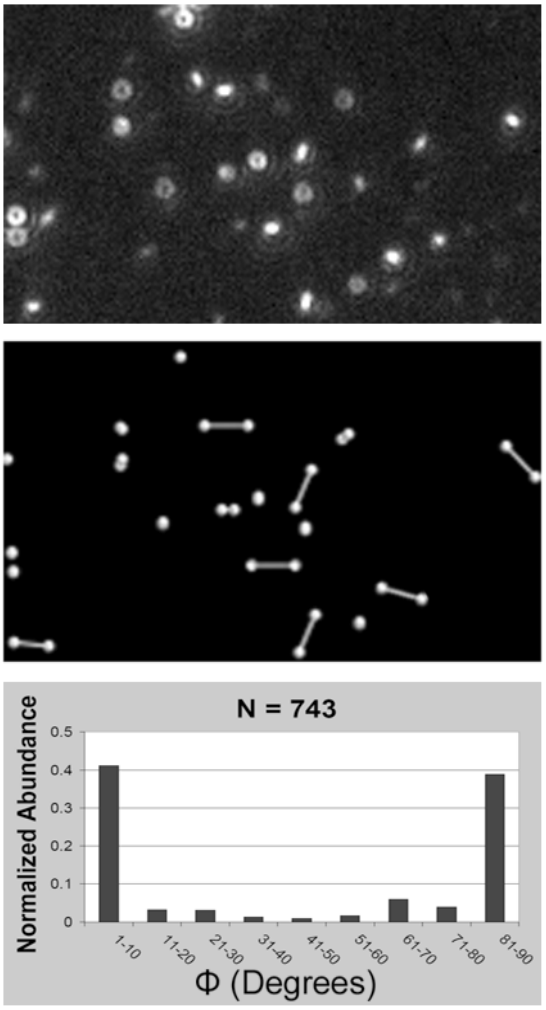

Figure 4.4. Representative single-molecule fluorescence image of a DPPC bilayer doped with ~10^{-8} mol% BODIPY-PC. Analysis of the single-molecule emission patterns results in the orientations shown schematically in the middle panel. Analysis of emission features from several bilayers results in the tilt angle histogram shown in the bottom panel. Using the percent of probes oriented normal to the surface and the plot in Fig. 4.3 results in an equivalent surface pressure of ~23 mN/m for DPPC bilayers.

The tilt angle histogram measured for supported bilayers in Fig. 4.4 can now be used to estimate the equivalence surface pressure of the bilayer using the data plotted for monolayers in Fig. 4.3. From the histogram in Fig. 4.4, the percentage of emission dipoles oriented normal to the membrane plane ($\Phi \leq 10^{\circ}$) in supported bilayers of DPPC is 41%. Single-molecule measurements on supported bilayers formed from both small unilamellar vesicles (SUV's) and giant unilamellar vesicles (GUV's) resulted in statistically identical results. The measured equivalent surface pressure of ~ 23 mN/m is somewhat smaller than the values obtained from other experiments (~30-35 mN/m).[1-5, 12-13]

4.3.3 Sterols – Effects of Additives on Monolayers and Bilayers at the "Equivalent Surface Pressure"

Having established the equivalent surface pressure for supported DPPC bilayers, the influence of sterol additives were compared in both LB monolayers transferred at 23 mN/m and DPPC bilayers. Cholesterol is widely distributed in biological membranes and exerts a well-known condensing effect.[14-17, 24-25] The profound influence of cholesterol on membrane properties can be traced to its structure, which is shown in Fig. 4.1. Cholesterol consists of a fused ring structure that is responsible for its rigid, planar geometry. There is a single hydroxyl group located at the C_3 position and an iso-octyl acyl chain extending from the opposite side of the ring at position C_{17}. Two methyl groups extend from the same side of the ring structure as the acyl chain, forming a β-configuration. When cholesterol inserts into lipid monolayers and bilayers, it orients with its polar hydroxyl group lying towards the hydrophilic phospholipid headgroups and the

hydrophobic ring structure aligned along the lipid acyl chains. The cohesive interactions between cholesterol and the lipid acyl chains are strongly linked with the degree of lipid saturation, making these interactions particularly important for lipids such as DPPC.

Figure 4.5 compares the effects of cholesterol on monolayers and bilayers of DPPC as probed through single-molecule orientation measurements. LB monolayers were transferred onto a glass substrate at a surface pressure of ~23 mN/m, which corresponds to the equivalent surface pressure of pure DPPC bilayers measured previously. Shown in Fig. 4.5 are the tilt angle histograms for monolayers and bilayers incorporating 0 mol%, 5 mol%, 10 mol%, and 33 mol% cholesterol. With no added cholesterol, the tilt angle histograms for both monolayers and bilayers are bimodal and closely agree with one another, as expected from their corresponding surface pressures. The population of BODIPY-PC molecules oriented normal to the film plane ($\Phi \leq 10^{\circ}$) is approximately 42% for both monolayers and bilayers, respectively.

As shown in Fig. 4.5, the addition of even small amounts of cholesterol (5 mol%) leads to a dramatic shift in the single-molecule tilt histograms. Upon the addition of 5 mol% cholesterol, the ordered abundance ($\Phi \leq 10^{\circ}$) increases from 42% to 59% in monolayers and from 41% to 52% in bilayers. The single-molecule tilt histograms summarized in Fig. 4.5 reveal a steady increase in the ordering of the acyl chains with increasing cholesterol content for both monolayers and bilayers. As cholesterol is increased, a steady rise in the number of BODIPY-PC molecules oriented normal to the plane ($\Phi \leq 10^{\circ}$) is observed with an associated drop in the population oriented in the membrane plane ($\Phi \geq 81^{\circ}$).

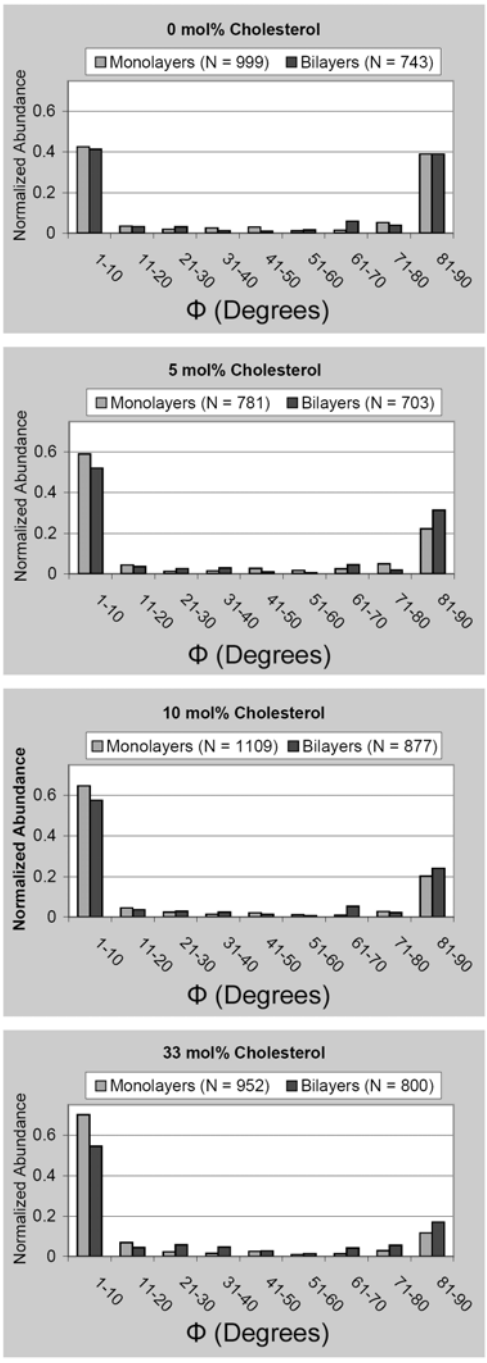

Figure 4.5. Comparison of tilt angle (Φ) histograms for DPPC monolayers (deposited at ~23 mN/m) and bilayers doped with increasing concentrations of cholesterol. At no added cholesterol, the tilt angle histograms for monolayers and bilayers reveal bimodal distributions that closely match one another, illustrating the corresponding surface pressure. As cholesterol increases, both films show large shifts in the single-molecule tilt populations toward more upright orientations ($\Phi \leq 10^{o}$). This is consistent with the well-known condensing effect of cholesterol.

Ergosterol and lanosterol provide useful structural analogs of cholesterol that can help clarify the unique role of cholesterol in modifying membrane properties. Ergosterol is generally found in the membranes of plants, while lanosterol predates cholesterol in the evolutionary pathway. As shown in Fig. 4.1, the structure of ergosterol is very similar to cholesterol and only differs slightly with a carbon-carbon double bond in the second steroid ring, an unsaturated side chain, and methylation at position C_{24}. Both cholesterol and ergosterol lead to condensing effects in membranes, although there is some disagreement regarding which has a larger effect.[19-21] Lanosterol, on the other hand, has three extra methyl groups on the α-surface of the ring system that are believed to increase the steric costs associated with membrane insertion (Fig. 4.1). Although lanosterol still has a condensing effect on membranes, studies agree that the effect is much smaller than that of either cholesterol or ergosterol.[19-21]

Figure 4.6 summarizes the results from defocused single-molecule PTIRF-M studies on monolayers and bilayers incorporating cholesterol, ergosterol, and lanosterol as a function of sterol concentration. Sterol concentrations of 0 mol%, 5 mol%, 10 mol%, and 33 mol% sterol are compared. Once again, LB monolayers were transferred at a surface pressure of ~23 mN/m to match the bilayer equivalent surface pressure determined earlier for pure DPPC. The results are summarized in Fig. 4.6 which plots the percentage of BODIPY-PC molecules oriented normal to the membrane plane ($\Phi \leq 10^{\circ}$) as a function of sterol concentration. The plot in Fig. 4.6 (top panel) shows that for both monolayers and bilayers, the population of dyes ordered normal to the membrane increases rapidly with cholesterol concentration and levels off at higher concentrations.

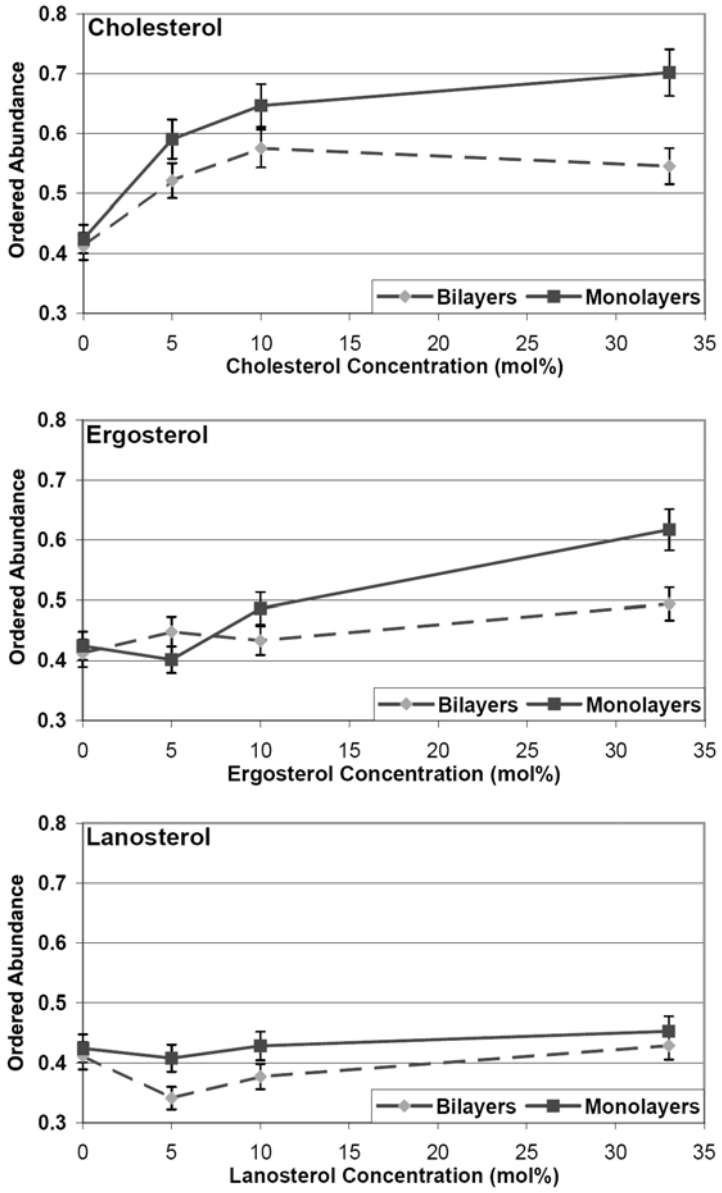

Figure 4.6. To compare the effects of cholesterol, ergosterol, and lanosterol on monolayers and bilayers of DPPC, the normalized population of BODIPY-PC probes oriented normal ($\Phi \leq 10^{o}$) to the surface is plotted versus sterol concentration. Monolayers were transferred at the bilayer equivalent surface pressure of ~23 mN/m. Small increases in cholesterol concentration lead to dramatic changes in both monolayers and bilayers while ergosterol is less effective at ordering the films. Lanosterol is the least effective at ordering DPPC films, with little or no change observed in the single-molecule tilt angle histograms.

The results for ergosterol, shown in Fig. 4.6 (middle panel), indicate a more subtle increase in membrane order with sterol concentration. Both monolayers and bilayers reveal an increase in order in the single-molecule PTIRF-M images, with monolayers being slightly more sensitive to ergosterol addition. Unlike the results for cholesterol, little effect on membrane ordering is observed at low ergosterol concentrations and only becomes significant in the single-molecule results at higher ergosterol concentration. For lanosterol, single-molecule orientation measurements reveal little influence on membrane ordering. Figure 4.6 (bottom panel) shows that the percentage of single-molecules oriented normal to the plane remains essentially constant for both monolayers and bilayers throughout the concentrations studied.

The bimodal distribution of single-molecule orientations observed in DPPC bilayers suggest coexisting lipid phases are present in both pure DPPC bilayers and those in which cholesterol has been added. Bulk fluorescence measurements on similar films find no evidence for coexisting domains on the sub-micron length scale.[26] However, both energy transfer measurements and some NMR studies have found evidence for coexisting domains in these systems.[27-30] These differences are often ascribed to the different length/time scales that are probed by the different techniques. The results shown here suggest single-molecule orientation measurements can provide a unique view of model lipid film properties that compliments other well established approaches.

The influence of cholesterol on high melting temperature lipids such as DPPC has been widely studied, yet a clear picture of its effects has yet to emerge. Different phase diagrams have been constructed based on results using different techniques, but most agree that these mixed bilayers can exist in the gel phase (S_o), liquid-crystalline (L_α), and

liquid-ordered (L_o) states. The latter is a cholesterol induced state whose name summarizes the combination of structural order with liquid-like dynamics in this state. The well-known condensing effects of cholesterol lead to extended acyl chains in this state, while translational diffusion and rotational motion remain liquid-like.[14-18]

4.3.4 Order Parameter – A Comparison with Literature Values

The single-molecule orientation measurements can be compared with previous bulk measures of membrane structure through the use of the order parameter, S. The order parameter is defined as

$$S = \tfrac{1}{2} (3\langle \cos^2\theta \rangle - 1)$$

where θ is the angle with respect to the membrane normal. Order parameters have been characterized in DPPC films as a function of cholesterol using techniques such as nuclear magnetic resonance (NMR), fluorescence anisotropy, and X-ray scattering.[19, 29, 31] The trends from these studies are summarized in Fig. 4.7 along with the results from our single-molecule measurements.

There is a striking similarity in the trends that are observed from our room temperature single-molecule studies and previous studies done above the transition temperature. Order parameters calculated using the average tilt angle from the single-molecule histograms show a sharp rise in S at low cholesterol concentration that levels off at higher concentrations. As shown in Fig. 4.7, this agrees closely with S values calculated from X-ray studies done at 45 ^{o}C.[31] Similar trends are also observed in the NMR and fluorescence studies carried out at 45 ^{o}C.

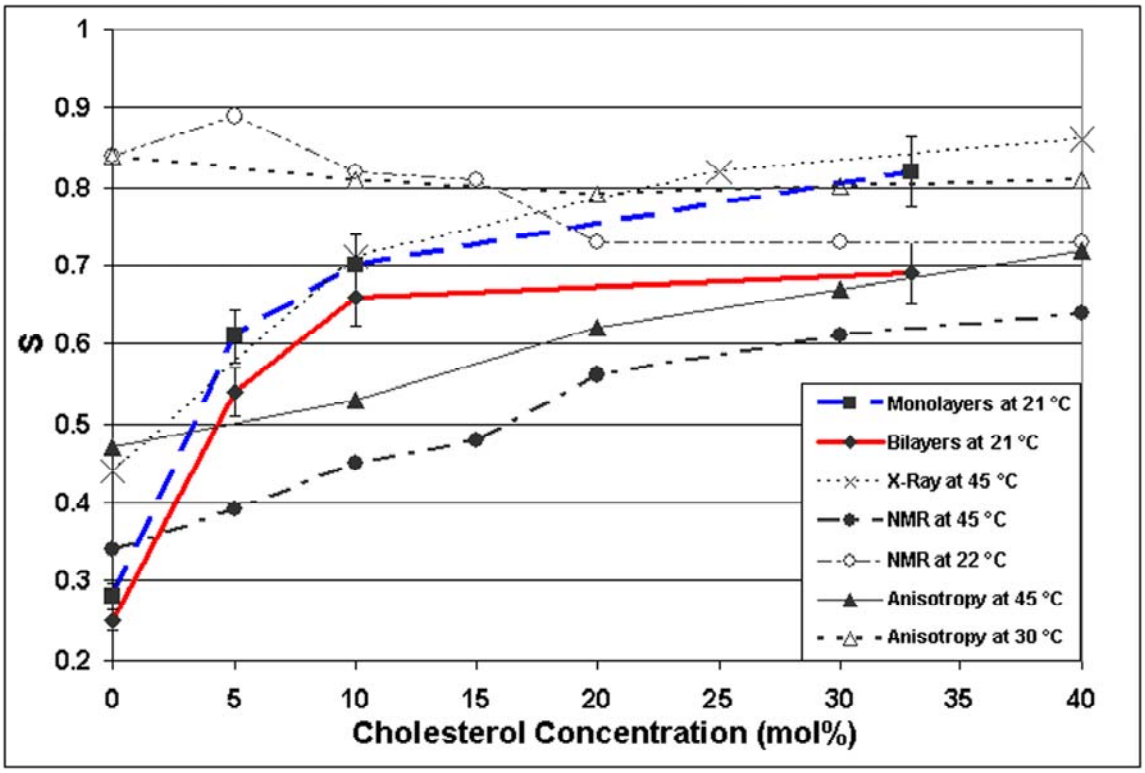

Figure 4.7. The order parameter, S, calculated from the average tilt angle found from the single-molecule tilt histograms is plotted as a function of cholesterol concentration. Also shown are trends in S found previously using NMR, fluorescence anisotropy, and X-ray measurements below and above the transition temperature for DPPC. (Adapted from references [19, 29, 31])

Also plotted in Fig. 4.7 are the results from NMR and fluorescence anisotropy studies done at room temperature that reveal high initial S values that decrease with cholesterol content.[19, 29] These changes do not track the changes we find in the single-molecule measurements which can be understood by recognizing that different techniques measure different aspects of membrane order. For example, S values derived from the NMR experiments provide a measure of the orientational freedom around the acyl chain axis. These measurements, therefore, provide insight into membrane packing. At room temperature, below the melting temperature for DPPC, NMR measurements of pure DPPC films yield high values for the order parameter. This results from the small degree of rotational freedom around the acyl chains and the high degree of lateral packing in the S_o phase. Upon the addition of cholesterol, however, the S values decrease due to the disruption of the gel state packing and increase in acyl chain freedom. Additional cholesterol further disrupts the lateral packing of the film and leads to the formation of the L_o phase, which has a greater degree of rotational freedom and thus a smaller S as compared to the gel phase.

Above the melting temperature, NMR studies of pure DPPC films in the fluid state yield S values that are small. The low S values arise from the increased freedom around the disordered acyl chains in this state. The addition of cholesterol, which has a condensing effect on DPPC, therefore, increases the order parameter as the L_o phase is formed. This transition is accompanied by a gel-like lateral packing with diffusional characteristics similar to the fluid phase.

For the single-molecule measurements summarized here at room temperature, the acyl chains in pure DPPC films have a high lateral packing and large tilt angles with

respect to the membrane normal which leads to the low calculated S values. The addition of cholesterol, which induces L_o phase formation, increases acyl chain order which is reflected in the PTIRF-M images as an increase in donut-like single-molecule emission features. This results in the large increase in S values calculated from the single-molecule measurements as cholesterol is increased. Since the NMR measurements track the lateral packing and rotational freedom of the acyl chains and the single-molecule measurements quantify the orientation of the acyl chains with respect to the membrane normal, the differences observed at room temperature in Fig. 4.7 are expected. At elevated temperature, however, the onset of the L_o phase increases lateral packing and decreases acyl chain tilt with respect to the membrane normal. This explains why the room temperature single-molecule measurements closely agree with previous studies done at 45 ^oC. Therefore, despite the differences in temperature between these studies, Fig. 4.7 reveals very good agreement between the single-molecule results and bulk measures of cholesterol added to DPPC membranes.

While the average single-molecule orientations leads to agreement with previous studies characterizing S in model mixed membranes of DPPC and cholesterol, the bimodal distribution observed illustrates the detailed information available from measuring the entire orientation distribution. Using single-molecules as probes of lipid environments can complement other more established techniques and provides a new tool for understanding these complicated systems at the molecular level.

4.4 Conclusions

Single-molecule fluorescence measurements taken using out-of-focus PTIRF-M are used to characterize the three-dimensional orientation of single BODIPY-PC dye molecules doped into model films of DPPC. For LB monolayers of DPPC, characterization of single-molecule orientation histograms as a function of surface pressure reveals an evolution in membrane order. At all surface pressures studied, a bimodal orientation histogram is observed which reflects the coexisting LE and LC phases present in the monolayer. There is a linear dependence in the number of BODIPY-PC molecules with transition dipoles oriented normal to the surface with surface pressure which is used to find the equivalent surface pressure in supported bilayers. Comparison of the single-molecule orientation histogram from DPPC bilayers with the results from the LB monolayers suggests an equivalent surface pressure of ~23 mN/m for bilayers. This is somewhat lower than the currently accepted value of ~30-35 mN/m.[1-3, 5, 12-13]

With the equivalent surface pressure for bilayers established, single-molecule studies comparing the effects of cholesterol, ergosterol, and lanosterol on membrane properties are compared between DPPC bilayers and LB monolayers transferred at ~23 mN/m. Single-molecule orientation as a function of sterol content tracked closely between monolayers and bilayers. Cholesterol had the largest effect on membrane order, increasing the number of BODIPY-PC molecules oriented normal to the surface even at low cholesterol content. Lanosterol had essentially no effect on the single-molecule orientations while ergosterol did affect orientations, but to a lesser extent than cholesterol. Using the average orientation from the histograms as a function of

cholesterol content, the order parameter S was calculated and compared with previous NMR and X-ray studies.[29, 31] Close agreement is observed between the room temperature single-molecule results and previous bulk measures of membrane order done at higher temperatures.

Now that we have a useful technique for tracking membrane order at the single molecule level, we can extend these studies to look at the affects the probe has on the films. As will be discussed in the next chapter, we can compare our experimental data with the results from a collaboration utilizing Molecular Dynamics studies. We can also study several different lipid analogs by simply changing the placement of the chromophore along the acyl chain, and use this to probe different aspects of membrane properties, as will be discussed in the future directions in Chapter 7.

4.5 References

1. Marsh, D., Lateral pressure in membranes. *Biochim. Biophys. Acta* **1996,** *1286* (3), 183-223.

2. Seelig, A., Local-Anesthetics and Pressure - a Comparison of Dibucaine Binding to Lipid Monolayers and Bilayers. *Biochim. Biophys. Acta* **1987,** *899* (2), 196-204.

3. Boguslavsky, V.; Rebecchi, M.; Morris, A. J.; Jhon, D. Y.; Rhee, S. G.; Mclaughlin, S., Effect of Monolayer Surface Pressure on the Activities of Phosphoinositide-Specific Phospholipase-C-Beta-1, Phospholipase-C-Gamma-1, and Phospholipase-C-Delta-1. *Biochemistry* **1994,** *33* (10), 3032-3037.

4. Portlock, S. H.; Lee, Y.; Tomich, J. M.; Tamm, L. K., Insertion and Folding of the Amino-Terminal Amphiphilic Signal Sequences of the Mannitol and Glucitol Permeases of Escherichia-Coli. *J. Biol. Chem.* **1992,** *267* (16), 11017-11022.

5. Schindler, H.; Quast, U., Functional Acetylcholine-Receptor from Torpedo-Marmorata in Planar Membranes. *Proc. Natl. Acad. Sci.* **1980,** *77* (5), 3052-3056.

6. Livanec, P. W.; Dunn, R. C., Single-Molecule Probes of Lipid Membrane Structure. *Langmuir* **2008,** *24* (24), 14066-14073.

7. Bartko, A. P.; Dickson, R. M., Imaging three-dimensional single molecule orientations. *J. Phys. Chem. B* **1999,** *103* (51), 11237-11241.

8. Bartko, A. P.; Dickson, R. M., Three-dimensional orientations of polymer-bound single molecules. *J. Phys. Chem. B* **1999,** *103* (16), 3053-3056.

9. Forkey, J. N.; Quinlan, M. E.; Goldman, Y. E., Measurement of single macromolecule orientation by total internal reflection fluorescence polarization microscopy. *Biophys. J.* **2005,** *89* (2), 1261-1271.

10. Patra, D.; Gregor, I.; Enderlein, J., Image analysis of defocused single-molecule images for three-dimensional molecule orientation studies. *J. Phys. Chem. A* **2004,** *108* (33), 6836-6841.

11. Toprak, E.; Enderlein, J.; Syed, S.; McKinney, S. A.; Petschek, R. G.; Ha, T.; Goldman, Y. E.; Selvin, P. R., Defocused orientation and position imaging (DOPI) of myosin V. *Proc. Natl. Acad. Sci.* **2006,** *103* (17), 6495-6499.

12. Gershfeld, N. L.; Tajima, K., Spontaneous Formation of Lecithin Bilayers at the Air-Water Surface. *Nature* **1979,** *279* (5715), 708-709.

13. Miller, C. E.; Majewski, J.; Watkins, E. B.; Mulder, D. J.; Gog, T.; Kuhl, T. L., Probing the local order of single phospholipid membranes using grazing incidence x-ray diffraction. *Phys. Rev. Lett.* **2008,** *100* (5), 058103.

14. Silvius, J. R., Role of cholesterol in lipid raft formation: lessons from lipid model systems. *Biochim. Biophys. Acta* **2003,** *1610* (2), 174-183.

15. Yeagle, P. L., The Roles of Cholesterol in the Biology of Cells. In *The Structure of Biological Membranes*, 2nd ed.; CRC Press LLC: 2005.

16. Mouritsen, O. G.; Zuckermann, M. J., What's so special about cholesterol? *Lipids* **2004,** *39* (11), 1101-1113.

17. Ohvo-Rekila, H.; Ramstedt, B.; Leppimaki, P.; Slotte, J. P., Cholesterol interactions with phospholipids in membranes. *Prog. Lipid Res.* **2002,** *41* (1), 66-97.

18. Quinn, P. J.; Wolf, C., The liquid-ordered phase in membranes. *Biochimica Et Biophysica Acta-Biomembranes* **2009,** *1788* (1), 33-46.

19. Bernsdorff, C.; Winter, R., Differential properties of the sterols cholesterol, ergosterol, beta-sitosterol, trans-7-dehydrocholesterol, stigmasterol and lanosterol on DPPC bilayer order. *J. Phys. Chem. B* **2003,** *107* (38), 10658-10664.

20. Cournia, Z.; Ullmann, G. M.; Smith, J. C., Differential effects of cholesterol, ergosterol and lanosterol on a dipalmitoyl phosphatidylcholine membrane: A molecular dynamics simulation study. *J. Phys. Chem. B* **2007,** *111* (7), 1786-1801.

21. Sabatini, K.; Mattila, J. P.; Kinnunen, P. K. J., Interfacial behavior of cholesterol, ergosterol, and lanosterol in mixtures with DPPC and DMPC. *Biophys. J.* **2008,** *95* (5), 2340-2355.

22. Hellen, E. H.; Axelrod, D., Fluorescence Emission at Dielectric and Metal-Film Interfaces. *J Opt Soc Am B* **1987,** *4* (3), 337-350.

23. Karolin, J.; Johansson, L. B. A.; Strandberg, L.; Ny, T., Fluorescence and Absorption Spectroscopic Properties of Dipyrrometheneboron Difluoride (Bodipy) Derivatives in Liquids, Lipid-Membranes, and Proteins. *J. Am. Chem. Soc.* **1994,** *116* (17), 7801-7806.

24. Ege, C.; Ratajczak, M. K.; Majewski, J.; Kjaer, K.; Lee, K. Y. C., Evidence for lipid/cholesterol ordering in model lipid membranes. *Biophys. J.* **2006,** *91* (1), L1-L3.

25. McMullen, T. P. W.; Lewis, R. N. A. H.; McElhaney, R. N., Cholesterol-phospholipid interactions, the liquid-ordered phase and lipid rafts in model and biological membranes. *Curr. Opin. Colloid Interface Sci.* **2004,** *8* (6), 459-468.

26. Keller, S. L., Coexisting liquid phases in lipid monolayers and bilayers. *Journal of Physics-Condensed Matter* **2002,** *14* (19), 4763-4766.

27. Brown, A. C.; Towles, K. B.; Wrenn, S. P., Measuring raft size as a function of membrane composition in PC-Based systems: Part 1 - Binary systems. *Langmuir* **2007,** *23* (22), 11180-11187.

28. Polozov, I. V.; Gawrisch, K., Characterization of the liquid-ordered state by proton MAS NMR. *Biophys. J.* **2006,** *90* (6), 2051-2061.

29. Scheidt, H. A.; Huster, D.; Gawrisch, K., Diffusion of cholesterol and its precursors in lipid membranes studied by H-1 pulsed field gradient magic angle spinning NMR. *Biophys. J.* **2005,** *89* (4), 2504-2512.

30. Silvius, J. R., Fluorescence energy transfer reveals microdomain formation at physiological temperatures in lipid mixtures modeling the outer leaflet of the plasma membrane. *Biophys. J.* **2003,** *85* (2), 1034-1045.

31. Mills, T. T.; Toombes, G. E. S.; Tristram-Nagle, S.; Smilgies, D. M.; Feigenson, G. W.; Nagle, J. F., Order parameters and areas in fluid-phase oriented lipid membranes using wide angle x-ray scattering. *Biophys. J.* **2008,** *95* (2), 669-681.

Chapter 5

Probing Lipid Membrane Properties using Orientation of Fluorescent Lipid Analog BODIPY-PC: Experimental and Simulation Studies

5.1 Introduction

The bulk of the research presented in this dissertation is directed towards obtaining a better understanding of lipid membrane structure at the single molecule level. By utilizing p-polarized total internal reflectance fluorescence microscopy and slightly defocusing the optics, the emission patterns from single molecules can be analyzed, and therefore, the emission dipole orientations found.[1-8] This chapter focuses on a collaboration with Dr. Wonpil Im and Kevin Song in the Bioinformatics Department at the University of Kansas, on molecular dynamics (MD) simulations of the lipid analog, BODIPY-PC, in monolayers and bilayers of DPPC. Comparisons between experiment and simulation provide detailed views of how BODIPY-PC inserts into lipid membranes and how monolayers and bilayers compare with one another.

5.2 Molecular Dynamics (MD) Simulations and Experimental Comparison

5.2.1 Introduction

As discussed before, model lipid membranes have been widely used as models for biological membranes due to the difficulties associated with studying intact tissues. These simplified models enable precise control over membrane components and experimental conditions. As such, these studies have collectively revealed detailed insights into membrane structure, phase behavior, and the influence of important membrane additives, such as cholesterol. As shown in the previous chapter, single-

molecule fluorescence measurements reveal insights into membrane properties in both monolayers and bilayers.[1-2] These studies utilized out-of-focus polarized total internal reflectance fluorescence microscopy (PTIRF-M) to characterize the three-dimensional orientation of the fluorescent lipid analog BODIPY-PC, doped into DPPC membranes. For Langmuir-Blodgett monolayers, these measurements showed that the tilt angle of the BODIPY-PC fluorophore is sensitive to surface pressure.[2] As surface pressure is increased, a linear evolution towards small tilt angles was observed, reflecting the increase in the acyl chain order. The tilt angle dependence on surface pressure was used to construct a calibration plot to find the equivalent surface pressure for bilayers.[1]

While trends in the single-molecule orientation measurements clearly reflect changes in membrane structure, many important questions remain unresolved: 1) what is the correspondence between monolayer and bilayer systems, 2) where does the probe position within the membrane, and 3) what are the microscopic driving forces determining the orientation of the reporter dye at different surface pressures. To address these questions, a total of 1.5 μs comparative molecular dynamics (MD) simulations of monolayer and bilayer DPPC systems incorporating one BODIPY-PC molecule per leaflet were carried out at low (~3 mN/m), mid (~10 mN/m), and high (~40 mN/m) pressures. The simulation results are compared with experimental data measured at 323 K. The orientation of reporter molecules will be compared between MD simulations and experimental results to evaluate the insertion of the fluorophore into the membranes and the microscopic driving forces responsible for their properties.

5.2.2 Molecular Dynamics (MD) Setup

Using Membrane Builder on www.CHARMM-GUI.org, a DPPC membrane with 64 lipids on each leaflet was created. Single BODIPY-PC molecules were inserted into the upper and bottom leaflets, respectively that contained a total of 4635 water molecules and 0.15M KCl. The simulations were carried out with fixed surface pressure and constant surface area. The temperature of the system was set to 323 K, and the simulations ran for 50 ns after 3 ns equilibration for each of 30 systems.

5.2.3 Varying Pressure Systems

Five bilayer and five monolayer systems were created at three different pressure systems: low pressure (~3 mN/m), medium pressure (~10 mN/m), and high pressure (~40 mN/m). While keeping the number of lipids on top and bottom leaflets constant, the surface area (i.e., the *XY* plane of the simulation box) was changed to alter the surface pressure applied to the membranes, as shown in Fig. 5.1. The surface areas of low pressure, medium pressure, and high pressure were 77 $Å^2$, 64 $Å^2$, 40 $Å^2$ per lipid, respectively. The five bilayer and five monolayer systems were assigned different velocities in order to increase the conformational sampling.

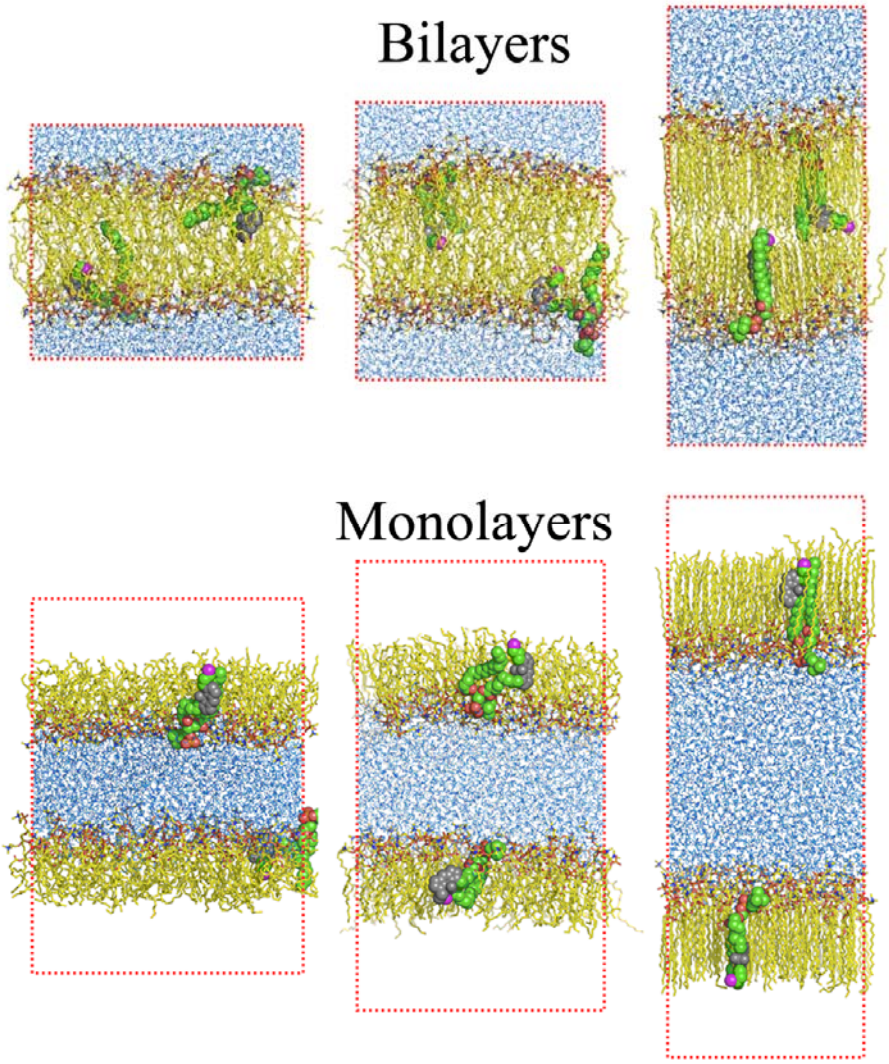

Figure 5.1 Molecular Systems of bilayer (top) and monolayer (bottom) systems at ~3 mN/m (low pressure, left), ~10 mN/m (medium pressure, middle), and ~40 mN/m (high pressure, right). The red boxes represent approximate system sizes.[9]

5.2.4 Experimental Setup

DPPC (Avanti Polar Lipids, Alabaster, AL) was obtained and used without further purification. The fluorescent lipid analog BODIPY-PC (Invitrogen Corporation, Carlsbad, CA, B3794) was used, as in the previous chapters. For the preparation of monolayers, DPPC was dissolved in chloroform (1mg/ml stock solutions). The solutions were doped with ~10^{-8} mol % BODIPY-PC reporter dye, and dispersed onto a subphase of ultra-pure water (18 MΩ) in a Langmuir-Blodgett trough (Type 611, Nima Technology, Coventry, England). For studies done above the transition temperature of DPPC, a water circulator bath (Neslab RTE-140, Thermo Scientific, Waltham, MA) was used to circulate water under the Teflon surface of the LB trough to maintain a temperature of 50 ±1˚C. Once the lipid/chloroform mixture was dispersed on the subphase, the chloroform was allowed to evaporate for 15 minutes. DPPC monolayers were compressed at a speed of 100 cm^2/min to approximately 45 mN/m and then expanded at a speed of 80 cm^2/min. The compression/expansion cycles were repeated twice to anneal the monolayer. The monolayer film was then compressed to the target pressure, held for approximately 15-20 minutes, and then transferred in a headgroup down geometry onto a Piranha cleaned glass substrate at a dipping speed of 25 mm/min. Monolayers were prepared above the transition temperature of DPPC (~50˚C).

All films were imaged using a total internal reflection fluorescence microscope (TIRF-M) (Olympus IX71, Center Valley, PA) equipped with a 100x objective (1.45 NA achromat). The 514 nm line from an argon ion laser (Coherent Innova 70 Spectrum, Santa Clara, CA) was directed through half-wave and quarter-wave plates (Newport, Irvine, CA) to generate p-polarized excitation. Excitation was directed through the

objective and fluorescence collected in an epifluorescence geometry with the optics defocused ~500 nm. The fluorescence was filtered with a combination of a dichroic mirror and long pass filters (Chroma, Rockingham, VT) and imaged onto a CCD camera (Cascade 650, Roper Scientific, Tucson, AR). Image collection was controlled with Slidebook software (Version 4.2, Intelligent Imaging Innovations, Denver, CO) and analyzed using MatLab software (Natick, MA).

5.3 Analysis

5.3.1 Tilt Angle Distributions

The orientation of BODIPY-PC molecules was characterized in terms of its tilt, azimuthal, and rotation angles by defining two primary vectors on the BODIPY-PC molecule. The tilt angle is defined by the angle between CL2-CR2 vector and the *Z*-axis (the membrane normal). Azimuthal angle is defined by the angle between CL2-CR2 vector and the Y-axis. Rotation angle is defined by projecting the *Z*-axis onto a plane that uses CL2-CR2 vector as normal and finding the angle between B-CC vector and the projected vector, as shown in Fig. 5.2.

5.3.2 Energetics

To characterize the microscopic driving forces of the dye molecule tilt, the non-bonded interaction energy between the dye molecule and the environment (DPPC and water molecules) as a function of dye tilt from the trajectories, was calculated. This energy is constituted as the enthalpic energy contribution on the tilt of the dye molecule as will be discussed later.

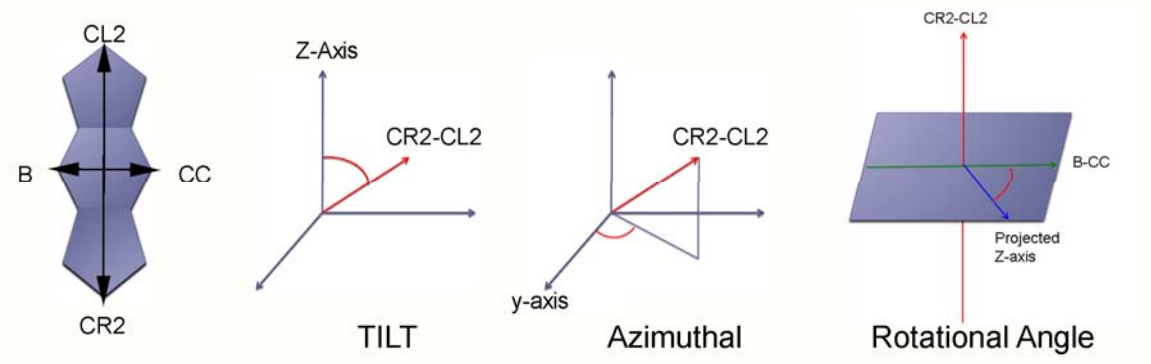

Figure 5.2 BODIPY-PC molecule and the definitions of the vectors. The CL2-CR2 vector is the principal vector that is used to calculate tilt and azimuthal angles by finding the angle between the vector and the z-axis and y-axis, respectively. The B-CC vector was used to calculate the rotation angle by projecting the z-axis onto a plane parallel to the B-CC vector and calculating the angle between the z-axis and the B-CC vector.

5.4 Comparison of Results for MD and Experimental

Figure 5.3 shows the distribution of BODIPY-PC tilt angles (CL2-CR2 vector shown in Fig. 5.2) in monolayer and bilayer MD simulations of DPPC at three different surface pressures. The tilt angle distributions reveal striking similarities between the monolayer and bilayer systems at each pressure. In addition, between monolayers and bilayers, the azimuthal and rotation angles show the same similarity (results not shown). At high surface pressure, the fluorophore molecule is predominantly aligned normal to the membrane with most of the population lying with tilt angles less than 20˚ from the membrane normal. As the pressure is reduced, the BODIPY-PC tilt angle becomes larger and broader in both monolayers and bilayers. A second peak around 40-50˚ in the high-pressure bilayer system, which is missing in the monolayer results, is due to a dye molecule trapped in a tilted conformation during the simulations. Interestingly, BODIPY-PC can have a tilt angle close to 180˚ intermittently. This can occur when the BODIPY fluorophore, which is located in the tailgroup, bends back around and interacts with the headgroup region. It is unclear whether this orientation would persist in longer simulations. The experiments cannot distinguish this tilt angle as 180˚ looks the same as 0˚. This shows that MD simulations can add new insight into how reporter probes insert into model membranes and what interactions occur on the mesoscale.

These results strongly suggest that the fluorescent lipid analog BODIPY-PC does respond to changes in the surrounding membrane environment and that its tilt angle is a sensitive marker of membrane surface pressure, as shown experimentally. In addition, a close agreement between the monolayer and bilayer systems suggests that monolayers can be used to approximate bilayer systems.

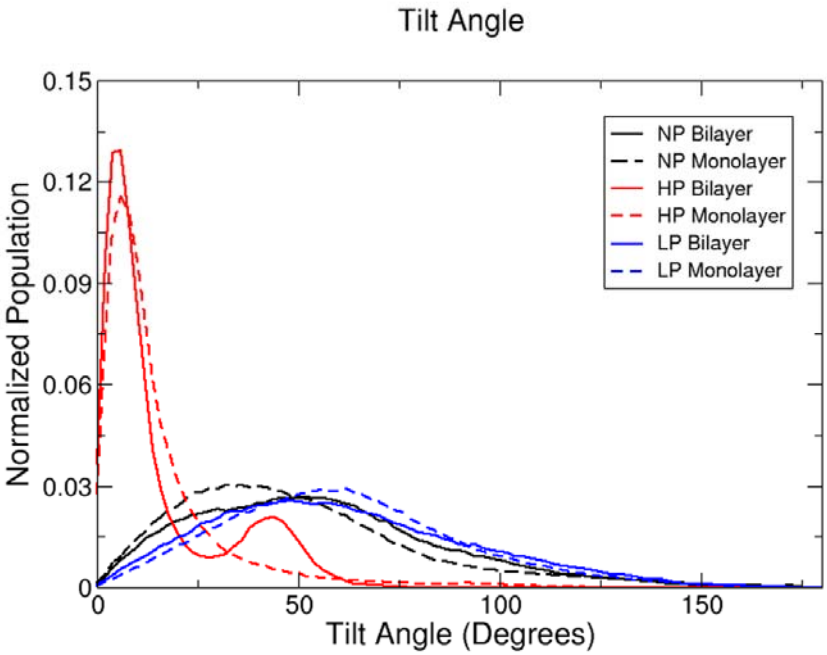

Figure 5.3 BODIPY tilt angle distributions from the Molecular Dynamics simulations of low (blue), mid (black), and high (red) pressure systems.[9]

The fluorescence from single BODIPY-PC dye molecules doped into membranes at ~10^{-8} mol % are also individually analyzed to extract the three-dimensional orientation of the emission dipole (approximated by vector CL2-CR2 shown in Fig. 5.2). Measurements such as these, therefore, enable a direct comparison to be made between the single molecule orientation measurements and the single molecule simulations discussed above. Langmuir-Blodgett (LB) monolayers of DPPC were transferred onto glass substrates at the low (3 mN/m), medium (10 mN/m), and high (40 mN/m) surface pressures to match those in the simulations. The films were transferred at a temperature of 323 K, above the transition temperature of DPPC. Figure 5.4 shows the distributions of BODIPY-PC tilt angles measured using the single molecule fluorescence measurements discussed in earlier chapters. Figure 5.4 shows the results from single molecule orientations at both low and high surface pressures.

A bimodal distribution in tilt angles is observed at both surface pressures, consistent with previous measurements done at room temperature.[1-2] At both pressures, large populations of molecules are observed oriented normal to the surface ($\leq 10^{o}$) and in the plane of film ($\geq 80^{o}$), with roughly 20 % oriented at intermediate angles, consistent with coexisting phases. The MD results are also plotted in Fig. 5.4 from 0^{o} to 90^{o}. The MD results shown in Fig. 5.3 have been re-weighted and plotted from 0° to 90^{o} since the experimental studies cannot distinguish between tilts separated by 180° from each other. As discussed earlier, the MD simulations at low pressure reveal a broad distribution of tilt angles centered at large angles, which sharpen and shift to smaller angles at higher pressure. There is a clear trend of increased order in the system as the surface pressure is increased in both the experiments and MD simulations.

Unlike the experimental results, however, the MD simulations do not show the bimodal distribution mostly due to the relatively small membrane areas simulated, which are not capable of capturing macroscopic phase behavior. The characteristic bimodal distributions in the experimental results arise from lipid phase coexistence that is not captured in the relatively small membrane areas used in the simulations. Nonetheless, the agreement between experiment and simulation, showing a shift in the tilt angle populations upon the increase of surface pressure, demonstrates that such experiments can capture the membrane properties.

To explore the order present in the lipid membranes, the order parameters of all the lipids in the monolayer and bilayer systems were calculated for each pressure in the MD simulations, as shown in Fig. 5.5. As expected, order parameters for all carbons are highest in the high-pressure systems and decrease as surface pressure decreases. Again, we find very close agreement between monolayers and bilayers with only a slight discrepancy in the low-pressure systems. This may arise from the increased interdigitation between the tail groups in bilayer systems at low surface pressure, which is absent in the monolayer systems.[10]

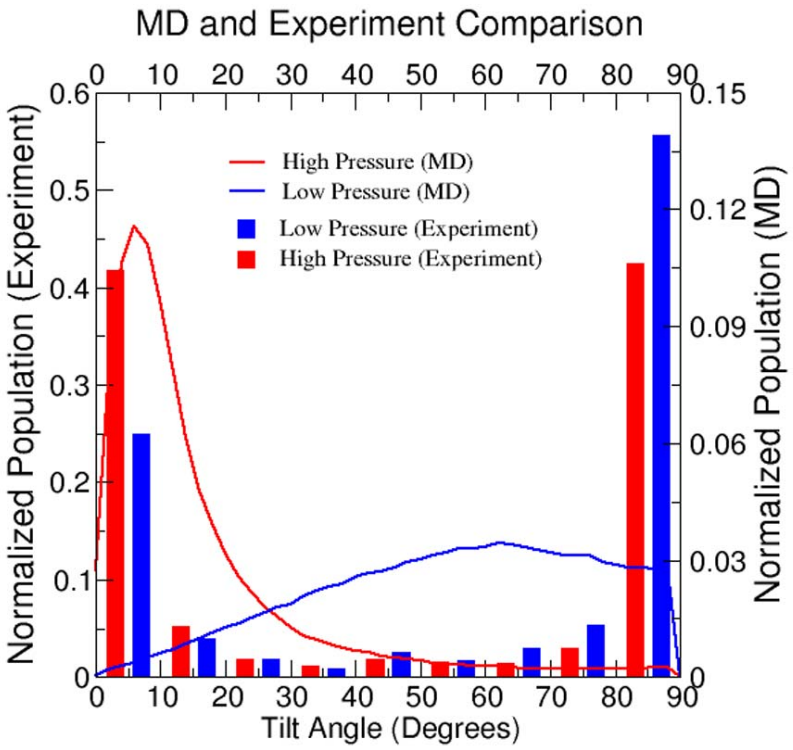

Figure 5.4 A comparison between the MD simulations and experimental results is shown. A clear trend of increased ordering in the system is seen as the surface pressure is increased. The bimodal distribution is also seen in both the MD simulations (combination of results) and the experimental data.[9]

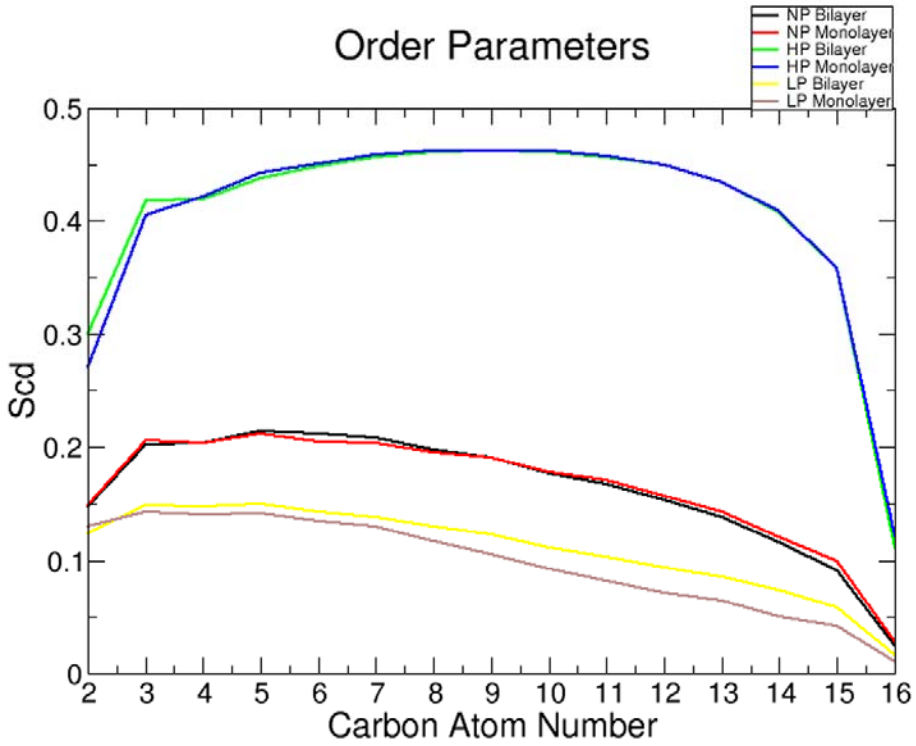

Figure 5.5 The order parameters for all lipids in the MD system are shown at low (LP), high (HP) and mid (NP) pressures. At high and mid pressures the results between monolayers and bilayers agree relatively well, but at low pressure, the monolayer and bilayer systems diverge slightly.

It is interesting to compare the order parameters from the MD simulations with those extracted from the single molecule orientation measurements. For comparison, order parameters are calculated from the experimental data by using the average tilt angle and from the MD simulations by averaging order parameters from all carbons (Fig. 5.5), using the equation:

$$S = \frac{3\cos^2\theta - 1}{2} \tag{5.1}$$

Where S is the order parameter and θ is the average tilt angle of the acyl chain. Both experiments and simulations reveal linear trends with similar slopes in the order parameter that increases with surface pressure. The offset obtained in Fig. 5.6likely arises from the phase coexistence in monolayer experiments.

Additional questions exist, such as, what are the microscopic driving forces that govern such orientational changes of the BODIPY-PC dye molecule with surface pressure changes? Lee and Im have previously shown that single-pass transmembrane helix tilting in membranes is governed by the intrinsic entropy from the helix precession around the membrane normal as well as specific helix-membrane interactions.[11-13] Using a similar approach, the interaction energies (i.e., the enthalpic contribution) on BODIPY-PC were calculated as a function of tilt angle for the BODIPY-PC / DPPC system. Figure 5.7 shows that at low and mid pressures, the enthalpic contribution remains approximately constant as a function of dye tilt angle. This illustrates that tilting of the dye molecule at these pressures is driven by the entropic contribution, which is consistent with the increased freedom of movement for the dye at these pressures. However, there is a significant interaction energy cost associated with larger tilt angles of BODIPY-PC at high surface pressure. Therefore, the enthalpic contribution becomes dominant due to the

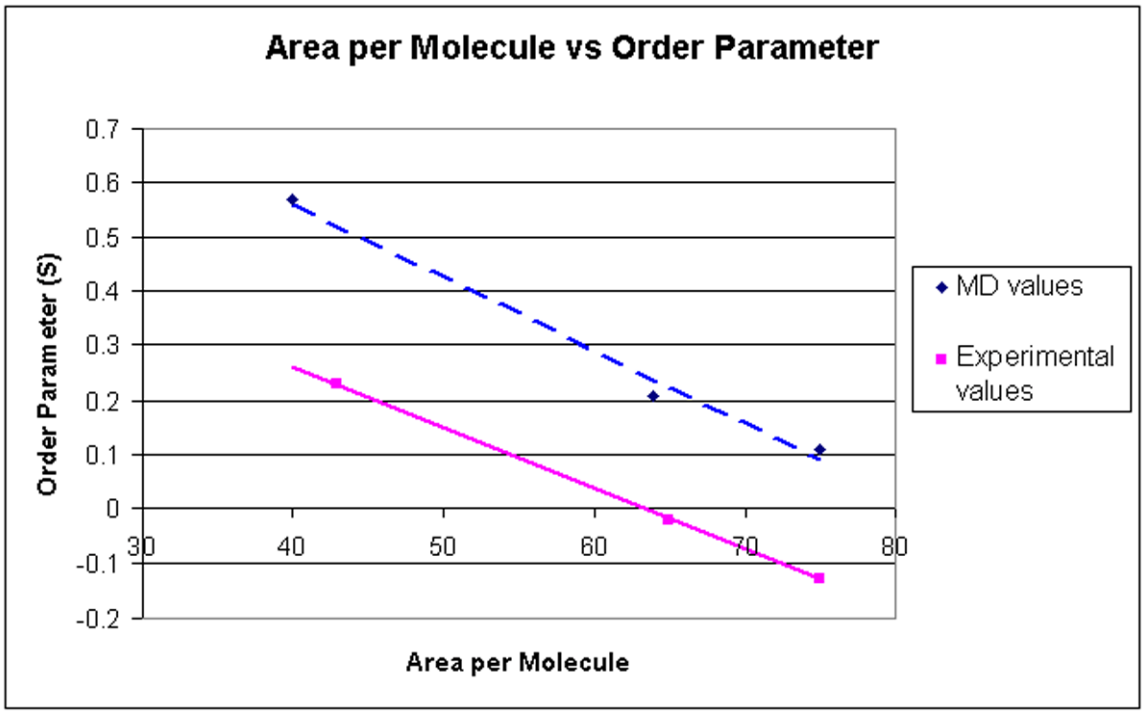

Figure 5.6 A plot of the order parameter vs. area per molecule for the experimental and MD monolayer results is shown. The MD values are plotted by the blue dashed line and were calculated from the average of all carbons in the acyl chain (from Fig. 5.5). The experimental values are plotted by the solid pink line and were calculated from the average tilt angle of the BODIPY molecule. The results agree relatively well with the offset most likely due to phase coexistence in the experimental results.

increased membrane packing at high surface pressure. This helps to identify the microscopic driving forces that reorient the reporter fluorophores with increasing surface pressures.

The BODIPY fluorophore interacts predominately with the lipid acyl chains. As shown in Fig. 5.8. In the low and mid pressure monolayer and bilayer systems, the BODIPY-PC fluorophore interacts slightly with the water molecules (shown in blue) and lipid headgroups (shown in red), but mostly interacts with the lipid acyl chain (shown in green). Also shown in Fig. 5.8, as the surface pressure is increased, the BODIPY-PC molecules interact almost exclusively with the lipid acyl chains (shown in green). This suggests that the fluorophore resides mainly in the lipid acyl chain region and can act as a good reporter molecule for the structure of the lipid acyl chains.

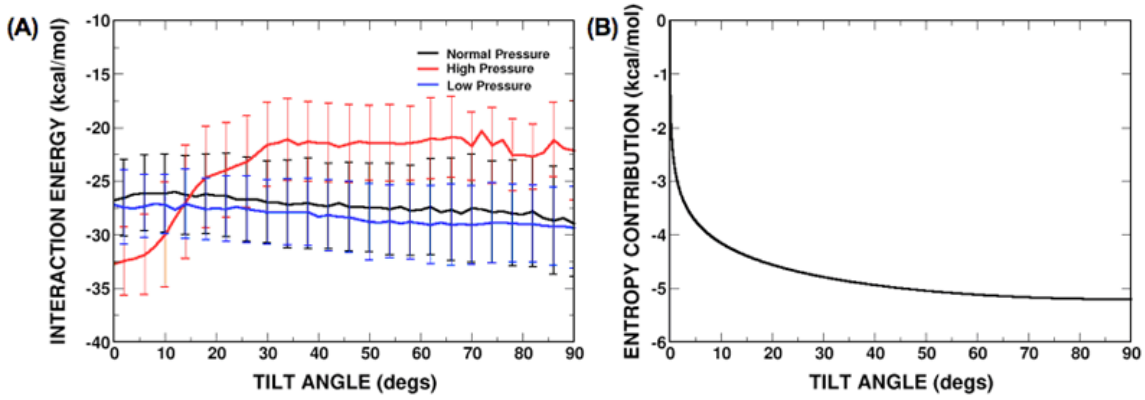

Figure 5.7 **(A)** Interaction energy vs. tilt angle is plotted showing at lower surface pressures, entropic contributions are dominant, but at high pressures, enthalpic contributions become dominant. Also illustrated in **(B)** is the entropic cost associated with larger tilt angles.[9]

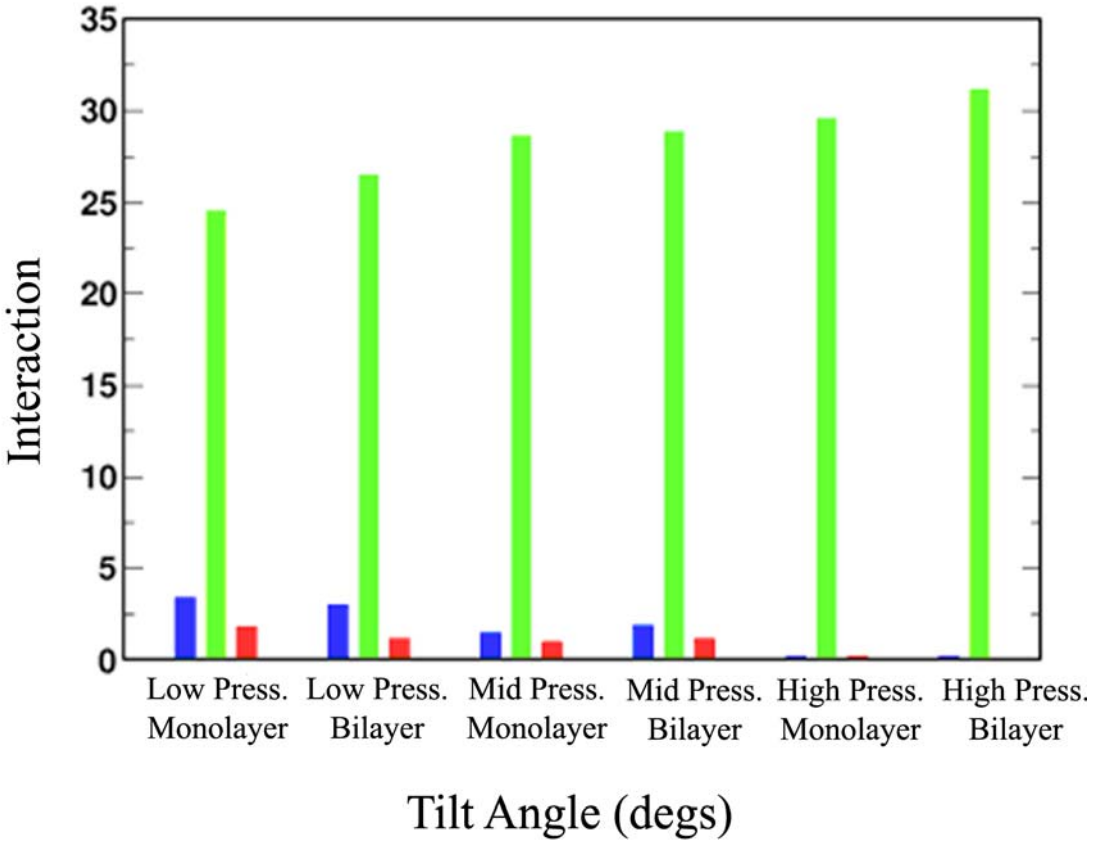

Figure 5.8 Average number of contacts with water (blue), lipid acyl chains (green), and lipid headgroups (red) with the BODIPY-PC fluorophore.[9] Low, mid, and high pressures for both monolayers and bilayers are listed.

5.5 Conclusions

In summary, the MD simulations of the BODIPY-PC dye molecule at three surface pressures reveal very close agreement between the monolayer and bilayer systems in terms of the dye orientation and lipid order. This observation suggests that monolayer experiments can be used to approximate bilayer systems. Such comparisons help reveal any similarities between the monolayer and bilayer systems and provide a basis for understanding the recent single molecule measurements characterizing BODIPY-PC tilt angles in similar films. Finally, the simulations provide new insights into the microscopic driving forces governing dye molecule tilting; the enthalpic contribution is dominant at high pressure conditions to have smaller tilt angles and the entropy contribution is dominant at medium and low pressures to have larger tilt angles. It is also shown that the BODIPY fluorophore resides mainly in the hydrophobic acyl chains, thereby providing a useful reporter of the acyl chain orientation.

5.6 References

1. Livanec, P. W.; Huckabay, H. A.; Dunn, R. C., Exploring the Effects of Sterols in Model Lipid Membranes Using Single-Molecule Orientations. *J. Phys. Chem. B* **2009,** *113* (30), 10240-10248.

2. Livanec, P. W.; Dunn, R. C., Single-Molecule Probes of Lipid Membrane Structure. *Langmuir* **2008,** *24* (24), 14066-14073.

3. Bartko, A. P.; Dickson, R. M., Imaging three-dimensional single molecule orientations. *J. Phys. Chem. B* **1999,** *103* (51), 11237-11241.

4. Bartko, A. P.; Dickson, R. M., Three-dimensional orientations of polymer-bound single molecules. *J. Phys. Chem. B* **1999,** *103* (16), 3053-3056.

5. Forkey, J. N.; Quinlan, M. E.; Goldman, Y. E., Measurement of single macromolecule orientation by total internal reflection fluorescence polarization microscopy. *Biophys. J.* **2005,** *89* (2), 1261-1271.

6. Patra, D.; Gregor, I.; Enderlein, J., Image analysis of defocused single-molecule images for three-dimensional molecule orientation studies. *J. Phys. Chem. A* **2004,** *108* (33), 6836-6841.

7. Toprak, E.; Enderlein, J.; Syed, S.; McKinney, S. A.; Petschek, R. G.; Ha, T.; Goldman, Y. E.; Selvin, P. R., Defocused orientation and position imaging (DOPI) of myosin V. *Proc. Natl. Acad. Sci.* **2006,** *103* (17), 6495-6499.

8. Hellen, E. H.; Axelrod, D., Fluorescence Emission at Dielectric and Metal-Film Interfaces. *J Opt Soc Am B* **1987,** *4* (3), 337-350.

9. Song, K. C.; Livanec, P. W.; Klauda, J. B.; Kuczera, K.; Dunn, R. C.; Im, W., Probing Lipid Membrane Properties using Orientation of Fluorescent Lipid Analog BODIPY-PC: Simulation and Experimental Studies. *In Preparation* **2009**.

10. Kaiser, R. D.; London, E., Determination of the depth of BODIPY probes in model membranes by parallax analysis of fluorescence quenching. *Biochimica Et Biophysica Acta-Biomembranes* **1998,** *1375* (1-2), 13-22.

11. Jo, S.; Kim, T.; Iyer, V. G.; Im, W., Software news and updates - CHARNIM-GUI: A web-based grraphical user interface for CHARMM. *J. Comput. Chem.* **2008,** *29* (11), 1859-1865.

12. Lee, J.; Im, W., Transmembrane helix tilting: Insights from calculating the potential of mean force. *Phys. Rev. Lett.* **2008,** *100* (1).

13. Jo, S.; Lim, J. B.; Klauda, J. B.; Im, W., CHARMM-GUI Membrane Builder for Mixed Bilayers and Its Application to Yeast Membranes. *Biophys. J.* **2009,** *97* (1), 50-58.

Chapter 6

Fuming Method for Micropatterning Structures on Diblock Copolymer and Langmuir-Blodgett Films and Reducing Photo-bleaching Rates in Single Molecule Studies

6.1 Introduction

Exploring and developing new methods for fabricating and manipulating structures on the submicron length scale have rapidly developed over the last decade. Interest in these structures revolves around potential applications in fields such as sensing, drug delivery, or analysis on miniaturized platforms.[1-3] These applications often take advantage of miniaturization to increase performance characteristics of a particular device or exploit unique phenomena that arise as a result of the reduced dimension. As a result, much activity has centered on developing new methods for rapidly patterning surfaces.[4]

Patterning techniques are often classified as conventional or unconventional depending on their stage of development.[5-7] Conventional techniques are considered the more developed methods that are commercially available and utilized in manufacturing. This category includes methods such as photolithography and particle beam lithography, which are widely adopted in industry and form the mainstay of many manufacturing processes in the microelectronics industry.[7-8] Photolithography approaches are rapid and allow for patterning large surface areas in parallel while serial techniques, such as particle beam lithography, are slower but generally enable higher spatial resolution. Together these techniques provide powerful capabilities for micropatterning surfaces. However, they often require expensive equipment, have limited flexibility in the materials

patterned, and generally do not work well on curved substrates. These and other limitations have led to research exploring unconventional micropatterning approaches.

A great deal of research has explored methods classified as soft lithographic approaches which have proven versatile for patterning structures onto surfaces.[5, 9] In general, these approaches use a master manufactured using a conventional approach to act as a form for creating a polymer mold or stamp.[5] These methods enable many replicas to be manufactured from a single master, thus relaxing the reliance on expensive instrumentation. These techniques can pattern large surface areas with sub-100 nm features and are amenable to patterning curved surfaces.[10] For even smaller features, scanning probe microscopy has proven useful.

Scanning probe techniques such as scanning tunneling microscopy (STM) and atomic force microscopy (AFM) have been adapted for patterning surfaces down to the atomic level.[11] Techniques such as dip-pen nanolithography use the transfer of material from an AFM tip to the substrate to write features as small as ~10 nm onto a substrate.[12-13] While these techniques offer exquisite control over the lateral feature size, the serial nature of the process makes them generally slow. This, however, is beginning to be addressed with the development of multi-tip platforms that enable the parallel writing of features.

Other approaches for micropatterning surfaces have taken advantage of natural structures formed in thin films. Inorganic films, self-assembled monolayers, and di-block copolymers can all be used to produce highly ordered, repeating structures on surfaces.[14-16] Self-assembly and self-organization processes have been extensively studied in the past decade. Diblock copolymers consist of two chemically distinct polymer chains

covalently bonded to each other. Usually, one chain is hydrophobic and the other hydrophilic. The two chains are immiscible and, therefore, undergo phase separation and self assemble into ordered patterns that are dependent on the length of each copolymer chain. Since the pattern dimensions depend on among other factors, the chain length, patterns on the order of tens to hundreds of nanometers and can be controlled by using copolymers with different chain lengths. The self-assembly process is self-initiated so simply spin coating the copolymer onto an atomically smooth surface, such as mica, and allowing time to anneal is all that is required for the self assembly process to occur.

Micro patterning surfaces using diblock copolymer thin films is advantageous for many reasons. The process is much cheaper and faster than most conventional lithography techniques. The copolymer chains can be tuned to change the features and properties of the resulting film. Also, the chains can have different etching rates, which can lead to preferential etching of the hydrophilic or hydrophobic chain to remove one chain. Diblock copolymer thin films can also be used for nano-reactors that provide high surface areas for the synthesis and catalysis of inorganic nano-particles, synthesis of nano-pores, and to fabricate vertical arrays of nano-wires with densities in excess of 1.9 x 10^{11} cm^{-2}.

The Langmuir-Blodgett (LB) technique has also been extensively used to study the two-dimensional phase structure present in lipid monolayers and multi-layer films transferred onto a solid support[17-23] as discussed in the previous chapter. The phase structure present in the resulting LB monolayer leads to long range patterns in the film, the particular structure of which is influenced by the components of the film and the conditions used to transfer the film onto the support. These two-dimensional films,

however, have found limited applications in microfabrication due to challenges associated with extending these structures into the third dimension. Therefore, while the LB approach allows for periodic structures to be patterned onto surfaces rapidly, modifying and controlling the feature height has proven problematic.

Here we demonstrate a technique for micropatterning surfaces that is rapid and offers a high degree of control over both the lateral and vertical feature size. One method uses di-block copolymers to pattern solid substrates and the other uses the LB technique to transfer a lipid monolayer onto a substrate under conditions that leads to the formation of distinct two-dimensional structures. We take advantage of the patterns formed in the di-block copolymer and LB film to template the growth of a polymer using a fuming method. In the fuming method, a supported di-block copolymer or lipid LB film is exposed to fumes from a cyanoacrylate, such as ethyl 2-cyanoacrylate.[24] The cyanoacrylate molecules undergo anionic polymerization in the presence of a weak Lewis base, such as water, to form a strong durable polymer. The varying hydration levels of the structures formed in the underlying organic films, therefore, template the growth of the polymer. This process leads to the growth of three-dimensional structures with lateral dimension controlled by the structure present in the underlying LB or diblock film and vertical dimension controlled by the length of the fuming process. Using this process, we show that structures can be fabricated onto both flat and curved surfaces with nanometric control.

In addition to patterning surfaces, we also show that we can greatly reduce the amount of photo-bleaching for fluorophores suspended in the underlying film using this process. BODIPY is a robust fluorophore, but still undergoes photo-bleaching quite

readily in the presence of oxygen. By fuming the same single molecule films as studied in Chapters 2-5, we show that we can greatly increase the lifetime of the fluorophores while the molecular structure in the monolayers remains unchanged. This may provide a very useful approach for applications that are plagued from loss of signal due to photo-bleaching.

6.2 Experimental and Methods

6.2.1 Langmuir-Blodgett Deposition

1,2-dipalmitoyl-*sn*-glycero-3-phosphocholine (DPPC) (Avanti Polar Lipids, Alabaster, AL) was dissolved in spectral grade chloroform (Fisher Scientific, Fairlawn, NJ) at a concentration of 1 mg/mL. Approximately 50 μL of the DPPC solution was dispersed onto a water subphase (18 MΩ) in a computer controlled Langmuir-Blodgett (LB) trough (Model 611, Nima Technology, Coventry, England). The suspended lipid monolayer was compressed at a rate of 100 cm^2/min to the desired surface pressure, which was monitored with a Wilhelmy pressure sensor. DPPC monolayers were transferred onto a freshly cleaved mica substrate in a head group down arrangement (Y-type). For experiments on curved substrates, DPPC monolayers were transferred onto 1.0 mm O.D. x 0.75 mm I.D. borosilicate glass capillaries (Sutter Instrument, Novato, CA). Films were transferred at a rates ranging from 10 - 40 mm/min, depending on the patterning desired. All films were transferred from a subphase held at ~ 21 ºC.

6.2.2 Di-block Copolymer Deposition

Asymmetric copolymers of polystyrene (PS) and polyethylene oxide (PEO) were used in this study. Poly(styrene-b-ethylene oxide) (PS-b-PEO = 19.0-6.4 (Mn x 10^3)) (Polymer Source, Inc.) was dissolved in HPLC grade benzene (Fisher Scientific) at a concentration of 5 - 10 mg/mL. Approximately 50 μL of this prepared solution was placed on a freshly cleaved mica substrate and spin coated. The prepared substrate was allowed to dry at room temperature for ~1 hour. Mica substrates were spin coated at different speeds (using a Variac controller) depending on the features and thickness desired. The same concentration solution can be used to coat the mica surface and let it dry without spin-coating. This will produce larger holes and thicker films.

The same asymmetric copolymer as above was used to coat curved surfaces. A piece of double sided tape was placed on a small round magnetic puck. Then a small piece of a stripped fiber optic (Nufern) diameter of 125μm ± 1.5μm (cleaned with isopropyl alcohol) was placed on the tape. Approximately 50μL of the diblock copolymer solution was placed onto the puck and spin coated the same as above. The prepared substrate was allowed to dry at room temperature for ~1 hour.

After spin coating the substrates, the thin film could then be exposed to approximately 5mL of HPLC grade benzene vapors in a closed container for ~ 10 minutes to 2 hours. The exposure to the benzene vapors helped to further "organize" the nanodomains. This was done when nanometric patterns were desired.

6.2.3 Cyanoacrylate Fuming

Following diblock copolymer or LB deposition of DPPC onto a substrate, films were exposed to fumes from the cyanoacrylic resin, ethyl 2-cyanoacylate (Sigma-Aldrich, St. Louis, MO). Briefly, the supported diblock copolymer film or DPPC monolayer was transferred into a sealed chamber containing approximately 0.03 g of ethyl 2-cyanoacrylate. Prior to sample introduction, the cyanoacrylate resin was heated to ~ 50 ºC using a heat lamp to accelerate the fuming process. Following cyanoacrylate heating, the diblock copolymer or LB film was introduced into the sealed chamber and exposed to the cyanoacrylate fumes for seconds to minutes, depending on the vertical feature size desired.

6.2.4 Atomic Force Microscopy

Atomic force microscopy (AFM) measurements (Nanoscope IIIa, Veeco Instruments, Santa Barbara, CA) were carried out in contact mode using silicon nitride cantilevers with a spring constant of 0.12 N/m (Veeco Instruments, Santa Barbara, CA).

6.2.5 Intensity Decay Measurements

DPPC (Avanti Polar Lipids, Alabaster, AL) was dissolved in spectral grade chloroform (Fisher Scientific, Fairlawn, NJ) at a concentration of 1 mg/mL. BODIPY-PC was added to a concentration of ~ 0.25 mol%. Approximately 50 μL of the DPPC solution was dispersed onto a water subphase (18 MΩ) in a computer controlled Langmuir-Blodgett (LB) trough (Model 611, Nima Technology, Coventry, England). The suspended lipid monolayer was compressed at a rate of 100 cm^2/min to the desired

surface pressure, which was monitored with a Wilhelmy pressure sensor. DPPC monolayers were transferred onto a freshly cleaved mica substrate in a head group down arrangement (Y-type). Films were transferred at the desired surface pressure. All films were transferred from a subphase held at ~ 21 ºC. Once the films were made, they were imaged using a total internal reflection fluorescence microscope (TIRF-M) (Olympus IX71, Center Valley, PA) equipped with a 100x objective (1.45 NA achromat). The 514 nm line from an argon ion laser (Coherent Innova 70 Spectrum, Santa Clara, CA) was measured with film in place, to be a constant 10.3 mW. The fluorescence was filtered with a combination of a dichroic mirror and long pass filters (Chroma, Rockingham, VT) and imaged onto a CCD camera (Cascade 650, Roper Scientific, Tucson, AR). Total integration time was 20-25 seconds, or until the fluorophores were photobleached. Image collection was controlled with Slidebook software (Version 4.2, Intelligent Imaging Innovations, Denver, CO).

6.3 Results and Discussion

6.3.1 LB film analysis

The pressure isotherm for DPPC, such as that shown in Chapter 2 (see Fig. 2.2), has been thoroughly studied and exhibits a plateau region at low surface pressures where the liquid-expanded (LE) and liquid-condensed (LC) phases coexist.[21] LB films of DPPC can exhibit distinct patterns that are sensitive to the surface pressure and conditions under which the film is transferred onto the substrate.[20] For example, LB monolayers of DPPC transferred in the phase coexistence region of the pressure isotherm exhibit distinctive semi-circular LC domains surrounded by LE regions in the monolayer (Fig. 2.4). At

lower surface pressures and faster dipping velocities, previous studies have found that hydrodynamic instabilities lead to the formation of stripes in the films.[18]

Figure 6.1A shows an AFM image of a typical DPPC monolayer transferred under conditions that lead to the formation of stripes. The DPPC monolayer was deposited onto a mica substrate at a surface pressure of 3.0 mN/m and a dipping velocity of 10 mm/min. Previous studies have shown that at these elevated dipping velocities, wetting instabilities lead to films with hydrophilic stripes separated by lipid regions that are hydrophobic. The stripes are observed as small height differences in the 20 μm x 20 μm AFM image shown in Fig. 6.1A. There is a small ~ 1 nm height difference between the hydrophilic stripes and the taller hydrophobic lipid regions as shown in the line-cut in Fig. 6.1A. Under these particular transfer conditions, the widths of the hydrophilic and hydrophobic stripes are ~0.85 μm and ~3.0 μm, respectively.

Figure 6.1B shows a similar DPPC film that was subsequently exposed to fumes of ethyl 2-cyanoacrylate for approximately 2 minutes following transfer onto the mica substrate. The stripes in the film are still clearly visible, however, as the line-cut displayed in Fig. 6.1B shows, the height differential has now grown to ~ 150 nm. By exposing the LB film to the cyanoacrylate fumes, a preferential polymerization reaction takes place in the hydrophilic regions of the film which can be used to build up three dimensional structures. The origin of this is understood from the reaction mechanism shown in Scheme 1 and the schematic shown in Fig. 6.2.

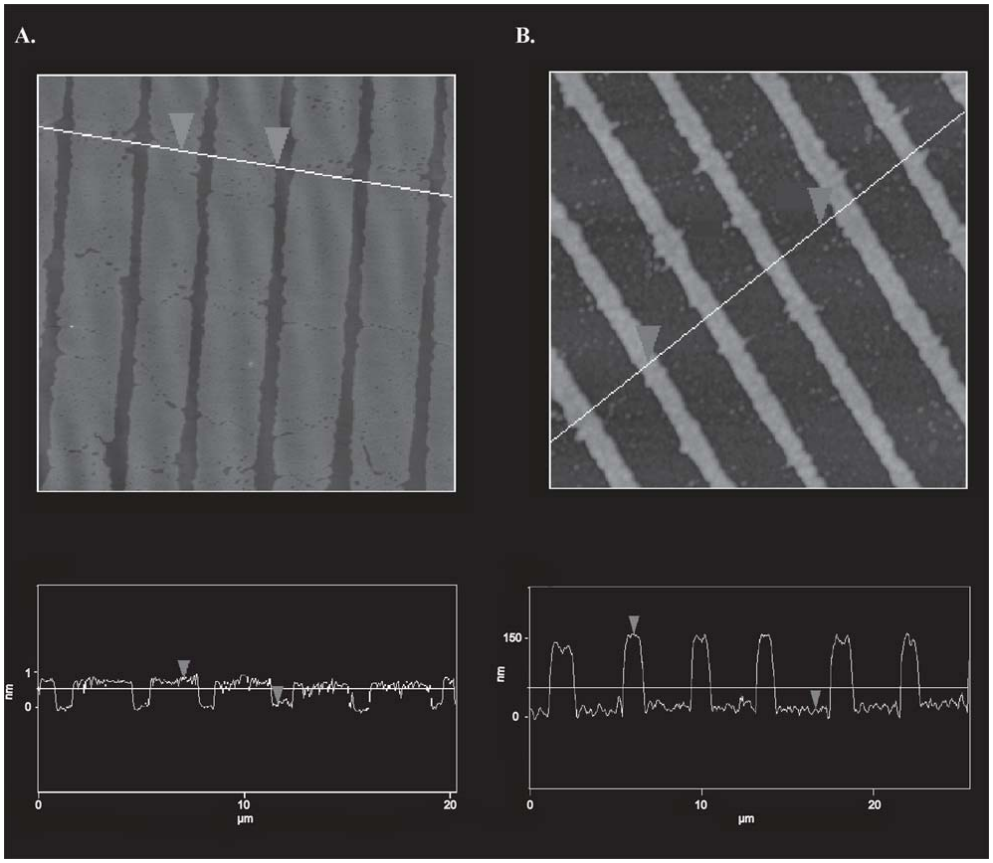

Figure 6.1 **(A)** AFM image of a LB film of DPPC transferred onto mica under conditions that lead to the formation of stripes in the film. The line-cut shown below reveals a ~ 1 nm height difference between the hydrophobic lipid stripes and the mica substrate. **(B)** A similar film following fuming with ethyl 2-cyanoacylate for approximately 2 minutes. Preferential polymerization in the hydrophilic regions of the film leads to the formation of channels. The line-cut below shows that the difference in feature height is now ~ 150 nm following polymer growth.

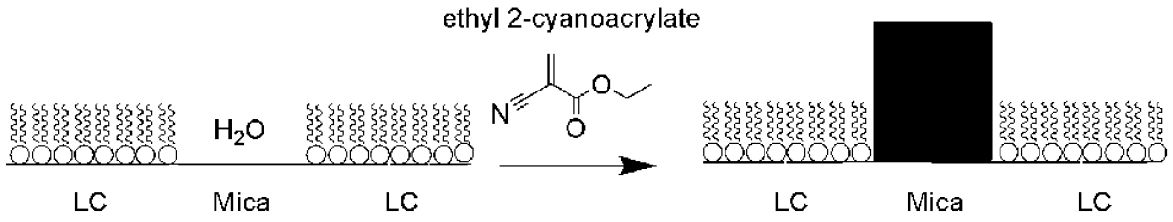

Figure 6.2 Schematic representation of the polymerization process. Hydrophilic regions in the deposited LB film lead to the preferential polymerization and growth of three dimensional structures.

Cyanoacrylate molecules undergo anionic polymerization in the presence of a weak Lewis base, such as water, to form a strong durable polymer. The patterned hydrophilic and hydrophobic areas in the LB film, therefore, provide a template that dictates where the polymerization reaction can proceed as shown in Fig. 6.2. For the films shown in Fig. 6.1, therefore, the narrow hydrophilic stripes preferentially support the polymerization reaction leading to the increase in their height.

Scheme 1

Initation

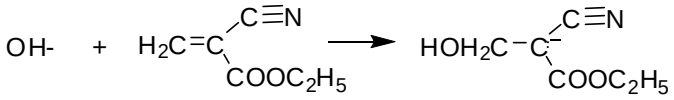

Propagation

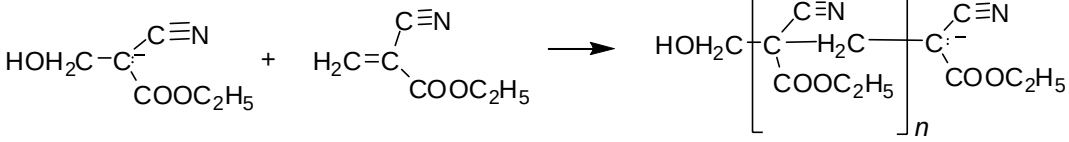

It is also straightforward to modify the size and spacing of the channels through changes in the film transfer conditions and fuming length. As an example, Fig. 6.3 shows a range of channels fabricated by varying these conditions. Figures 6.3A, 6.3B, and 6.3C display channels that are 530 nm, 700 nm, and 3.0 μm wide, respectively, templated by increasing the velocity at which the LB film was transferred. The average height profiles displayed, moreover, show that the channel depths are 15 nm, 100 nm, and 150 nm, respectively, reflecting changes in exposure times during the fuming process. With this approach, vertical features from a few nanometers to microns can be fabricated in minutes.

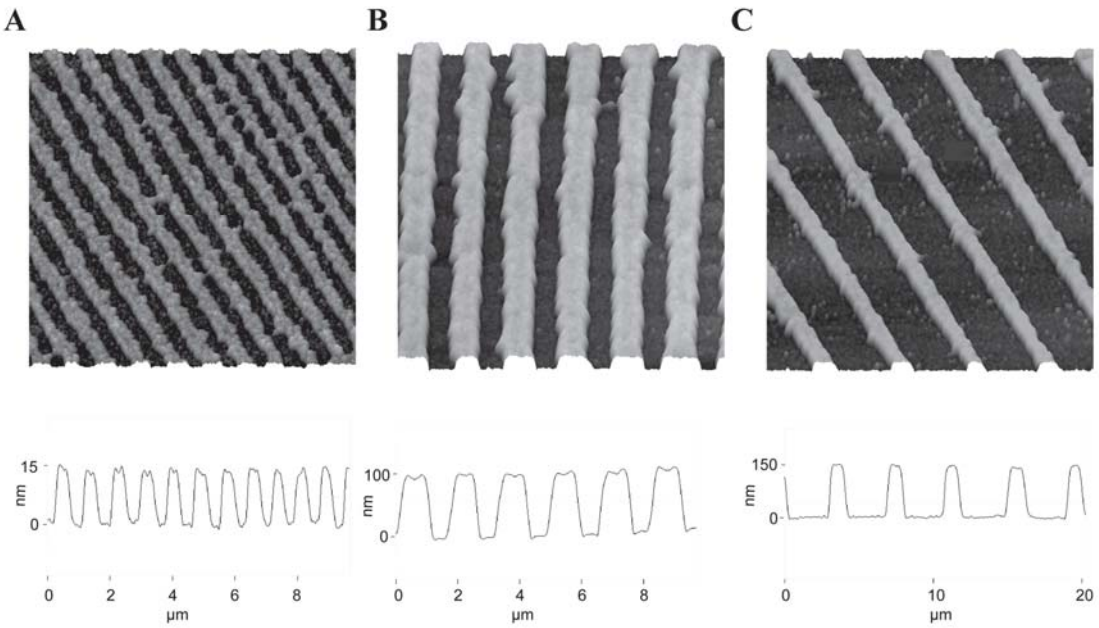

Figure 6.3 Series of AFM images illustrating the flexibility in channel dimensions created with the fuming method. The channels shown are **(A)** 530 nm wide and 15 nm deep (Π = 3 mN/m, dipping velocity = 40 mm/min, fumed for 2 minutes); **(B)** 700 nm wide and 100 nm deep (Π = 3 mN/m, dipping velocity = 25 mm/min, fumed for ~ 1 minute); and **(C)** 3.0 μm wide and 150 nm deep (Π = 3 mN/m, dipping velocity = 10 mm/min, fumed for ~ 30 seconds). The channel width is controlled by the underlying LB film and the depth is controlled by fuming duration.

Another advantage of this approach is that large surfaces can quickly be micropatterned since the entire surface is exposed during the fuming process. As an example, Fig. 6.4 shows a 60 μm x 60 μm region of a film that was templated with a DPPC monolayer transferred to mica at a surface pressure of 3.0 mN/m and a dipping velocity of 10 mm/min. Exposure to cyanoacrylate fumes for ~ 1 minute leads to the formation of enclosed channels, approximately 100 nm deep. The line-cut shown below the image in Fig. 6.4 reveals the long range order present in these microfabricated structures.

The fuming process can also be used to grow three dimensional structures directly onto the lipid monolayer. Monolayers of DPPC transferred in the LE/LC phase coexistence region of the pressure isotherm lead to distinct patterns in the resulting films. Generally, these films consist of semi-circular LC lipid domains surrounded by the more expanded LE phase. While these monolayers lead to generally hydrophobic surfaces due to the exposed lipid tail groups, greater access to the polar headgroups and underlying hydrophilic mica substrate in the disordered LE phase leads to preferential hydration compared to the more ordered and closely packed LC phase.

Transferring DPPC monolayers to a mica substrate at slower speeds and higher surface pressures enables wells to be patterned onto the substrate, as shown by the films displayed in Fig. 6.5. For the films shown in Fig. 6.5, DPPC monolayers were transferred onto mica at a surface pressure of 8.5 mN/m and dipping velocity of 10 mm/min. Under these conditions, the films contain semi-circular LC domains that are 5-8 Å taller than the surrounding LE phase, consistent with previous measurements on similar films. Figure 6.5A shows a film transferred under these conditions, following

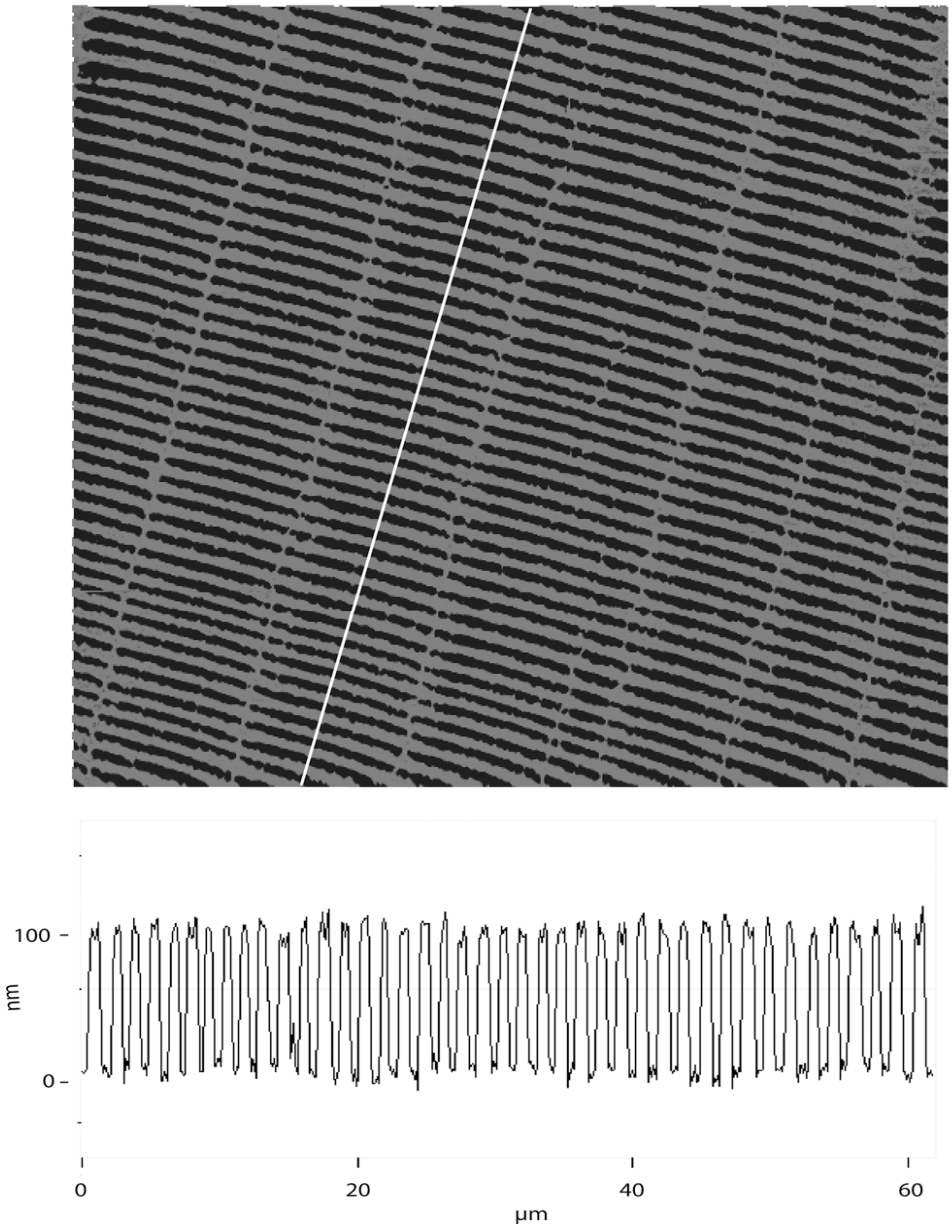

Figure 6.4 A 60 µm x 60 µm AFM image of a fumed film with enclosed channels approximately 100 nm deep. The line-cut shown below illustrates the long range consistency in the features grown on the underlying LB film.

fuming with cyanoacrylate for 2 minutes. The line-cut shown indicates that the vertical structures in this film are 140 nm. The fuming process leads to polymer growth in the LE regions of the film, creating wells in the film where the semi-circular LC domains are located. The film shown in Fig. 6.5B was fumed for 10 minutes and the well depth is ~ 450 nm.

The series of films shown in Figs. 6.3 and 6.5 help to illustrate that the fuming method provides a fast, flexible approach for micropatterning surfaces with nanometer to micron control over both the lateral and vertical feature size. While the LB film on the substrate templates the lateral features, the vertical feature size is controlled through the fuming step. Using LB films to template the lateral pattern offers several advantages: different surface active molecules lead to other geometrical patterns, film transfer is rapid even for large surface areas, a range of substrates can be used, and films can be transferred to both flat and curved surfaces. To illustrate the latter, fuming experiments were conducted on LB films transferred onto the outer walls of small glass capillaries.

Figure 6.6 shows the results from fuming a DPPC monolayer transferred onto the outer surface of a glass capillary (outer diameter = 1.0 mm) at a surface pressure of 8.5 mN/m and dipping velocity of 10 mm/min. As shown in Fig. 6.6, a fluorescence image (middle panel) of the capillary surface reveals coexisting bright and dark structures in the film that are indicative of DPPC phase coexistence. This confirms that an intact monolayer is transferred onto the outside of the glass capillary using the LB method. Also shown in Fig. 6.6 is an AFM image of the capillary surface following fuming (right panel). The AFM image shows that the lateral structure present in the film is preserved following fuming while the height difference is increased to ~ 30 nm. In contrast to films

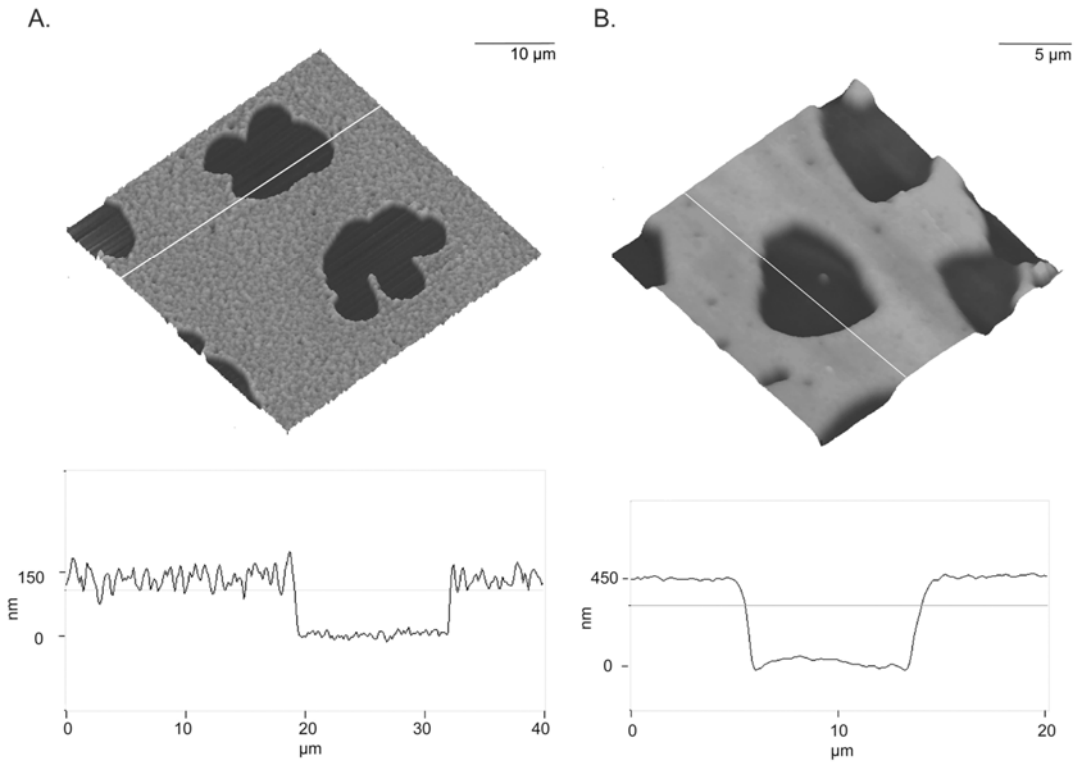

Figure 6.5 AFM images of DPPC monolayers transferred in the LE/LC phase coexistence region following fuming. Fuming leads to preferential polymerization in the LE regions of the film, leading to the formation of wells in the semi-circular LC domains. The wells in the films are **(A)** ~ 140 nm and **(B)** ~ 450 nm deep.

transferred onto hydrophilic mica surfaces where polymerization occurs in the LE regions of the film, those transferred onto glass exhibit preferential polymerization in the LC regions of the monolayer. This reflects the more hydrophobic nature of the underlying glass substrate and shows that both the LB film and substrate are important in directing polymer growth. The results presented in Fig. 6.6 show that the fuming method can be used to micropattern highly curved surfaces, which have proven problematic for other approaches.

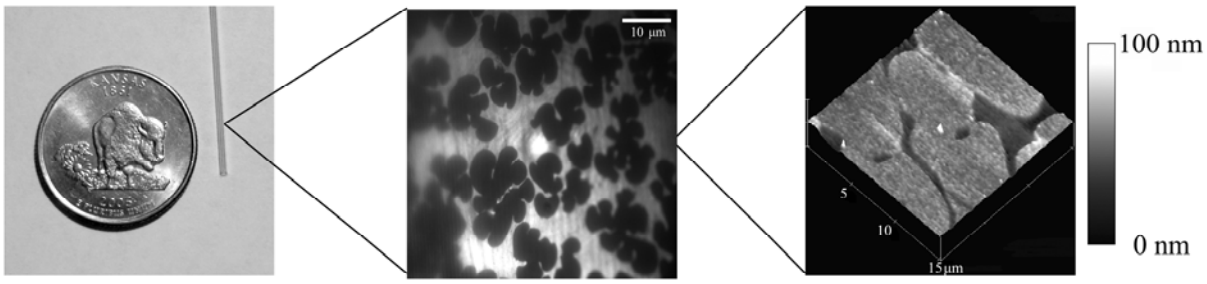

Figure 6.6 (Left panel) A Glass capillary tube (1.0 mm O.D. 0.75 mm I.D.) shown next to a U.S. quarter (23 mm diameter) for scale. **(Center panel)** Fluorescence image of a DPPC monolayer transferred onto the outer surface of a capillary tube using the LB technique. The bright and dark structures observed in the fluorescence image are typical of DPPC monolayers transferred in the LE/LC phase coexistence region of the pressure isotherm (~8.5 mN/m). **(Right panel)** A 15 μm X 15 μm AFM image of the outer surface of the DPPC coated capillary following fuming. Following fuming, the height differences in the DPPC film increase to ~ 30 nm while the lateral structure remains the same.

6.3.2 Diblock Copolymer film analysis

Diblock copolymers can form many distinct shapes that depend on many factors. Spheres, cylinders, gyroids, and lamellae are some of the shapes that can be formed when the chain lengths, annealing times and conditions, and/or fraction volumes of the copolymer are varied.[25-26] When imaged with AFM, the shapes appear as holes due to the separation of the hydrophilic and hydrophobic chains of the diblock copolymer. The hydrophilic regions are, therefore, available for polymer growth through the fuming method as described above.

Various diblock copolymer patterns were investigated using atomic force microscopy. A number of different pattern types and sizes can be fabricated depending on the copolymer used, the spin casting speed, and annealing times. For example, Fig. 6.7A and 6.7B show AFM images of the diblock copolymer PS-b-PEO spin-casted onto a mica substrate. Features as small as ~ 20 nm - 30 nm, as shown in the AFM image in Fig. 6.7B were made using this method. Smaller sizes and uniform patterns were made by allowing the thin film to be exposed to benzene vapors for different periods of time, which helps organize the diblock copolymer patterns, as shown in the AFM image in Fig. 6.7B. Before exposure to benzene vapors, the patterns are ~ 250 nm wide as shown in Fig. 6.7A. The preferential interactions of the blocks with the substrate and the air promote orientations of the microdomains parallel to the surface.[26] Exposure to benzene vapors which acts as a good solvent for both blocks leads to phase mixing, as opposed to phase segregation. As the thin film is exposed to the vapors, the fumes must diffuse through the film, which causes a gradient normal to the film surface. This gradient progresses through the thin film and translates to an ordering front. Since benzene is a

good solvent for both blocks, preferential affinity of the blocks to the substrate surface is reduced, causing the orientation to be normal to the substrate. As this ordering front moves through the thin film, microphase separation is templated by the existing domains present causing the domains to orient normal to the substrate.[27]

By spin-casting at slower speeds and using higher concentrations of the diblock copolymer, larger patterns (~400 nm – 700 nm) can be fabricated as shown in the AFM image displayed in Fig. 6.8. The conditions at which the diblock copolymer is deposited dictates the structures formed. The larger patterns are spin-casted slower and for shorter periods of time as compared to the smaller patterns. Thicker films and larger holes are also made by simply dripping the copolymer solution onto the mica slide and allowing it to dry. This causes patterns similar to spin-casting at lower speeds with higher concentrations.

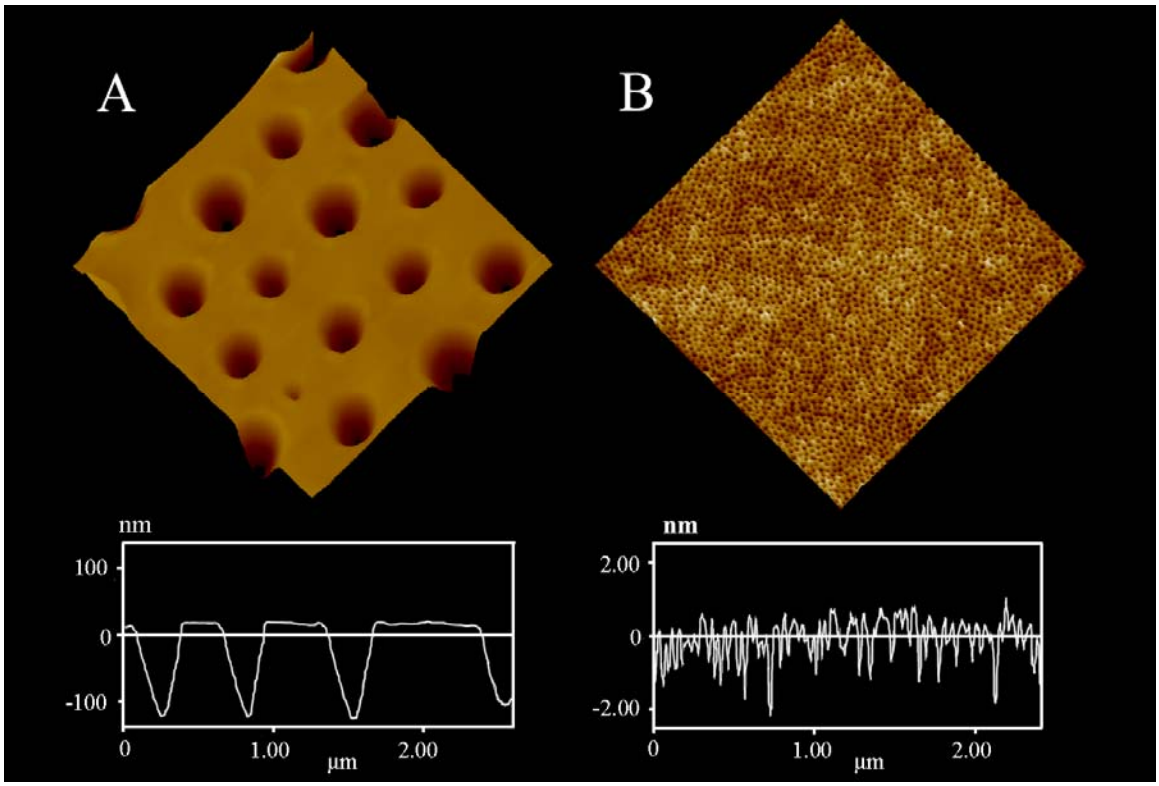

Figure 6.7 A 2.5 µm x 2.5 µm AFM scan of the diblock copolymer, PS-b-PEO spin-casted onto a mica substrate showing different sized holes. **(A)** Line cuts of the holes showing that the holes are approximately 250 nm wide and 100-150 nm deep before exposing to benzene vapors. **(B)** Line cuts showing that after exposing the copolymer to benzene vapors for 1.5 hours, the holes become approximately 30 nm. (**(B)** was exposed to benzene vapors reorganizing the diblock copolymer chains.)

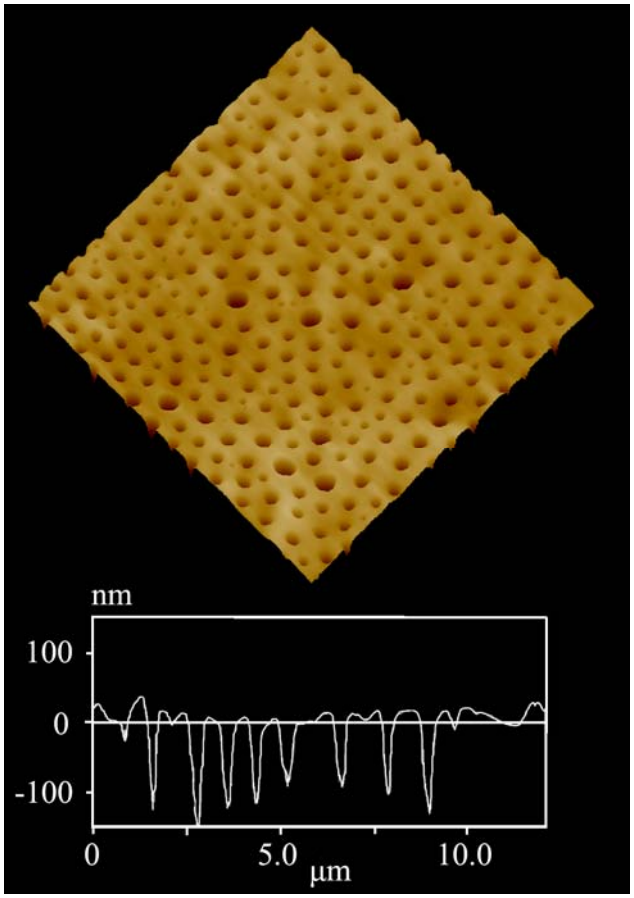

Figure 6.8 A 10 µm x 10 µm AFM scan of the diblock copolymer, PS-b-PEO showing holes that are ~400 nm – 750 nm wide and ~ 200 nm deep. This film was made by spin-casting the copolymer solution onto the mica slide at slow speeds and letting it dry.

By allowing the film to be fumed with cyanoacrylate, three-dimensional structures can be made. The cyanoacrylate selectively bonds to the hydrophilic regions of the film (the holes) and therefore pillars are made as shown in Fig. 6.9 and 6.10. Exposing the films to cyanoacrylate fumes for longer periods of time in attempt to make larger three dimensional structures results in the structures eventually merging together to form 'worm like' features.

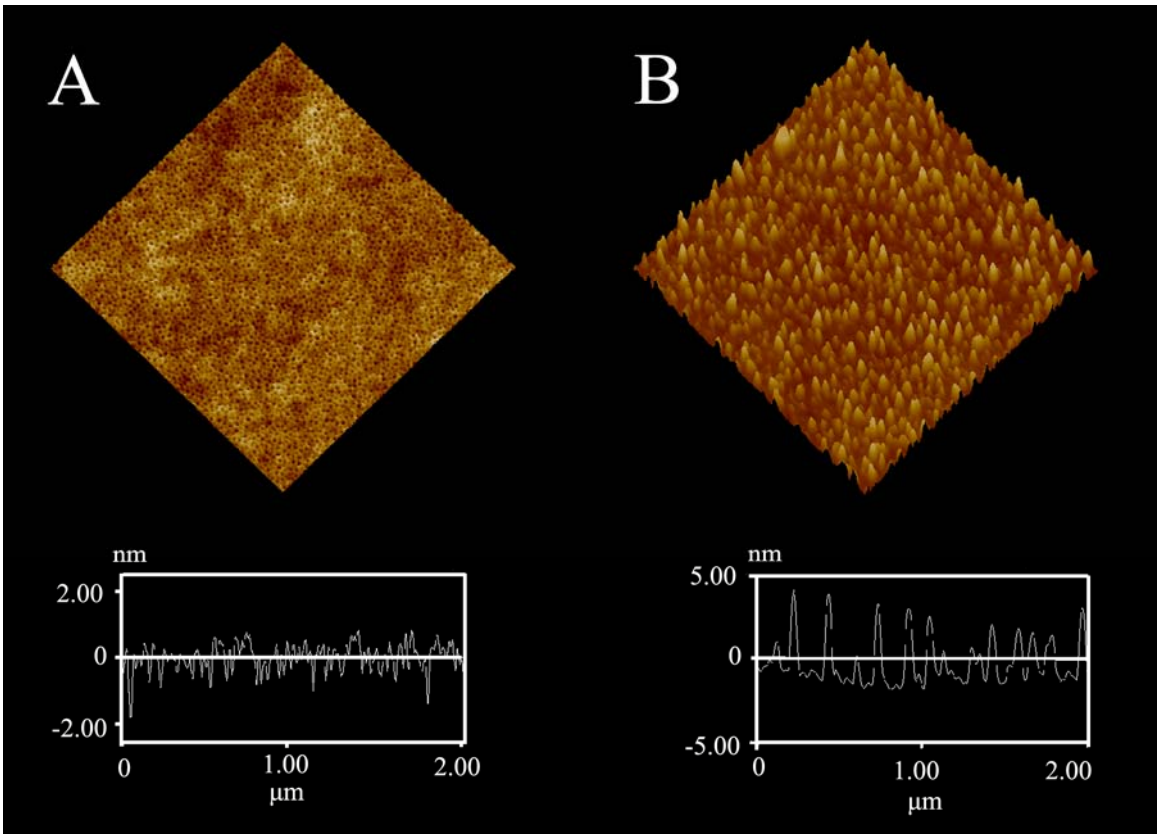

Figure 6.9 A 2 µm x 2 µm AFM scan of the diblock copolymer, PS-b-PEO spin-casted onto a mica substrate showing before and after fuming. **(A)** Line cuts of the holes showing that the holes are approximately 30 nm wide before fuming. **(B)** Line cuts showing that after fuming the copolymer film for ~ 2 minutes, the holes become pillars of ~ 5-10 nm in height. (**(A)** was exposed to benzene vapors reorganizing the diblock copolymer chains before fuming process.)

Diblock copolymer patterns were also made by spin-casting the copolymer onto a stripped fiber optic cable as shown in Fig. 6.10. In the past, it has proven difficult to grow submicron patterns onto curved surfaces. By using this method, the diblock copolymer can simply be spin-cast onto a stripped, cleaned fiber optic cable. By just spin-casting the copolymer onto the fiber, patterns of 100 nm can consistently be made. Smaller patterns can be made by allowing the thin film to undergo benzene vapor treatment as described before and shown in Fig. 6.9. Also shown in Fig. 6.10B is the same diblock copolymer film shown in Fig. 6.10A, but after fuming for 1.5 minutes. The hydrophilic regions that appeared as holes before, now have become pillars that are ~ 25nm tall.

These patterns could potentially be used for many applications. As stated before, photonic crystals have become of interest due to their unique properties as waveguides. The telecommunications industry is very interested in photonic technology because this would create a way to 'bend' or direct light around a very sharp corner with little or no loss. The films created in this chapter could potentially be used for this new technology. New and better ways to anneal these thin films will be needed to achieve the extreme uniformity that photonic crystals need to function properly.

These results show that diblock copolymer and LB films transferred onto both flat and curved substrates can be used to template lateral features for micropatterning using the fuming method. The vertical feature size is controlled through the fuming step, which offers advantages that compliment current micropatterning techniques. In the fuming method, vertical features can be easily tuned from nanometers to microns by controlling the exposure time to the cyanoacrylate fumes, providing a large dynamic range of feature

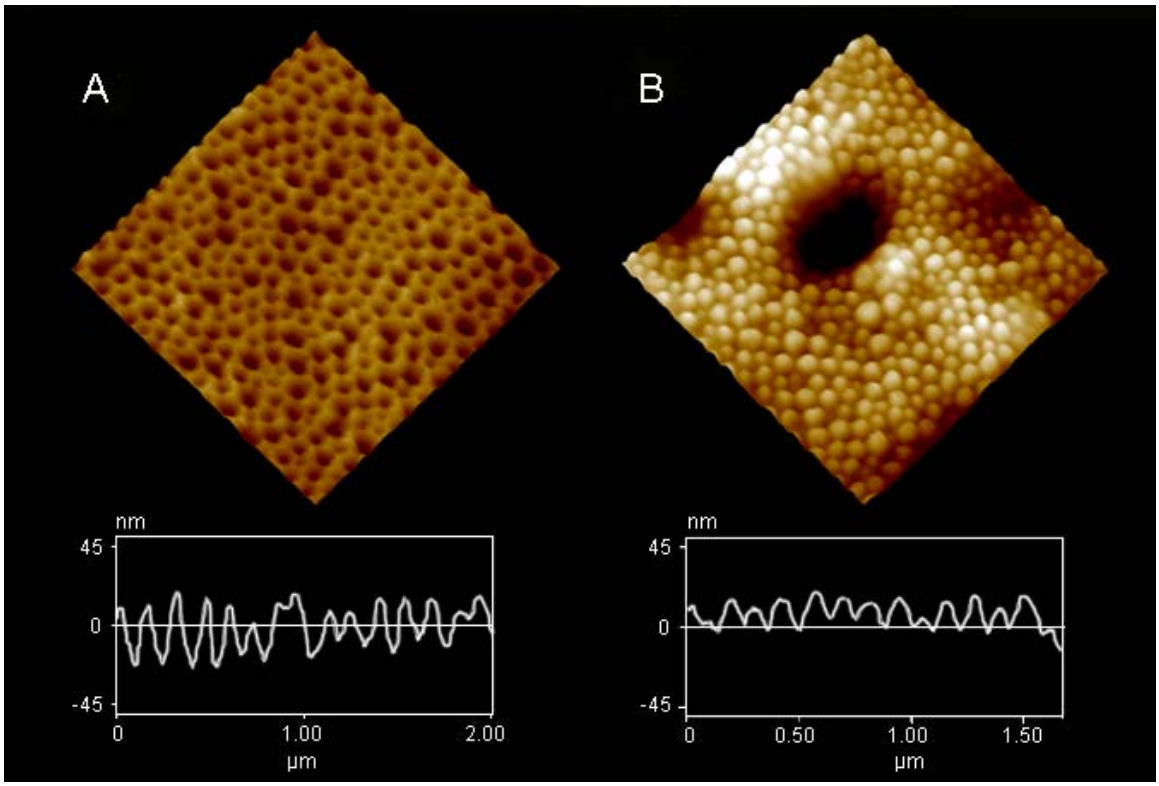

Figure 6.10 A 2 µm x 2 µm AFM scan showing the diblock copolymer (PS-b-PEO) thin film on a curved surface. **(A)** Holes are ~75 - 100 nm wide and 25nm deep. **(B)** After cyanoacrylate fuming for 1.5 minutes, the holes become pillars that are ~75 - 100 nm wide ~20-25 nm tall.

sizes. Since it is a parallel approach, fuming takes minutes regardless of substrate size and cyanoacrylates have easily accessible functional groups for chemically modifying the surface properties of the patterned substrate. Cyanoacrylates are also amenable to autoclaving for biological applications and are transparent which should facilitate the development of applications involving optical approaches.[28]

6.4 Reduction of Photo-bleaching Rates by Cyanoacrylate Fuming

With any fluorescence technique, photobleaching can be a major problem. Photobleaching occurs when a fluorophore permanently loses the ability to fluoresce due to photon-induced chemical damage. When a fluorophore transitions from an excited singlet state to an excited triplet state, fluorophores may interact with other molecules and produce irreversible covalent modifications. The excited triplet state is relatively long lived in comparison to the excited singlet state, thereby giving the excited molecule more time to undergo chemical reactions with any environmental components that may be present. For a given fluorophore, the average number of excitation and emission cycles that the fluorophore undergoes before photobleaching, is dependent on the properties of the molecule and its environment.

When analyzing single molecules, as done in the previous chapters, it can be difficult to capture images with good signal-to-noise (S/N) ratio before the fluorophore signal is lost due to photobleaching. There are several ways to help reduce photobleaching such as reducing the amount of oxygen present, using anti-fade reagents, and decreasing the intensity of the excitation source (which will also decrease the signal). There are also several factors such as the survival time, quantum yield and extinction

coefficient of the fluorophore that can limit the signal-to-noise when obtaining single molecule images. In the previous chapters, BODIPY fluorophores were selected for our single molecule measurements because they are robust fluorophores with high quantum yields and large absorption cross-sections. Moreover, they are relatively insensitive to their environment.

The presence of oxygen is one major limiting factor that can affect the survival times of fluorophores. In order to decrease the photobleaching rate of the fluorophores, we can reduce the amount of oxygen accessible to the film by creating a barrier. Photobleaching rates in single molecule measurements can be improved by using the fuming method discussed above to deposit a physical barrier above the lipid films. After depositing a LB monolayer of DPPC onto a solid substrate, the film was exposed to the cyanoacrylate fumes for short amounts of time to apply a very thin film. The thin film dramatically reduces the photobleaching rates of the dyes, but its effect on the underlying structure of the monolayer must be explored. Figure 6.11 shows single molecule orientation histograms from a DPPC monolayer doped with 33 mol % cholesterol, deposited onto a glass substrate at 25 mN/m. The film was doped with ~ 10^{-8} mol % BODIPY-PC. The blue bars represent the single molecule orientations before fuming and the red bars represent the single molecule orientations after fuming. As can be seen, there is no statistically relevant difference, illustrating that the fuming process does not perturb the molecular order in the underlying lipid films.

Having established that the fuming process does not alter the underlying lipid film structure, we now turn to the photobleaching rates. Figure 6.12 compares the fluorescence intensity decay plots for representative monolayers at two surface pressures.

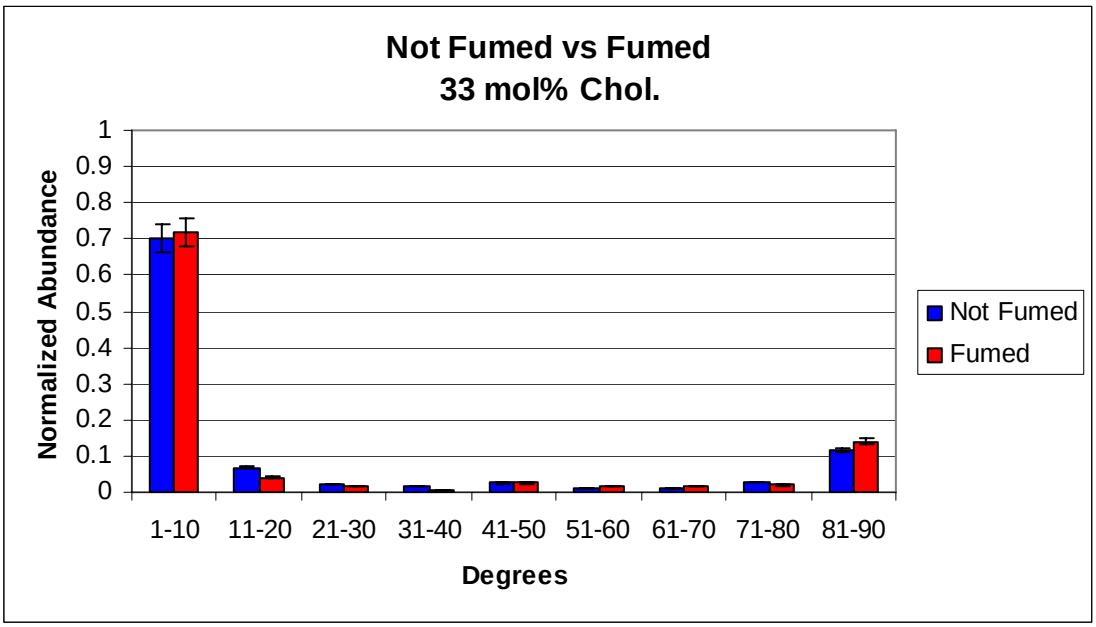

Figure 6.11 Monolayers of DPPC before and after fuming deposited at 25 mN/m with 33 mol % cholesterol. This example helps to illustrate that the thin film of cyanoacrylate does not affect the single molecule orientations in the lipid membranes.

In this experiment, monolayers of DPPC were made as described in Chapter 2 and doped with ~0.25 mol % BODIPY-PC. The monolayer was positioned for imaging and the excitation power was held constant at 10.3 mW. Each monolayer was imaged for approximately 20-25 seconds with a frame integration time of 1 second. The total intensity was calculated from each frame and used to create decay plots such as those shown in Fig. 6.12. At a surface pressure of 15 mN/m, the initial decay rates of the monolayers before fuming are fast, as shown by the pink line Fig. 6.12. This is due to the loose packing of the lipid acyl chains in which the fluorophores are more accessible to oxygen. At a higher surface pressure of 25 mN/m, the initial intensity decay rates of the monolayers before fuming are slower due to the increased lateral packing of the acyl chains. The increased packing of the lipid acyl chains decreases the accessibility of the oxygen to interact with the fluorophores.

By fuming the monolayers for a short period of time, thereby depositing a thin layer of cyanoacrylate and reducing the oxygen access to the film, the intensity decay rate for both films slows dramatically as shown by the blue lines in Fig. 6.12. As stated before, when performing single molecule studies, photobleaching can be a limiting factor, therefore, the fuming process presented here to decrease the photobleaching rates of the reporter molecules can be very useful in single molecule imaging.

A common accepted pathway of photobleaching is the reaction of triplet state oxygen with the fluorophore as discussed before. If the oxygen can be partially blocked from reacting with the fluorophore, photobleaching rates can be decreased. Thus, by

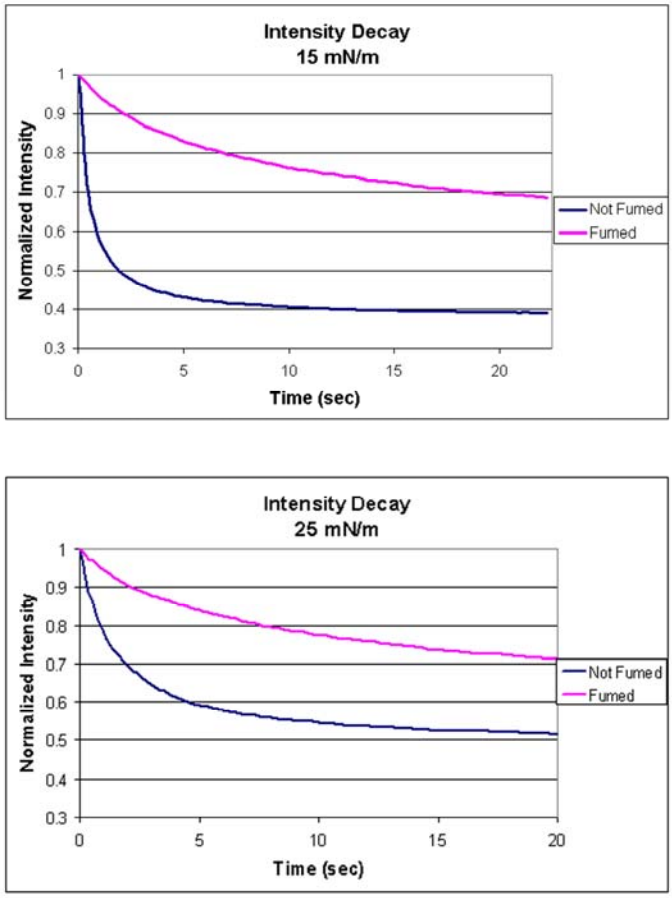

Figure 6.12 Two representative plots of fumed vs. not fumed monolayers are shown. As can been seen, at 15 mN/m, the intensity of not fumed monolayers decreases rapidly, then after fuming for a short period of time, the intensity decreases at a much slower rate. At 25 mN/m the intensity of the not fumed monolayers decreases at a slower rate than the lower surface pressure, but after fuming the intensity still decreases at a much slower rate.

coating the surface with a thin film of cyanoacrylate, this can be achieved. With this fuming technique, it was shown that the fuming process does not affect the molecular order of the films, yet drastically reduces the photobleaching rates, helping to obtain longer lifetimes of the fluorophores.

6.5 Conclusions

A method for micropatterning flat and curved surfaces is developed that uses LB films to template the growth of a polymer on a substrate. Patterns in LB films arising either from hydrodynamic instabilities during the dipping process or phase partitioning in the lipid monolayer are used to template different hydration levels across the film. Upon exposure to fumes from ethyl 2-cyanoacrylate, anionic polymerization occurs in the hydrated regions of the film leading to polymer growth in those areas. Feature height is controlled by the duration of the fuming step and structures from nanometers to microns can be fabricated in minutes. This method offers a general approach for patterning surfaces that is rapid, amenable to different substrates and films, will work on both flat and curved surfaces, and does not require expensive instrumentation.

The diblock copolymer method of creating submicron patterns has proven to be a fast and cost-effective way to create patterns on flat and curved surfaces. Lateral patterns ranging from ~ 20 nm to ~ 1 micron can be easily achieved. By simply changing the conditions, i.e. chain link sizes and spin-casting speed, a variety of sizes can be quickly fabricated. This method has also been proven efficient for coating curved surfaces, which has proven difficult in the past with most other nano-lithography techniques. Combining this method with the fuming technique proves to be a quick and simple way

to ‘grow’ three dimensional structures from a template of the diblock copolymer thin film patterns.

It is also shown that fuming for very short periods of time, we can greatly reduce the photo destruction rates of the fluorophores used in single molecule orientation measurements. It was shown that the thin layer of cyanoacrylate does not affect the molecular order of the films, but greatly reduces the photobleaching rates. This method can easily be used to improve the signal to noise in single molecule images.

6.6 References

1. Pihl, J.; Karlsson, M.; Chiu, D. T., Microfluidic technologies in drug discovery. *Drug Discovery Today* **2005,** *10* (20), 1377-1383.

2. Rosi, N. L.; Mirkin, C. A., Nanostructures in biodiagnostics. *Chem. Rev.* **2005,** *105* (4), 1547-1562.

3. Soper, S. A.; Hashimoto, M.; Situma, C.; Murphy, M. C.; McCarley, R. L.; Cheng, Y. W.; Barany, F., Fabrication of DNA microarrays onto polymer substrates using UV modification protocols with integration into microfluidic platforms for the sensing of low-abundant DNA point mutations. *Methods* **2005,** *37* (1), 103-113.

4. Sanchez, C.; Boissiere, C.; Grosso, D.; Laberty, C.; Nicole, L., Design, synthesis, and properties of inorganic and hybrid thin films having periodically organized nanoporosity. *Chem. Mater.* **2008,** *20* (3), 682-737.

5. Gates, B. D.; Xu, Q. B.; Stewart, M.; Ryan, D.; Willson, C. G.; Whitesides, G. M., New approaches to nanofabrication: Molding, printing, and other techniques. *Chem. Rev.* **2005,** *105* (4), 1171-1196.

6. Xia, Y. N.; Rogers, J. A.; Paul, K. E.; Whitesides, G. M., Unconventional methods for fabricating and patterning nanostructures. *Chem. Rev.* **1999,** *99* (7), 1823-1848.

7. Xia, Y. N.; Whitesides, G. M., Soft lithography. *Angew. Chem. Int. Ed.* **1998,** *37* (5), 551-575.

8. Ito, T.; Okazaki, S., Pushing the limits of lithography. *Nature* **2000,** *406* (6799), 1027-1031.

9. Rodgers, J. A.; Nuzzo, R. G., *Mater. Today* **2005,** *8*, 50-56.

10. Gates, B. D.; Whitesides, G. M., Replication of vertical features smaller than 2 nm by soft lithography. *J. Am. Chem. Soc.* **2003,** *125* (49), 14986-14987.

11. Stroscio, J. A.; Eigler, D. M., Atomic and Molecular Manipulation with the Scanning Tunneling Microscope. *Science* **1991,** *254* (5036), 1319-1326.

12. Ginger, D. S.; Zhang, H.; Mirkin, C. A., The evolution of dip-pen nanolithography. *Angew. Chem. Int. Ed.* **2004,** *43* (1), 30-45.

13. Piner, R. D.; Zhu, J.; Xu, F.; Hong, S. H.; Mirkin, C. A., "Dip-pen" nanolithography. *Science* **1999,** *283* (5402), 661-663.

14. Childs, W. R.; Nuzzo, R. G., Large-area patterning of coinage-metal thin films using decal transfer lithography. *Langmuir* **2005,** *21* (1), 195-202.

15. Park, M.; Harrison, C.; Chaikin, P. M.; Register, R. A.; Adamson, D. H., Block copolymer lithography: Periodic arrays of similar to 10(11) holes in 1 square centimeter. *Science* **1997,** *276* (5317), 1401-1404.

16. Ulman, A., Formation and structure of self-assembled monolayers. *Chem. Rev.* **1996,** *96* (4), 1533-1554.

17. Florsheimer, M.; Mohwald, H., Development of Equilibrium Domain Shapes in Phospholipid Monolayers. *Chem. Phys. Lipids* **1989,** *49* (4), 231-241.

18. Gleiche, M.; Chi, L. F.; Fuchs, H., Nanoscopic channel lattices with controlled anisotropic wetting. *Nature* **2000,** *403* (6766), 173-175.

19. Helm, C. A.; Mohwald, H.; Kjaer, K.; Alsnielsen, J., Phospholipid Monolayers between Fluid and Solid States. *Biophys. J.* **1987,** *52* (3), 381-390.

20. Hollars, C. W.; Dunn, R. C., Submicron structure in L-alpha-dipalmitoylphosphatidylcholine monolayers and bilayers probed with confocal, atomic force, and near-field microscopy. *Biophys. J.* **1998,** *75* (1), 342-353.

21. Kaganer, V. M.; Mohwald, H.; Dutta, P., Structure and phase transitions in Langmuir monolayers. *Rev Mod Phys* **1999,** *71* (3), 779-819.

22. Mcconnell, H. M.; Tamm, L. K.; Weis, R. M., Periodic Structures in Lipid Monolayer Phase-Transitions. *Proceedings of the National Academy of Sciences of the United States of America-Physical Sciences* **1984,** *81* (10), 3249-3253.

23. Spratte, K.; Chi, L. F.; Riegler, H., Physisorption Instabilities during Dynamic Langmuir Wetting. *Europhys. Lett.* **1994,** *25* (3), 211-217.

24. Lewis, L. A.; Smithwick, R. W.; Devault, G. L.; Bolinger, B.; Lewis, S. A., Processes involved in the development of latent fingerprints using the cyanoacrylate fuming method. *Journal of Forensic Sciences* **2001,** *46* (2), 241-246.

25. Fredrickson, G. H.; Bates, F. S., Dynamics of block copolymers: Theory and experiment. *Annu. Rev. Mater. Sci.* **1996,** *26*, 501-550.

26. Park, C.; Yoon, J.; Thomas, E. L., Enabling nanotechnology with self assembled block copolymer patterns (vol 44, pg 6725, 2003). *Polymer* **2003,** *44* (25), 7779-7779.

27. Lin, Z. Q.; Kim, D. H.; Wu, X. D.; Boosahda, L.; Stone, D.; LaRose, L.; Russell, T. P., A rapid route to arrays of nanostructures in thin films. *Adv. Mater.* **2002,** *14* (19), 1373-1376.

28. Stonehill, A. A. U.S. Patent 3,360,124, 1967.

Chapter 7

Conclusions and Future Directions

7.1 Dissertation Summary

The bulk of the research outlined in this dissertation is directed towards obtaining a better understanding of lipid membrane structure. Biological membranes are highly complex and heterogeneous structures that compartmentalize membrane components. Biological membranes serve as the dividing barrier between the inside of the cell and its environment, making their structure and function important. Bilayer membranes are made of a variety of phospholipid molecules, cholesterol, and proteins, and as discussed in Chapter 1, there is great diversity in the number of phospholipid molecules that compose biological membranes. There have been numerous techniques utilized to study the structure and function of biological and model membranes, and these studies have suggested the presence of small domains found in membranes.

The fluid mosaic model proposed by S.J. Singer to describe the nature of membranes has since been adapted. Through many experimental results, it is now understood that while some molecules can diffuse freely through the membrane, others congregate to form small heterogeneous structures. The term, lipid raft has been coined to describe these small regions of coexisting lipid phases or microdomains in which segregate or isolate different membrane components. The small size, typically <100 nm, and dynamic nature of lipid rafts, makes them difficult to directly visualize.

Because of the complex nature of natural membranes, model membranes are commonly used to simplify the analysis. There is a long standing history of utilizing

model membranes for the analysis of membrane structure and function. As discussed in Chapter 2, we utilized monolayers made by the Langmuir-Blodgett (LB) technique and bilayers made from the vesicle fusion technique. Fluorescence microscopy is a technique that is commonly used to elucidate domains in membranes. Fluorescence imaging utilizes the propensity of fluorescent lipid analogs to partition into less ordered regions in the membrane. Model membranes were examined to probe the domains present in DPPC monolayers using a phase sensitive membrane dye.

High resolution AFM measurements were also performed on model systems. The LC and LE regions seen in the fluorescence measurements were visible in the topographical AFM images as small 6-8 Å height differences. However, it was found that there were also coexisting nanometric sized domains within the LE phase that were not resolved with the fluorescence measurements. These nanometric sized domains have driven the need for further studies with high resolution techniques.

Near field scanning optical microscopy (NSOM) was used to probe the nanometric domains present by simultaneously collecting topographical measurements with high spatial resolution optical measurements. This provides a pixel-to-pixel mapping of the topography and fluorescence and a direct correlation is observed between bright domains with regions of lower topography, confirming that these areas represent regions of LE phase. This illustrates the utility of NSOM when analyzing submicron sized domains.

The bulk of this dissertation covers single molecule orientation measurements in model membranes. We can utilize the way that fluorophores emit light, as described in Chapter 2, to analyze the structure of model membranes at the molecular level. As

shown previously, by utilizing p-polarized total internal reflectance fluorescence microscopy (PTIRF-M) and slightly defocusing the optics, the emission patterns from single molecules may be used to determine the 3-D orientation of reporter molecules. The emission patterns arise from a distortion of the anisotropic emission characteristics of the fluorescent probes. In Chapter 3, experiments showed that by inserting the tailgroup labeled fluorescent lipid analog, BODIPY-PC into DPPC monolayers as a reporter molecule, the ordering of the lipid acyl chains with increasing surface pressure was tracked at the single molecule level.

Monolayers are often used as mimics of biological membranes because they offer a reproducible and simple way to control many properties such as lateral surface pressure and compressibility. Therefore, it is important to be able to directly compare monolayers and bilayers. Bilayers offer a more faithful representation of biological membranes, but exist in a tension free state at equilibrium. While direct measurements of surface pressure in bilayers is not possible, the monolayer-bilayer equivalence pressure can be estimated through indirect studies comparing membrane properties. In order to find a monolayer/bilayer "equivalent surface pressure", in Chapter 4 we show that the ordered abundance ($\leq 10^{\circ}$ tilt away from the membrane normal) can be plotted with respect to surface pressure to create a calibration curve that describes the linear response of the lipid acyl chain tilt to surface pressure. This can then be used for studies comparing properties of monolayers and bilayers and for establishing conditions under which monolayers can be used as bilayer mimics. This equivalent surface pressure was found to be ~ 23 mN/m, which is somewhat lower than current literature values.[1-7]

After developing a reliable way to track membrane order in monolayers and bilayers, we examine the effects of membrane additives such as cholesterol which was also analyzed in Chapters 3 and 4. It has previously been shown that cholesterol causes a condensing effect on lipid membranes.[8-13] The condensation of lipid acyl chains induces a new phase known as the liquid ordered state (l_o) in which has the ordered properties of the solid ordered state (s_o) and the fluid properties of the liquid disordered state (l_d), which is important for the elucidation of lipid rafts. We have shown that with the addition of small amounts of cholesterol to monolayers of DPPC, this condensing effect can be clearly observed in the single molecule measurements. For example, with the addition of just 5 mol % cholesterol, the ordered abundance ($\leq 10^\circ$ tilt) increases from ~ 42 % to ~ 60 %.[14]

The condensing effect of cholesterol and two other biologically relevant sterols, ergosterol and lanosterol, were studied in monolayers and bilayers of DPPC at the "equivalent surface pressure" found previously. A clear condensing effect was seen with the addition of both cholesterol and ergosterol, but not with lanosterol. This is attributed to the non-planar structure of the lanosterol molecule.

In a collaboration initiated with Dr. Wonpil Im and Kevin Song at the University of Kansas, we compared our single molecule measurements with molecular dynamics (MD) simulations to analyze how BODIPY-PC inserts into monolayers and bilayers of DPPC. A clear trend in ordering of the lipid acyl chains with respect to surface pressure was shown for both MD simulations and experimental results above the transition temperature of DPPC. The MD studies also analyzed the microscopic driving forces that determine the orientation of the reporter molecule at different surface pressures. At low

and medium surface pressures, it was found that entropic contributions are dominant but at high surface pressures, enthalpic contributions are dominant.

Finally, in Chapter 6, a method was developed to reproducibly fabricate micro- and nanoscopic patterns onto solid substrates.[18] By utilizing diblock copolymers and monolayers created by the Langmuir-Blodgett (LB) deposition technique, surfaces were patterned in parallel on flat or curved surfaces. By fuming with cyanoacrylate, two-dimensional structures were "grown" into three-dimensional structures in a short period of time. The fuming process was also found to decrease the photobleaching rates in single molecule imaging without altering the structure of the underlying film. Fuming creates a thin physical barrier that decreases the access of oxygen to the fluorophores, thereby decreasing chemical modifications to the fluorophores.

7.2 Future Directions

7.2.1 Probing Different Lipid Analogs for the Placement of the Fluorophore Along the Lipid Acyl Chain

The BODIPY-PC fluorophore used throughout this dissertation was chosen because of its properties as discussed previously. As shown in Fig. 7.1, the BODIPY fluorophore can be placed at many positions along the lipid acyl chain, thereby enabling the depth dependence of the reporter molecule to be probed. Other analogs such as the FM 1-43, BODIPY C4,C9 and BODIPY C8, C5 shown in Fig. 7.1, can also analyze the depth dependence of the fluorophore.

The initial studies of ordered abundance ($\leq 10^{\circ}$ tilt) vs. surface pressure are reported for three different lipid analogs, as shown in Fig. 7.2. Initial studies show that

the probe placement affects the sensitivity of the reporter probe to the membrane packing. The original BODIPY-PC (C9) is the most sensitive to lipid acyl chain ordering, while C5 and C12 BODIPY-PC molecules are less sensitive. This could be due to the insertion depth of the fluorophore in the membrane. The original BODIPY-PC molecule also contains a 4-carbon chain on the terminal end of the fluorophore, in which seems to have an effect on insertion into membranes. By utilizing different reporter molecules, different aspects of the membrane structure and properties may be probed.

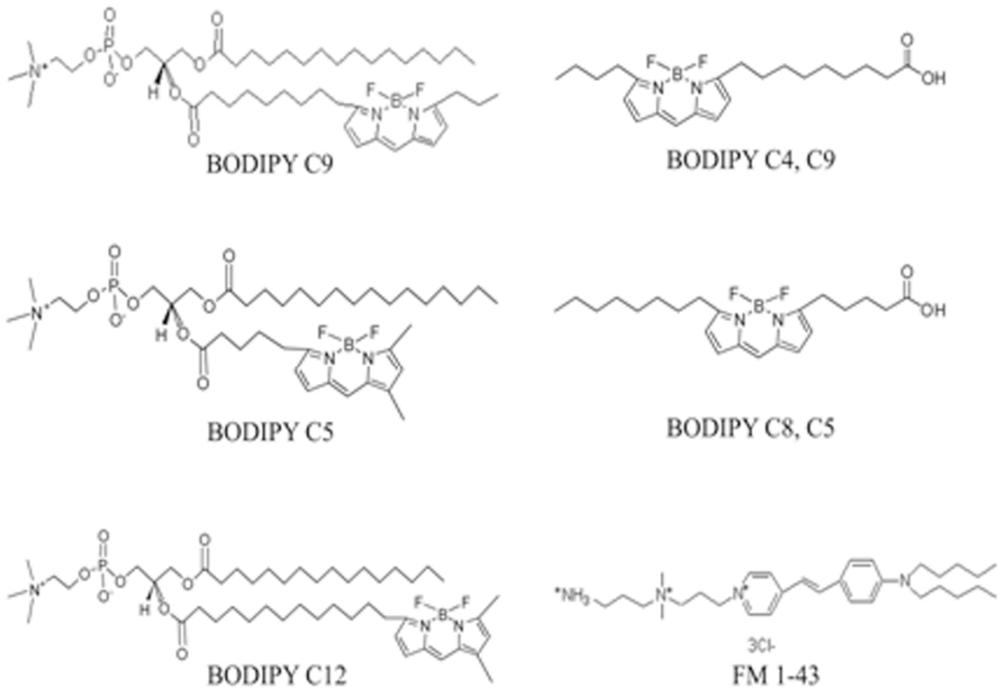

Figure 7.1 Schematic representation of several different lipid analogs. The BODIPY fluorophore can be placed at several different places along the acyl chain. The membrane dye FM 1-43 is also shown. The depth dependence of the BODIPY fluorophore can be probed.

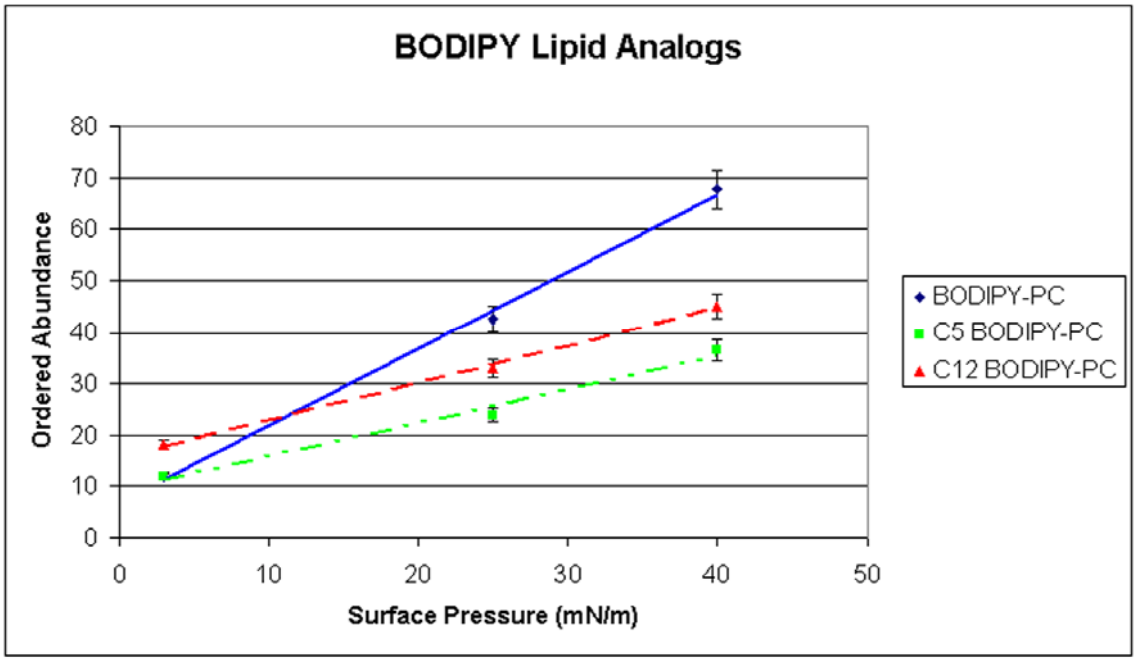

Fig. 7.2 Three different BODIPY-PC lipid analogs are graphed. The original BODIPY-PC analog (shown in blue) has the highest sensitivity (slope = 1.50) to membrane packing, while the C5 BODIPY-PC and C12 BODIPY-PC (shown in green and red, respectively) have lower sensitivity (slope = 0.65 and 0.72, respectively).

7.2.2 Direct Observation of Antibody Orientation Through Single Molecule Orientations

Antibodies are gamma globulin proteins that are used by the immune system to identify foreign objects in the body. Antibodies can be arranged onto a solid substrate and used for purification of proteins and bio-sensing application. Numerous studies have been performed to arrange antibodies onto a solid substrate in an oriented fashion. The orientation of the antibody on the surface directly affects the binding of the antigen. Methods such as selective polymer-protein noncovalent interactions,[19] use of protein A,[20] and self assembled monolayers,[21] just to name a few, have been used to improve the binding of antigens to antibodies.

The most common way to analyze the orientation of an antibody deposited on a substrate is by performing an affinity assay. By simply analyzing how much of the antigen binds to the antibody, a correlation between binding and the orientation of the antibody can be made. This, however, still does not show the true orientation of the antibody. We would like to develop a method to directly probe the orientation of antibody on a surface by utilizing the single molecule method as described in this dissertation.

The antibody can be attached to the surface by utilizing several well-known methods of attachment and orientation. Then by using a fluorescently tagged antigen, binding will occur and the orientation can be analyzed, as described in Chapter 2. For the orientation of the antibody to be analyzed, the fluorescent tag has to be attached to the antigen in a rigid fashion. The tag could also possibly be attached to the antibody itself in

order to obtain structural orientation. This method should prove useful for the determination of antibody orientations, and should be amenable to a variety of antibodies.

We have shown that the single molecule orientations can probe membrane structure at the molecular level. This molecular level structure can help reveal the heterogeneity and complex structure of membranes. The further exploration of other membrane dyes may enable tuning the sensitivity and sense the different aspects of membrane structure and function and future exploration of orientation measurements to other biological applications such as antibody/antigen binding may also be useful.

7.3 References

1. Boguslavsky, V.; Rebecchi, M.; Morris, A. J.; Jhon, D. Y.; Rhee, S. G.; Mclaughlin, S., Effect of Monolayer Surface Pressure on the Activities of Phosphoinositide-Specific Phospholipase-C-Beta-1, Phospholipase-C-Gamma-1, and Phospholipase-C-Delta-1. *Biochemistry* **1994,** *33* (10), 3032-3037.

2. Gershfeld, N. L.; Tajima, K., Spontaneous Formation of Lecithin Bilayers at the Air-Water Surface. *Nature* **1979,** *279* (5715), 708-709.

3. Marsh, D., Lateral pressure in membranes. *Biochim. Biophys. Acta* **1996,** *1286* (3), 183-223.

4. Miller, C. E.; Majewski, J.; Watkins, E. B.; Mulder, D. J.; Gog, T.; Kuhl, T. L., Probing the local order of single phospholipid membranes using grazing incidence x-ray diffraction. *Phys. Rev. Lett.* **2008,** *100* (5), 058103.

5. Portlock, S. H.; Lee, Y.; Tomich, J. M.; Tamm, L. K., Insertion and Folding of the Amino-Terminal Amphiphilic Signal Sequences of the Mannitol and Glucitol Permeases of Escherichia-Coli. *J. Biol. Chem.* **1992,** *267* (16), 11017-11022.

6. Schindler, H.; Quast, U., Functional Acetylcholine-Receptor from Torpedo-Marmorata in Planar Membranes. *Proc. Natl. Acad. Sci.* **1980,** *77* (5), 3052-3056.

7. Seelig, A., Local-Anesthetics and Pressure - a Comparison of Dibucaine Binding to Lipid Monolayers and Bilayers. *Biochim. Biophys. Acta* **1987,** *899* (2), 196-204.

8. Ege, C.; Ratajczak, M. K.; Majewski, J.; Kjaer, K.; Lee, K. Y. C., Evidence for lipid/cholesterol ordering in model lipid membranes. *Biophys. J.* **2006,** *91* (1), L1-L3.

9. McMullen, T. P. W.; Lewis, R. N. A. H.; McElhaney, R. N., Cholesterol-phospholipid interactions, the liquid-ordered phase and lipid rafts in model and biological membranes. *Curr. Opin. Colloid Interface Sci.* **2004,** *8* (6), 459-468.

10. Mouritsen, O. G.; Zuckermann, M. J., What's so special about cholesterol? *Lipids* **2004,** *39* (11), 1101-1113.

11. Ohvo-Rekila, H.; Ramstedt, B.; Leppimaki, P.; Slotte, J. P., Cholesterol interactions with phospholipids in membranes. *Prog. Lipid Res.* **2002,** *41* (1), 66-97.

12. Silvius, J. R., Role of cholesterol in lipid raft formation: lessons from lipid model systems. *Biochim. Biophys. Acta* **2003,** *1610* (2), 174-183.

13. Yeagle, P. L., The Roles of Cholesterol in the Biology of Cells. In *The Structure of Biological Membranes*, 2nd ed.; CRC Press LLC: 2005.

14. Livanec, P. W.; Huckabay, H. A.; Dunn, R. C., Exploring the Effects of Sterols in Model Lipid Membranes Using Single-Molecule Orientations. *J. Phys. Chem. B* **2009,** *113* (30), 10240-10248.

15. Bernsdorff, C.; Winter, R., Differential properties of the sterols cholesterol, ergosterol, beta-sitosterol, trans-7-dehydrocholesterol, stigmasterol and lanosterol on DPPC bilayer order. *J. Phys. Chem. B* **2003,** *107* (38), 10658-10664.

16. Cournia, Z.; Ullmann, G. M.; Smith, J. C., Differential effects of cholesterol, ergosterol and lanosterol on a dipalmitoyl phosphatidylcholine membrane: A molecular dynamics simulation study. *J. Phys. Chem. B* **2007,** *111* (7), 1786-1801.

17. Sabatini, K.; Mattila, J. P.; Kinnunen, P. K. J., Interfacial behavior of cholesterol, ergosterol, and lanosterol in mixtures with DPPC and DMPC. *Biophys. J.* **2008,** *95* (5), 2340-2355.

18. Erickson, E. S.; Livanec, P. W.; Frisz, J. F.; Dunn, R. C., Fuming Method for Micropatterning Structures on Langmuir-Blodgett Films. *Langmuir* **2009,** *25* (9), 5098-5102.

19. Clarizia, L. J.; Sok, D.; Wei, M.; Mead, J.; Barry, C.; McDonald, M., Antibody orientation enhanced by selective polymer-protein noncovalent interactions. *Anal Bioanal Chem* **2009,** *393* (5), 1531-1538.

20. Ikeda, T.; Hata, Y.; Ninomiya, K.; Ikura, Y.; Takeguchi, K.; Aoyagi, S.; Hirota, R.; Kuroda, A., Oriented immobilization of antibodies on a silicon wafer using Si-tagged protein A. *Anal. Biochem.* **2009,** *385* (1), 132-137.

21. Vareiro, M. L. M.; Liu, J.; Knoll, W.; Zak, K.; Williams, D.; Jenkins, A. T. A., Surface plasmon fluorescence measurements of human chorionic gonadotrophin: Role of

antibody orientation in obtaining enhanced sensitivity and limit of detection. *Anal. Chem.* **2005,** *77* (8), 2426-2431.